Iris effects, radiator fins, and the tropopause

Submitted by Brett McKim to the University of Exeter as a thesis for the degree of Doctor of Philosophy in Mathematics in February 2024.

I certify that all material in this thesis which is not my own work has been identified and that any material that has previously been submitted and approved for the award of a degree by this or any other University has been acknowledged.

Brett McKim

Abstract

The ways in which clouds, circulation, and climate sensitivity interact are grand challenges of climate science. All of these phenomena depend on water vapor's condensable nature and strong radiative absorption. In this thesis, we take up the premise that a closer study of water vapor may provide a master key for unlocking how clouds, circulation, and climate sensitivity interact. We begin with simple models of tropical climate, water vapor's thermospectric properties, and the water vapor feedback (Chapter 1), then pursue an understanding of how thermospectric properties interact with the general circulation and climate stability in the form of subtropical radiator fins (Chapter 2) and how these properties can constrain the general circulation in the form of the radiative tropopause (Chapter 4). We use this understanding to constrain the anvil cloud area feedback (Chapter 3), a longstanding source of uncertainty in estimating climate sensitivity.

Chapter 2 shows how, at tropical surface temperatures, the spectral width of the water vapor window, a key parameter in setting the strength of the longwave clear-sky feedback, is controlled by variations in tropospheric relative humidity owing to water vapor continuum absorption's quadratic dependence on vapor pressure. In Earth's tropics, strong meridional gradients of humidity exist due to the large scale overturning circulation, which implies meridional variations in Earth's longwave feedback. Regions of ascending motion are warm and wet, so water vapor is effective at blocking increased surface emission from escaping to space. Regions of subsidence are warm yet dry, and act as "radiator fins" by letting more surface emission escape to space, thereby stabilizing the tropics as a whole. To complement this clear-sky picture, a simple theory of cloud radiative effects is developed. High clouds mask clear-sky emission in proportion to their optically thick area fraction. Owing to their relatively fixed temperatures, they destabilize the tropics as a whole.

Chapter 3 builds on this model of cloud radiative effects to include both longwave and shortwave radiation, and high clouds and low clouds and their change with warming. Combining this formalism with observations of the present day cloud radiative effect, the anvil cloud area feedback can be constrained with a form of hypothesis testing we call the "storyline approach". For the anvil cloud area feedback to be significant, their area would need to change by 50% K^{-1}, but theory connecting anvil cloud area to the large scale circulation, observations of interannual variability, and simulations suggest they vary by about 4% K^{-1}. These multiple lines of evidence rule out a strong area feedback. On the other hand, only a 2% K^{-1} change in albedo is needed to induce a strong anvil cloud albedo feedback, but evidence for such is unclear. This suggests that a major source of uncertainty in estimating

climate sensitivity is due to changes in anvil cloud optical depth.

Chapter 4 looks again at water vapor spectroscopy, but this time at how the histogram of absorption coefficients controls the vertical profile of radiative cooling and the location of the radiative tropopause, where radiative cooling goes to zero. Previous theories of tropopause temperature based on skin temperature-like arguments break down due to the additional degrees of freedom that spectral radiative transfer allows. Tropopause temperature decouples from outgoing longwave radiation and is coupled instead to the spectral emission from the most optically thick wavenumber. Thus, radiative cooling can only extend to where water vapor is optically thick. The highest height (lowest temperature) to which water vapor is optically thick is determined by Clausius-Clapyeron scaling and the maximum effective absorption coefficient of water vapor. With these constraints, a simple model of tropopause temperature predicts a relatively fixed radiative tropopause temperature with warming and can successfuly predict changes in tropopause temperature as a result of changes in surface temperature, column relative humidity, and spectroscopic absorption.

Chapter 5 looks back on the preceding chapters and analyzes what made this approach of studying water vapor's thermospectric properties so fruitful. One of the key reasons for this success was linking water vapor's thermodynamic *and* spectroscopic properties. The former's role in climate is far more appreciated than the latter, which means there are likely more problems that could benefit from a deeper study of water vapor spectroscopy. Another reason for success was that these clear-sky insights helped build an idealized, yet sophisticated enough model of cloud radiative effects to better interpret observations and led to hypothesis testing which could incorporate different lines of evidence. Overall, this thesis stresses the need for physical understanding to be incorporated into formal methods of analysis (such as feedback decompositions) used in community efforts like CMIP. Methods of analysis should be updated as knowledge of the climate system improves and be developed to make it as easy as possible to incorporate multiple lines of evidence. This gives the best chance to more quickly constrain climate sensitivity.

Dedication

This thesis is dedicated to my parents, Sheree and Paul, for always supporting my interests throughout the years; to *Stargate* for introducing me to physics; to my high school physics teacher, Bill, for igniting a love of physics; to my undergraduate advisors, Tengiz and Sara, and the College of Creative Studies at UC Santa Barbara for teaching me how be collaborative; to my friends, Nick, Dolev, Mitchell, and Anoop, for showing how me how groups can achieve far more than what individuals can alone; to my undergraduate research advisors, Libe, Jeff, and Mike, for introducing me to oceanographic research; to my PhD advisor Nadir for his steady guidance and love of science; to my undergraduate research advisor Alexander for showing how physics can bridge different cultures; to my PhD advisor Geoff for giving me the freedom to pursue my interests; to my Fulbright advisors, Sandrine and Jean-Louis, for showing me just how far a single idea can be taken, to my partner, Veronica, for making life far richer; and to her parents, Melissa and James, for offering their home during the Covid-19 Pandemic.

Committee

Examiners
Prof. Dr John Thuburn
Chair in Geophysical Fluid Dynamics
University of Exeter

Dr Paulo Ceppi Senior Lecturer in Climate Science
Imperial College London

Primary Supervisors
Prof. Dr Geoffrey K. Vallis
Chair in Mathematics
University of Exeter

Dr Nadir Jeevanjee
Research Physical Scientist
Geophysical Fluid Dynamics Laboratory

Secondary Supervisor
Dr Stephen Thomson
Lecturer in Geophysical and Astrophysical Fluid Dynamics
University of Exeter

Fulbright Scholarship Supervisors
Dr Sandrine Bony
Senior Research Scientist
Laboratoire de Météorologie Dynamique

Dr Jean-Louis Dufresne
Senior Research Scientist
Laboratoire de Météorologie Dynamique

List of publications

McKim, B. A., Jeevanjee, N., & Vallis, G. K. (2021). Joint dependence of longwave feedback on surface temperature and relative humidity. *Geophysical Research Letters*, 48 (18), e2021GL094074. doi: https://doi.org/10.1029/2021GL094074

Henry, M., Vallis, G. K., Lutsko, N. J., Seeley, J. T., & **McKim, B. A.** (2023). State-Dependence of the Equilibrium Climate Sensitivity in a Clear-Sky GCM. *Geophysical Research Letters*, 50, e2023GL104413. https://doi.org/10.1029/2023GL104413

McKim, B. A., Bony, S., & Dufresne, J.L. (2024). Weak anvil cloud area feedback suggested by physical and observational constraints. *Nature Geoscience*. https://doi.org/10.1038/s41561-024-01414-4

McKim, B. A., Jeevanjee, N., Vallis, G. K., & Lewis, N. T. (2024). Water vapor spectroscopy and thermodynamics constrain Earth's Tropopause Temperature. *AGU Advances*, in review.

Risi, C., ..., **McKim, B. A.**, ... (2024). Amplification of temperature changes with altitude in the tropics and subtropics. In preparation for submission to *Reviews of Geophyiscs.*

Contents

Contents vi

List of Figures viii

List of Tables xii

1 Introduction 2
- 1.1 Water vapor and Earth's climate . . . 3
- 1.2 Subtropical radiator fins and the longwave feedback . . . 6
- 1.3 Anvil cloud feedbacks . . . 9
- 1.4 The radiative tropopause . . . 14
- 1.5 What lies ahead . . . 15

2 Longwave feedbacks 16
- 2.1 Abstract . . . 17
- 2.2 Introduction . . . 17
- 2.3 Results . . . 18
- 2.4 Discussion . . . 25
- 2.5 Acknowledgements . . . 27
- 2.6 Supporting Information . . . 27

3 Anvil cloud feedbacks 29
- 3.1 Abstract . . . 30
- 3.2 Introduction . . . 30
- 3.3 Methods . . . 31
- 3.4 Conceptualizing cloud radiative effects . . . 38
- 3.5 Analytic feedbacks and the storyline approach . . . 38
- 3.6 Climatology . . . 40
- 3.7 Constraining the anvil cloud area feedback . . . 41
- 3.8 Uncertainty in the anvil cloud albedo feedback . . . 45
- 3.9 Implications of uncertainty . . . 46
- 3.10 Further uses of our framework . . . 47
- 3.11 Acknowledgements . . . 48
- 3.12 Data . . . 51

4 Tropopause temperature 52

4.1 Abstract . . . 53
4.2 Introduction . . . 53
4.3 Formulating the thermospectric constraint . . . 55
4.4 Testing the thermospectric constraint . . . 59
4.5 From spectroscopy to the general circulation . . . 61
4.6 Reconciling different constraints . . . 63
4.7 Discussion . . . 65
4.8 Supporting Information . . . 66

5 Conclusions, reflections, and outlook **70**
5.1 Reinterpreting radiator fins with the longwave clear-sky feedback . . . 71
5.2 Constraining the radiative response of anvil clouds to warming . . . 72
5.3 Water vapor's role in constraining the radiative tropopause temperature . . . 74
5.4 Takeaways . . . 75
5.5 Personal reflections . . . 78

6 References **80**

List of Figures

1.1 **The Blue Marble**. Earth on December 7, 1972 from the Apollo 17 spacecraft. Photo taken either by Ron Evans or Harrison Schmitt. 4

1.2 **From spectroscopy to the general circulation.** (a) Composite image of North and South America from GOES-16/GOES-17. (b) Tropical Atlantic and the ITCZ from the VIIRS instrument on the NOAA-20 spacecraft. (c) Anvil clouds over eastern Brazil from the International Space Station. (d) Mesoscale cloud field over the western Atlantic from the International Space Station. (e) Schematic figure of microphysical processes within a cumulonimbus cloud, taken from Morrison et al. (2020). (f) Hydrometeors and water vapor spectroscopy, taken from Stevens and Bony (2013). 5

1.3 **A canonical example of the two box model of the coupling between moisture, cloudiness, and the general circulation.** Figure taken from Larson et al. (1999). 12

2.1 **Exploration of state dependence of longwave clear-sky feedback λ_{cs} in a column model**. (a) λ_{cs} phase space as a function of surface temperature T_s and column relative humidity RH, with contours indicating values of λ_{cs} and stipples indicating values between 2.2 ± 10% $\mathrm{Wm^{-2}K^{-1}}$. See Equation (2.2) for details of the calculation. Typical temperatures and humidity ranges spanned by the Earth are shaded in green. The subtropics and deep tropics are noted as ∼295 K/30%, and ∼300 K/60%, respectively. The gray arrows indicate different pathways to move from the subtropics to the deep tropics. (b) Cross section of λ_{cs} phase space at 275 K and 300 K. (c) Cross section of λ_{cs} phase space at 20% and 80% relative humidity. 19

2.2 **The closing of the H_2O window is sensitive to relative humidity at high surface temperatures.** The surface-to-space transmission $\mathcal{T}_\nu$ is plotted as a function of wavenumber ν for a surface temperature of 275 K (a) and 300 K (b), and a relative humidity of 12.5%, 25%, 50%, and 100%. The H_2O window is where $\mathcal{T}_\nu \approx 1$ and surface emission escapes directly to space. We use a Savitzky–Golay filter with a 5 $\mathrm{cm^{-1}}$ width to smooth these plots. 21

2.3 **Furnaces and radiator fins manifest as meridional variations in longwave clear-sky feedback λ_{cs}.** (a) Zonal-mean λ_{cs} is diagnosed from Figure 2.1, using the reanalysis zonal-mean RH (b) and the reanalysis zonal-mean T_s (c) as inputs (see text for details). The shaded region in (a) represents the global mean value of $2.2 \pm 10\%$ $\mathrm{Wm^{-2}K^{-1}}$ reported in other studies. We posit that the local maxima and minimum of λ_{cs} that lie outside this range should be considered the "radiator fins" and "furnace", respectively, of the tropics. Note the equal-area scaling of the x-axis. 22
2.4 **A simple model for zonal-mean all-sky emission.** (a) cloud-top fraction f, (b) cloud-top temperature T_{ct}, (c) clear-sky emission OLR_{cs}, and (d) all-sky emission OLR_{as}. The black curves are from ERA5 reanalyis. The dashed-red curve in (d) is our simple estimate produced by the equation above the panels (see Equation 2.3). Note the equal-area scaling of the x-axis. 24
2.5 **Incorporating clouds into the longwave feedback.** Zonal-mean all-sky feedback (λ_{as}, dashed-red) is diagnosed from zonal-mean clear-sky feedback (λ_{cs}, solid-black) and zonal-mean cloud-top fraction f. See Equation 2.4 for details. Note the equal-area scaling of the x-axis. 26
2.6 **Identifying zonal-mean cloud-top properties.** a) We identify the zonal-mean cloud-top fraction f by selecting the maximum of the zonal-mean cloud fraction profile above a 550 hPa cutoff. b) We identify the zonal-mean cloud-top temperature T_{ct} as the atmospheric temperature at which cloud fraction peaks. Data is shown for a select number of latitude bands. 28

3.1 **Conceptualizing cloud radiative effects.** We idealize the vertical cloud profile into two distinct layers that represent anvil clouds and low clouds with random overlap, a reasonable assumption for clouds separated by more (Oreopoulos et al. 2022). Equations indicate the domain-averaged contribution of high clouds, low clouds, and the surface to TOA energy balance. Their sum in the longwave and shortwave is given by Equation 3.1 and 3.3, respectively. See Table 3.1 for symbol meanings and values. 39
3.2 **Observed net, shortwave, and longwave cloud radiative effects (C, $C^{\mathbf{sw}}$, $C^{\mathbf{lw}}$) from CERES compared to their inferred counterparts.** Tropical mean values are shown in the upper left of each panel. The West Pacific Warm Pool and East Pacific regions are boxed in (a). The colorbar is the same for all plots. 41
3.3 **Climatological values of tropical quantities.** Effective anvil cloud fraction (a) and low cloud fraction from CALIPSO (b). The West Pacific Warm Pool and East Pacific regions are boxed to indicate regions of maximum anvil and low cloud coverage, respectively. (c–h) Inferred cloud radiative effects from Equations 3.5, 3.6, 3.8. Tropical mean values and standard deviations are shown in the upper left of each panel. Refer to Figure 3.6 to see $m_{\ell h}$ and C_h plotted with a finer color scale. 42

3.4 **Interannual changes in tropical mean anvil cloud area (a) and anvil cloud albedo (b) as a function of surface temperature.** Each point represents one year from 2006–2016. In each subplot, the slope, correlation of the best fit line and its standard error are shown. Standard error in the slope due to limited sampling is indicated by shading. In (b), the regression is calculated excluding the 2015–2016 El Niño. See Figure 3.8 for regression calculated including the El Niño and the regression calculated for low cloud albedo. 45
3.5 **Illustration of effective cloud fraction.** The high cloud fraction profile in the Warm Pool and low cloud fraction profile in the East Pacific are from CALIPSO. The full width-half maximum and effective cloud fraction of each profile are shown. The high cloud and low cloud profiles are clipped below 8 km and above 4 km, respectively, in accordance with our detection method. 48
3.6 **Climatological values of tropical quantities.** Top) Inferred cloud overlap effect from Equation 3.8. Bottom) Inferred anvil cloud radiative effect from Equation 3.5. Tropical mean values and standard deviations are shown in the upper middle of each panel. Refer to Figure 3.3 to see $m_{\ell h}$ and C_h and other quantities plotted with a broader color scale. 49
3.7 **Interannual changes in tropical mean anvil cloud height (a) and temperature (b).** In each subplot, the slope, correlation for the best fit line and its standard error are shown. Standard error in the slope due to limited sampling is indicated by shading. 49
3.8 **Interannual changes in tropical mean anvil cloud albedo (red) and low cloud albedo (blue).** (a) The line of best fit is calculated with the 2015–2016 El Niño included. (b) The line of best of fit is calculated without the El Niño. . 51

4.1 **The max absorption strength of water vapor spectroscopic absorption is hypothesized to constrain Earth's tropopause.** (a) Water vapor absorption strength as a function of wavenumber. (b) The rotational branch (150 to 1000 cm^{-1}) of absorption strength as a normalized histogram (plotted vertically), with units of $\ln \kappa_{\mathrm{H_2O}}$. (c) Spectrally-resolved radiative cooling from a single column model with line-by-line radiative transfer, PyRADS. (d) Spectrally-integrated radiative cooling. We make a rough estimate of the maximum absorption coefficient as $\kappa_{\mathrm{max}} \sim 10^3 - 10^4$ $\mathrm{m^2 kg^{-1}}$, which we hypothesize relates to the tropopause. $\kappa_{\mathrm{kink}} = 40$ $\mathrm{m^2\ kg^{-1}}$ refers to where the density of lines begins to decline rapidly, which has been hypothesized to relate to anvil clouds (Jeevanjee and Fueglistaler 2020b). Spectral data plotted at a resolution of 0.1 cm^{-1} using PyRADS (Koll and Cronin 2018). 56

4.2 **The thermospectric constraint, Equation 4.5 and 4.6, can quantitatively capture the change in tropopause temperature ($T_{\mathbf{tp}}$).** (a) Isca's single column model control simulation's temperature profile. (b) Control simulation's radiative cooling profile. (c) The surface temperature is varied and RH kept fixed at 0.7. Simulations (dots), theory (solid lines). (d) The relative humidity is varied and T_s fixed at 290 K. (e) The absorption coefficients of water vapor are scaled uniformly and T_s and RH fixed at 290 K and 0.7, respectively. Water vapor and CO_2 (280 ppmv) are the only greenhouse gases present in these simulations. 57

4.3 **Water vapor spectroscopy affects the radiative and lapse rate tropopauses.** (a) Zonal-mean temperature profile of the control Isca aquaplanet simulation. (b) Zonal-mean radiative cooling profile of the control. (c) Zonal-mean mass flux profile of the control. (d-g) Water vapor absorption coefficients are increased geometrically by [1/2, 1, 2] and the resulting changes in radiative- and lapse rate-tropopause temperature and height are recorded. The lack of ozone in these simulations accounts for the high (25 km) lapse rate tropopause. 59

4.4 **Moisture is essential to capturing a fixed tropopause temperature and spectral radiative transfer decouples tropopause temperature from outgoing longwave radiation.** (a) Outgoing longwave radiation (OLR) of Isca single column model with various types of radiative transfer. (b) Tropopause temperature for the same simulations. (c) Predicted tropopause temperature from the OLR constraint (Equation 4.1). (d-f) The radiative cooling profile plotted in temperature coordinates for $T_s = 270, 280, 290, 300, 310$ K for each model setup. Each profile has been normalized by its maximum tropospheric value and is plotted starting at the lifting condensation level for clarity. See Supporting Information for details. 63

4.5 **Zonal-mean profiles from control Isca aquaplanet simulation.** (a) Relative humidity. (b) Lapse rate. The dashed line indicates the radiative tropopause. The globally averaged tropospheric lapse rate is 7 K km^{-1}, defined here as the region between the average lifting condensation level ($\approx$ 950 hPa) and the average tropopause height ($\approx$ 150 hPa). 67

List of Tables

3.1 **Climatological values of tropical quantities (30°S − 30°N) used in this study**. All radiative quantities are evaluated at the top of atmosphere. $C^{\mathrm{lw}}_{\mathrm{obs}}$ and $C^{\mathrm{sw}}_{\mathrm{obs}}$ refer to the observed longwave and shortwave cloud radiative effects from CERES. See Climatology section for details. 50

4.1 **Definition of symbols used**. See main text for details on computing κ_{max}. See Jeevanjee and Fueglistaler (2020b) for more details and derivations of many of these quantities. 69

Author's Declaration

Most of the work in Chapter 3 was completed during an interruption of my PhD, while receiving a Fulbright Scholarship at Laboratoire de Météorologie Dynamique under the supervision of Sandrine Bony and Jean-Louis Dufresne. I have been advised by the Postgraduate Research Administration that I am welcome to include this work because the interruptions system can be used to undertake a placement which involves research relevant to the rest of the thesis.

Chapter 1

Introduction

1.1 Water vapor and Earth's climate

On December 7, 1972, 45000 km from home, a photo was taken by astronauts on *Apollo 17* that would shape the way humans viewed their planet. From the Indian to the Atlantic Ocean, from ice-covered Antarctica to desert North Africa, from pop-corn like Equatorial clouds to whirling tropical cyclones — somehow, these diverse worlds were in fact one world. *The Blue Marble* reveals not a mote of dust suspended in a sunbeam, but an engine that transforms the sun's energy into winds, clouds, deserts, and forests, or what we call Earth's climate.

This engine has as much power to foster development as it has to destroy. When *The Blue Marble* was taken, the cyclones it captured had just brought flooding and high winds to India. But these disturbances wash out on annual, multi-decadal timescales, and even multi-millennium timescales, which has enabled human development to flourish (Xu et al. 2020). Earth's climate has varied by less than 1 K (0.3%) from its 288 K global mean from the first written works to the steam engine (IPCC 2021). A natural question thus arises: How does this system stabilize itself?

Answering this question has only become more relevant as humans continue to push and prod the climate with greenhouse gasses such as Carbon Dioxide (CO_2). Since the steam engine, humans have warmed the globe by over 1 K (IPCC 2021), a blink of time in comparison to the human history that precedes it. Humans continue to emit CO_2, thus motivating one of the central questions of climate science: How much will the Earth warm in response?

Attempts to understand this question are epitomized by quantifying Equilibrium Climate Sensitivity (ECS), an idealized metric defined as the global mean surface temperature increase that results from an instantaneous doubling of CO_2:

$$\text{ECS} \equiv -\frac{F_{2\times}}{\lambda}, \tag{1.1}$$

where $F_{2\times}$ is the forcing (Wm^{-2}) due to an instantaneous doubling of CO_2 from its pre-industrial concentration of 280 ppmv, and λ is the net feedback parameter ($\text{Wm}^{-2}\text{K}^{-1}$) which quantifies how much Earth's top of atmosphere energy balance changes in response to a unit K of warming. This definition is shaped by two important aspects of Earth's climate: First, although we are interested in surface warming, the planet ultimately warms and cools by what enters and exits its top-of-atmosphere (TOA). Second, Earth's warming can be usefully decomposed into a push (the forcing) and a temperature-mediated response (the feedback). While quantifying and understanding the forcing is important and a fully-fledged sub-field in its own right (Forster et al. 2021), we will simply take it as a given that $F_{2\times} \approx 3.7$ Wm^{-2} and focus here on the feedback and what physical processes control it.

Consider the limit in which $\lambda \to 0$ $\text{Wm}^{-1}\text{K}^{-1}$. In this regime, even a small perturbation at TOA would require a large change in surface temperature to restore the TOA balance. At $\lambda = 0$ $\text{Wm}^{-2}\text{K}^{-1}$, Earth's climate would enter a runaway state where no amount of warming could ever balance a radiative perturbation. In the opposite limit of $\lambda \to -\infty$ $\text{Wm}^{-1}\text{K}^{-1}$,

Figure 1.1: **The Blue Marble**. Earth on December 7, 1972 from the Apollo 17 spacecraft. Photo taken either by Ron Evans or Harrison Schmitt.

a perturbation at TOA could be balanced with just a slight change in surface temperature. In reality, the best estimate for Earth is $\lambda = -1.3$ Wm^{-2}K^{-1} (Sherwood et al. 2020), which implies an ECS value of $-F_{2\times}/\lambda = (4.0 \text{ Wm}^{-2})/(1.3 \text{ Wm}^{-2}\text{K}^{-1}) \approx 3$ K. However, the uncertainty spans from from $2.6 - 3.9$ K, primarily because of uncertainty in clouds and how they respond to warming and couple to the atmospheric circulation (Bony et al. 2015; Sherwood et al. 2020).

It took forty years to narrow the uncertainty in ECS from 1.5 – 4.5 K (Charney et al. 1979) to its present day estimate. Part of this difficulty was (and still is) that water vapor and clouds have out-sized impacts on Earth's energy balance, but depend on scales from the microscopic to the planetary. Their mass fraction is small too. Water vapor only accounts for 0.25% of the total mass of the atmosphere, and clouds only 0.0125%. If all of this rained out, atmospheric water vapor would make a pool across Earth's surface only 2.5 cm deep, and clouds would make a pool only 1 mm deep (Stevens and Bony 2013). And yet changes in water vapor with warming are known to halve λ (Held and Soden 2000; Manabe and Wetherald 1967), and about 3000 convective updrafts throughout the Intertropical Convergenze Zone power the Earth's Hadley circulation (Riehl and Malkus 1958). The multi-scale nature of the problem is illustrated by displaying the relative scales between radiative absorption and the general circulation in Figure 1.2.

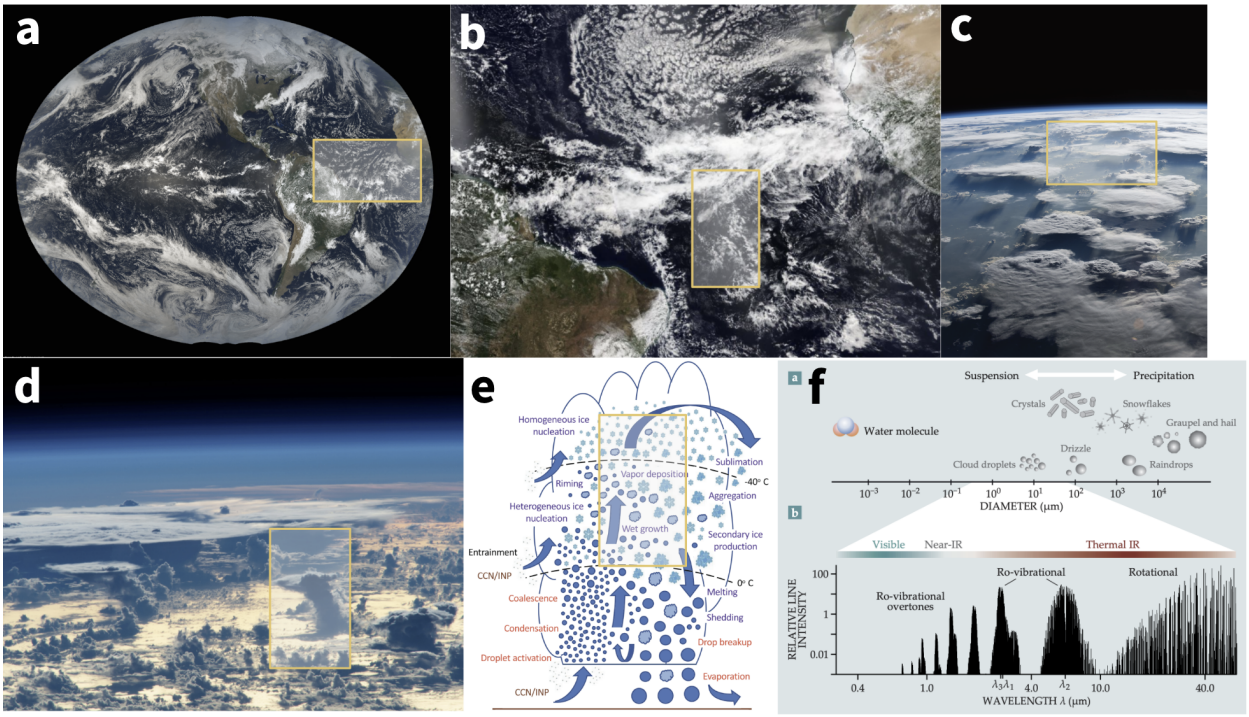

Figure 1.2: **From spectroscopy to the general circulation.** (a) Composite image of North and South America from GOES-16/GOES-17. (b) Tropical Atlantic and the ITCZ from the VIIRS instrument on the NOAA-20 spacecraft. (c) Anvil clouds over eastern Brazil from the International Space Station. (d) Mesoscale cloud field over the western Atlantic from the International Space Station. (e) Schematic figure of microphysical processes within a cumulonimbus cloud, taken from Morrison et al. (2020). (f) Hydrometeors and water vapor spectroscopy, taken from Stevens and Bony (2013).

Our goal here, broadly speaking, is to better understand this coupling between clouds, circulation, and climate sensitivity by regarding water vapor as the bridge between these entities. More specifically our goal is three-fold.

1. How do water vapor and atmospheric circulation tie together to influence climate stability (i.e. λ), particularly as one transitions from the moist, ascending deep tropics to the dry, descending subtropics?

2. How important are anvil clouds produced by deep convection, and their change with warming, for constraining Earth's climate stability and sensitivity?

3. How does water vapor's thermodynamic and radiative properties conspire to constrain the general circulation's radiative tropopause temperature?

These questions are introduced broadly here, but let us now further organize their context, motivation, and underlying physics to set the stage for following chapters.

1.2 Subtropical radiator fins and the longwave feedback

The first credible estimate of climate sensitivity was made in Manabe and Wetherald (1967). When they increased CO_2 in their single column climate model, the warming would double if they kept the *relative humidity* fixed rather than the *specific humidity*. This "water vapor feedback", in which surface evaporation increases with warming so as to maintain a nearly constant relative humidity, is the single largest contribution to Earth's net feedback (Held and Soden 2000). Owing to this large contribution, the water vapor feedback is the starting point for our study into how the general circulation interacts with evaporation and humidity to modulate climate stability.

Radiative convective equilibrium

Given the success of Manabe and Wetherald (1967) in estimating climate sensitivity, we will follow their approach and begin with a single column model (SCM) in radiative convective equilibrium (RCE) with the following essential ingredients (Jeevanjee et al. 2022):

1. A single column setting that emphasizes the role of vertical energy transfers.
2. Surface fluxes that strongly couple surface temperatures to tropospheric temperatures and constrain the tropospheric lapse rate via convective adjustment. This coupling allows us to focus on the simpler TOA energy balance rather than the surface energy balance.
3. A sufficiently realistic representation of water vapor radiative transfer, that is, a *spectral* (wavenumber-dependent) representation which permits a quantitatively accurate radiative response from perturbations in water vapor.
4. The assumption of fixed tropospheric relative humidity (RH) to capture the water vapor feedback.

In this paradigm, water vapor is optically thick across most wavenumbers, except for a region between roughly $800-1200$ cm^{-1} known as the "water vapor window". Water vapor's opacity "masks" or "blocks" much of the surface emission from escaping to space (a notion we will make more precise). Water vapor also re-emits much of this absorbed radiation back to the surface, so the surface must cool primarily via conduction and evaporation. These surface sensible and latent heat fluxes warm and moisten the boundary layer, and then convection transports that water vapor into the troposphere. This water vapor condenses and precipitates, heating the atmosphere at an altitude where the atmosphere can then cool radiatively to space owing to the optically thin atmosphere above it (Jeevanjee and Romps 2018).

To see how these ingredients lead to the water vapor feedback, consider what happens when CO_2 is increased in RCE. First, the outgoing longwave radiation decreases owing to

the increased atmospheric opacity from CO_2. Then, convection and precipitation decrease since condensation heating balances tropospheric radiative cooling (this is what Radiative-Convective Equilibrium means). Since the depth of convection is constrained to remain at a fixed isotherm of about 220 K (Hartmann and Larson 2002a), the rate at which convection converts boundary layer moisture to precipitation has decreased and the boundary layer moistens as a result. This increased relative humidity inhibits evaporation, which causes surface temperatures to increase in response. As surface temperature increases, the convectively coupled troposphere must warm too. Specific humidity must increase as a result so as to maintain a constant relative humidity (Romps 2014). The increased water vapor traps yet more radiation, which must be compensated by further warming by the process just described.

Simpson's Law of water vapor emission

This water vapor feedback can be quantified and understood most easily by focusing on spectrally-resolved TOA fluxes and the emergent property that water vapor is an "invariant emitter" that follows "Simpson's Law" (Ingram 2010; Jeevanjee et al. 2021b; Stevens and Kluft 2023). We will outline this approach, pursued in many papers (Jeevanjee 2023; Jeevanjee and Romps 2018; Koll et al. 2023; Seeley and Jeevanjee 2020; Stevens and Kluft 2023), here.

Ultimately, the incident solar radiation S must be balanced by the outgoing longwave radiation OLR. This outgoing radiation emanates from the surface only in the window region, and from the troposphere for all other wavenumbers (ignoring CO_2 and O_3 here). These contributions can be formalized with the spectrally resolved emission temperature as a function of wavenumber:

$$\mathrm{OLR}_\nu = \pi B_\nu(T_{\mathrm{em}}(\nu)), \tag{1.2}$$

where OLR_ν ($\mathrm{Wm^{-2}cm}$) is the spectrally resolved OLR (and which satisfies $\mathrm{OLR} = \int \mathrm{OLR}_\nu d\nu$), $B_\nu(T)$ is the Planck emission ($\mathrm{Wm^{-2}cm\ sr^{-1}}$), and T_{em} is the emission temperature (sometimes called the "brightness" temperature).

The longwave feedback, which accounts for most of the water vapor feedback (Jeevanjee 2023), will be controlled by the response of emission temperatures to a changing surface temperature:

$$\lambda_{\mathrm{LW}} = -\frac{d\mathrm{OLR}}{dT_s} = -\int_{0\ \mathrm{cm^{-1}}}^{\infty\ \mathrm{cm^{-1}}} \frac{\partial \mathrm{OLR}_\nu}{\partial T}\bigg|_{T=T_s} d\nu = -\int_{0\ \mathrm{cm^{-1}}}^{\infty\ \mathrm{cm^{-1}}} \pi \frac{\partial B_\nu}{\partial T}\bigg|_{T=T_{\mathrm{em}}} \frac{dT_{\mathrm{em}}}{dT_s} d\nu, \tag{1.3}$$

so T_{em} and dT_{em}/dT_s for optically thick water vapor should be understood.

$T_{\mathrm{em}}(\nu)$ is determined by where the optical depth τ of the atmosphere is about 1, a sweet spot where greenhouse gasses have a relatively clear view to space, but their density is high

enough to have substantial emission (Jeevanjee 2023). Water vapor's optical depth can be shown to be a roughly single valued function of temperature (Jeevanjee and Romps 2018), that is:

$$\tau_{\mathrm{H_2O}} = \tau_{\mathrm{H_2O}}(T) = \int_{T_{\mathrm{tp}}}^{T} \kappa_{\mathrm{H_2O}} \rho_v^* \mathrm{RH}(T') \frac{dT'}{\Gamma}, \tag{1.4}$$

where T_{tp} is the tropopause temperature, $\kappa_{\mathrm{H_2O}}$ is the mass absorption coefficient ($\mathrm{m^2 kg^{-1}}$) of water vapor, Γ is the lapse rate, and ρ_v^* is the density of saturation water vapor. This is because ρ_v^* is an exponentially varying function of temperature due to Clausius-Clapyeron scaling, and RH, κ, and Γ only weakly vary with pressure by comparison (Koll and Cronin 2018; Romps 2014). When using T as a vertical coordinate, the profile of $\tau_{\mathrm{H_2O}}$ is universal and independent of surface temperature, which means that $T_{\mathrm{em}}(\nu)$ is also independent of surface temperature as long as RH is fixed. This yields Simpson's "Law": Assuming fixed relative humidity, emission temperatures and spectrally-resolved OLR are independent of surface temperature (to first order) at wavenumbers where water vapor is optically thick. Expressed mathematically:

$$\left.\frac{d\mathrm{OLR}_\nu}{dT_s}\right|_{\mathrm{RH}} \approx 0 \quad \text{because} \quad \left.\frac{dT_{\mathrm{em}}}{dT_s}\right|_{\mathrm{RH}} \approx 0 \quad \text{(when } \nu \text{ is optically thick from } \mathrm{H_2O}\text{)}. \tag{1.5}$$

Conversely, if we continue to ignore the contribution from the net feedback from CO_2 radiator fins (Kluft et al. 2021; Seeley and Jeevanjee 2020; Stevens and Kluft 2023), then in the optically thin window region where surface emission sees directly to space,

$$\left.\frac{dT_{\mathrm{em}}}{dT_s}\right|_{\mathrm{RH}} \approx 1 \quad \text{(when } \nu \text{ is optically thin from } \mathrm{H_2O and\ CO_2}\text{)}. \tag{1.6}$$

With these approximations, and with ignoring shortwave absorption by water vapor, the water vapor feedback in radiative convective equilibrium can be computed with a simple integration determined by surface Planck emission within the water vapor window:

$$\lambda_{\mathrm{RCE}} = -\frac{d\mathrm{OLR}}{dT_s} = -\int_{0\ \mathrm{cm^{-1}}}^{\infty\ \mathrm{cm^{-1}}} \left.\frac{\partial \mathrm{OLR}_\nu}{\partial T}\right|_{T_s=290\ \mathrm{K}} d\nu = -\int_{800\ \mathrm{cm^{-1}}}^{1200\ \mathrm{cm^{-1}}} \pi \left.\frac{\partial B_\nu}{\partial T}\right|_{T_s=290\ \mathrm{K}} d\nu \approx -2\ \mathrm{Wm^{-2}K^{-1}}. \tag{1.7}$$

This value is close to the observed slope of linearity between outgoing longwave radiation and surface temperature across much of Earth (Koll and Cronin 2018) (although deviations seem to occur at the warmest surface temperatures). Evidently, fixed relative humidity radiative-convective equilibrium and Simpson's law can quantitatively capture much of the

water vapor feedback. It also sheds some insights on the relevant thermospectric physics at play.

In Equation 1.7, the feedback is determined by a competition between the increasing value of $\partial B_\nu / \partial T|_{T=T_s}$ with increasing T_s (when integrated over all wavenumbers, this term is $4\sigma T_s^3$), and the decreasing width of the water vapor window as water vapor opacity increases (Koll and Cronin 2018). We have included the first effect in arriving at our semi-analytic estimate of $\lambda_{\text{RCE}} \approx -2$ Wm^{-2}K^{-1} at $T_s = 290$ K, but calculating the decrease in width of the water vapor analytically is more involved (see Equations 37 - 39 of Koll et al. (2023)) and will not be treated here. Thus, we can predict that $\lambda_{\text{RCE}} \approx -2$ Wm^{-2}K^{-1} in the present day climate, but we cannot fully understand its state dependence without including this contribution. We take up this task in Chapter 2, where the presented numerical radiative transfer calculations include the effect of a decreasing width in the water vapor window.

This balanced competition could be modulated by variations in column relative humidity, which would change the width of the water vapor window at a given surface temperature. It is unclear how much these variations matter in controlling λ_{RCE}, but they may relate to the contrast in climate stability between the moist tropical"furnaces" and dry subtropical"radiator fins" (Pierrehumbert 1995). This brings us to the first question to be addressed in this thesis: *How do water vapor and atmospheric circulation tie together to influence climate stability (i.e. λ), particularly as one transitions from the moist, ascending deep tropics to the dry, descending subtropics?*

1.3 Anvil cloud feedbacks

Single column RCE and Simpson's law are powerful models for understanding Earth's climate, but they say little about where clouds form and their role in climate change. Clouds have a strong influence on the energy balance of the present day climate (Hartmann 2015) and likely influence Earth's climate sensitivity (Ceppi and Nowack 2021). A more comprehensive model of tropical dynamics is needed to answer how clouds will change with warming, and a more comprehensive model of how clouds modify Earth's TOA energy balance is needed to say whether changes in cloudiness will matter for climate sensitivity. Here, we focus primarily on anvil clouds, the horizontally extensive ice clouds that cap regions of deep convection (Gasparini et al. 2023).

Two box model of tropical climate

Earth's insolation depends on latitude (ϕ), which forces a circulation to balance this energetic gradient. This circulation is dynamically constrained by the weak Coriolis force at tropical latitudes, which has fundamental implications for deep convection and cloudiness that will now be explored.

More solar radiation is received in the deep tropics ($\phi \lesssim |15°|$) than the subtropics ($|15°| \lesssim \phi \lesssim |30°|$). Consequently, the deep tropics are warmer than the subtropics and also moister because of surface evaporation's exponential temperature dependence:

$$E = C_d u \rho_v^*(T_s)(1 - \mathrm{RH_{bl}}), \tag{1.8}$$

where C_d is a drag coefficient, u is the surface wind speed, $\mathrm{RH_{bl}}$ is the boundary-layer relative humidity, and $\rho_v^*(T_s)$ is the surface saturation vapor density:

$$\rho_v^*(T_s) = \frac{p_v^{\mathrm{ref}}}{R_v T_s} \exp\left(- \frac{L}{R_v T_s} \right), \tag{1.9}$$

where $p_v^{\mathrm{ref}} = 2.5 \times 10^{11}$ Pa is a reference pressure from Clausius-Clapeyron scaling (Romps 2014), $L \approx 2.5 \times 10^6$ J kg^{-1} is the latent heat of vaporization, and $R_v = 461$ J kg^{-1} K^{-1} is the vapor gas constant.

As a result, the deep tropics tends to have more surface moist static energy (h_s) (Zhang and Fueglistaler 2020), which quantifies the conserved measure of energy of an adiabatically lifted air parcel that is allowed to condense:

$$h_s \equiv c_p T_s + \frac{L R_d T_s}{p_s} \rho_v^*(T_s) \mathrm{RH_{bl}} + g z_s, \tag{1.10}$$

where T_s is surface temperature, $R_d = 287$ J kg^{-1} K^{-1} is the dry gas constant, $p_s \approx 1000$ hPa is the surface pressure, and $z_s = 0$ m is the surface height. This is in contrast to the tropical free troposphere (ft), where gravity waves efficiently homogenize the horizontal distribution of saturated moist static energy (Bretherton and Smolarkiewicz 1989; Charney 1963; Neelin and Held 1987; Sobel et al. 2001). This has implications for the tropical circulation and the location of anvil clouds (Neelin and Held 1987), because it is the saturation value of the moist static energy of the environment (h_{ft}^*) that determines whether a perturbed, saturated surface air parcel will convect (Arakawa and Schubert 1974), since a moist adiabatic temperature profile is associated with vertically constant saturation moist static energy (Romps 2020).

For instance, if $h_{\mathrm{s}} < h_{\mathrm{ft}}^*$, an upwardly perturbed surface air parcel (par) condensing in that region would be cooler than its surroundings and then return to the surface due to its negative buoyancy:

$$h_s = h_{\mathrm{par}}^* = c_p T_{\mathrm{par}} + \frac{L R_d T_{\mathrm{par}}}{p_s} \rho_v^*(T_{\mathrm{par}}) + g z_{\mathrm{par}} < h_{\mathrm{ft}}^* = c_p T_{\mathrm{ft}} + \frac{L R_d T_{\mathrm{ft}}}{p_s} \rho_v^*(T_{\mathrm{ft}}) + g z_{\mathrm{ft}}, \tag{1.11}$$

Since $z_{\mathrm{par}} = z_{\mathrm{ft}}$, this inequality implies that $T_{\mathrm{par}} < T_{\mathrm{ft}}$, and thus a negative buoyancy b, since

$$b = g \frac{T_{\mathrm{par}} - T_{\mathrm{ft}}}{T_{\mathrm{ft}}}. \tag{1.12}$$

Note that we have ignored virtual temperature and condensate loading influences on buoyancy (Bao et al. 2022; Parodi and Emanuel 2009) for simplicity.

Conversely, if $h_s > h_{ft}$, then a surface air parcel that is perturbed upwards would be warmer than its surroundings and continue to rise and condense into clouds, or in other words, *convect*. This convection takes the form of deep, precipitating clouds (Riehl and Malkus 1958) that quickly adjusts the h^*_{ft} to h_s (Arakawa and Schubert 1974; Emanuel 2008; Zhang and Fueglistaler 2020), which adjusts the atmospheric column temperature profile to a moist adiabat (Raymond 1995; Romps 2020). Because the moist adiabat is more dynamically stable than the dry adiabat, the descending, dry-adiabatically heated branch of the circulation must equilibrate to the temperature profile of the ascending branch rather than vice versa. This equilibration is carried out by gravity waves (Bretherton and Smolarkiewicz 1989) that horizontally homogenize the rest of the free troposphere to this "convective subcloud h" (Zhang and Fueglistaler 2020).

The higher h_s in the deep tropics means it is more likely to convect there and form anvil clouds, although determining the precise location and timing of this convection depends not only on surface fluxes, but convective downdrafts and entrainment between the boundary layer and the free troposphere (Raymond 1995). Returning to the bigger picture, this rising air loses its moisture via condensation and then travels polewards, but it can only go so far before conservation of angular momentum constrains it to descend in the subtropics (Held and Hou 1980). (Although there can be departures from this constraint due to zonal asymmetries that are unaccounted for in the theory.) This subsiding branch of the circulation is dryer and heats adiabatically without phase changes as it sinks. Because of this dry descent, one might expect it to follow a dry adiabat, but then the air would be strongly buoyant relative to the deep tropical moist adiabat profile of temperature. In fact, radiative cooling (Q, K day^{-1}) cools the air below the dry adiabat, allowing it to sink or "subside" at the rate:

$$w_{\text{sub}} = \frac{Q}{\Gamma_d - \Gamma_m}. \tag{1.13}$$

This coupling between temperature, moisture, cloudiness, and circulation can be described most simply by a box model of the tropics that divides the atmosphere into a moist "warm pool" and a dry "cold pool" (e.g. Larson et al. 1999; Lindzen et al. 2001; Pierrehumbert 1995 and shown in Figure 1.3).

Thermostats and iris effects

This idealized picture of tropical climate can help refute or support hypotheses for the strength of proposed anvil cloud feedbacks. For instance, anvil clouds were hypothesized to function as a thermostat by forming preferentially at the warmest end of tropical sea surface temperatures and blocking incident solar radiation from heating the surface further (Ramanathan and Collins 1991). However, this inference was based on the surface energy budget rather than the TOA energy budget, which is the more relevant budget for determining whether clouds have a stabilizing or destabilizing effect on surface temperature (Jeevanjee et al. 2022; Manabe and Wetherald 1967; Pierrehumbert 1995). Anvil clouds have an almost neutral impact on the TOA energy balance (Hartmann and Berry 2017; Kiehl 1994;

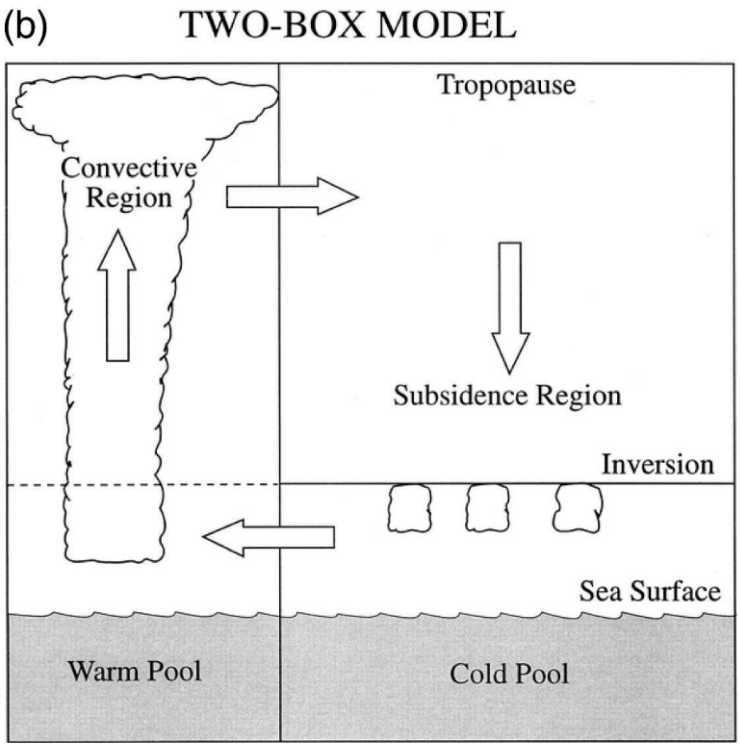

Figure 1.3: **A canonical example of the two box model of the coupling between moisture, cloudiness, and the general circulation.** Figure taken from Larson et al. (1999).

Ramanathan et al. 1989), which could affect surface temperature gradients but not the tropical mean temperature, which is constrained instead by the tropical mean TOA balance (Pierrehumbert 1995). Furthermore, the relationship between anvil clouds and the surface temperature distribution can be explained by the physics of convective thresholds described in the previous section (Williams et al. 2009), without having to invoke any temperature stabilization mechanism.

With the two box model of tropical climate and its derivatives, the thermostat class of anvil cloud feedbacks could be ruled out (Hartmann and Michelsen 1993; Lau et al. 1997; Pierrehumbert 1995; Wallace 1992). In place of a thermostat mechanism, Pierrehumbert (1995) argued for the primacy of subtropical dry regions in stabilizing climate. However, they did not present any candidate mechanism that could control the relative area of dry and moist regions, and they rely on the assumption that deep convective anvil clouds have and continue to have a small cloud radiative effect. This mechanistic gap opened the door for considering the "Iris effect", where anvil cloud evolution is hypothesized to control this relative area of dry and moist areas and which leads to the idea that anvil clouds and their change with warming may constitute a significant feedback (Lindzen et al. 2001).

In particular, Lindzen et al. (2001) hypothesized that anvil cloud area and detrained water

in the upper troposphere might both decrease with warming because of increases in precipitation efficiency (although the presumably microphysical mechanism for *why* the efficiency might change was never specified, and the quantitative link between efficiency and cloud area was never established). Using monthly variations in observed cloud amount, they inferred a fractional change in anvil cloud area of about -22% per degree surface temperature (K^{-1}). They then used a box model of tropical climate like the one described previously to show that this iris effect might have a strong influence on Earth's climate sensitivity. Note that Lindzen et al assumed that anvil clouds have a strong positive cloud radiative effect, contradicting previous observations showing their radiative neutrality (Ramanathan et al. 1989). However, strong critiques of this study soon followed based on issues with methodology such as the unrealistic cloud radiative effect (Lin et al. 2002) and neglecting the dynamical contribution to cloud changes (Bony et al. 2004; Hartmann and Michelsen 2002) when inferring cloud feedbacks. To this day, there has been limited evidence to link changes in precipitation efficiency with anvil cloud area (Ito and Masunaga 2022), casting doubt on the iris hypothesis (at least as originally proposed). Furthermore, When changes in precipitation efficiency are explicitly imposed in GCM experiments, changes in climate sensitivity relative to control simulations are much more modest than the original iris hypothesis suggests (Mauritsen and Stevens 2015), and are more affected by changes in anvil cloud optical depth than anvil cloud area (Li et al. 2019). We will revisit this point in Chapter 3.

The iris effect became a polemical issue due partly to the people involved and partly because it was (and still is) difficult to verify or refute the microphysical precipitation efficiency mechanism suggested in Lindzen et al. (2001). Progress has come instead from understanding how anvil clouds' macrophysical properties tie to large-scale controls like those displayed in the box model of tropical circulation. The Fixed Anvil Temperature (FAT) hypothesis is one example of this type of constraint (Harrop and Hartmann 2012; Hartmann and Larson 2002b; Zelinka and Hartmann 2010). But here, we will focus on the stability iris hypothesis, which argues that tropical anvil cloud areas should decrease with warming because of mass conservation and moist thermodynamics (Bony et al. 2016).

First, one assumes that anvil cloud cloud area (f_h) is proportional to the detrainment (i.e. the divergence) of cloudy air from the convective region in the upper troposphere $-\rho^{-1}\partial_z M$, where M is the convective mass flux and ρ the density of air. This detrained cloudy air is equal to the horizontal convergence of air in clear-sky regions (CSC). By conservation of mass and the continuity equation, this horizontal convergence must balance the vertical divergence of clear-air subsidence ($\partial_z w_{\text{sub}}$). Stated mathematically:

$$f_h = -\mu\rho^{-1}\partial_z M = \mu \text{CSC} = \mu\partial_z w_{\text{sub}} = \mu\partial_z\left(\frac{Q}{\Gamma_m - \Gamma_d}\right), \tag{1.14}$$

where μ represents the microphysical and vertical advection time tendencies for log cloud condensate (Beydoun et al. 2021; Jeevanjee 2022) and the lapse rate is now assumed equal to a moist adiabat. Because at fixed temperatures levels, moist adiabatic lapse rates decreases with surface warming (Jeevanjee 2022), the denominator in the right most side of Equation 1.14 should increase. Increases in radiative cooling are less significant (Bony et al. 2016;

Knutson and Manabe 1995), so if one assumes that variations in μ are small by comparison, the overall effect should be for anvil cloud area to decrease. Despite the disregard of potential changes in cloud microphysics (Beydoun et al. 2021; Gasparini et al. 2023; Jeevanjee 2022), the stability iris hypothesis is consistent with observations (Ito and Masunaga 2022; Saint-Lu et al. 2020, 2022).

While the stability iris provides a way to understand changes in anvil cloud area, it is still unclear how strong the resulting radiative feedback would have because confounding factors such as cloud overlap (i.e. exposing low clouds beneath anvils), uncertainty in the precise magnitude of the area change, and potentially a changing cloud radiative effect may modulate the result. Changes in anvil cloud area are still one of the largest sources of uncertainty in estimating climate sensitivity (Forster et al. 2021; Sherwood et al. 2020), which leads us to the second question of our thesis: *How important are anvil clouds produced by deep convection, and their change with warming, for constraining Earth's climate stability and sensitivity?*

1.4 The radiative tropopause

Much of the discussion so far has focused on climate stability and radiative feedbacks, but in revisiting *The Blue Marble* and in particular the oblique views of anvil clouds from the International Space Station in Figure 1.2c,d, another question arises: what sets the depth of the troposphere? Or in other words, why do convection and eddies extend so far? As we have seen, the thermodynamic and radiative constraints that accompany water vapor play a role in setting the atmosphere's temperature profile, at least in the tropics, and they also constrain the decrease in convective mass fluxes (Betts 1998; Chadwick et al. 2013; Held and Soden 2006; Jenney et al. 2020) and tropical overturning strength with warming (Betts and Ridgway 1989; Knutson and Manabe 1995; Vecchi and Soden 2007), as well as the temperature of anvil clouds (Harrop and Hartmann 2012; Hartmann and Larson 2002b), so it might be that water vapor plays a role in tropospheric depth depth too.

The connection between water vapor, radiative cooling, and the circulation (Manabe and Strickler 1964 and Chapter 1) motivates studying the radiative tropopause (defined by the lowest level where radiative cooling goes to zero and neglecting dynamical warming associated with processes like the Brewer-Dobson circulation). A simple argument for how water vapor constrains the temperature of the radiative tropopause goes as follows: Water vapor decreases as temperature decreases, which itself decreases with altitude until water vapor becomes so optically thin that its radiative emission becomes negligible. By continuity, convection must also become negligible because its latent heating ultimately balances this radiative cooling. The temperature at which water vapor becomes optically thin and stops radiative cooling has not been made precise, but this reasoning has been used to argue for the relatively constant temperature of anvil clouds (Hartmann and Larson 2002b) and may even be more apt in constraining tropopause temperature (Seeley et al. 2019).

However, it is possible to constrain the tropopause without any notion of water vapor, and instead constrain it with a notion of dynamical and radiative consistency: the tropopause is the height to which dynamical effects extend and the height needed to satisfy planetary

energy balance (Held 1982; Thuburn and Craig 1997, 2000; Vallis 2017). Using gray radiative transfer theory, one can show that the tropopause temperature should be a skin-like temperature tied to OLR (Pierrehumbert 2010). Models based on this type of thinking can reproduce the meridional structure of the tropopause (Hu and Vallis 2019) and its vertical shift with warming (Vallis et al. 2015).

It is not clear whether these two types of thinking are necessarily consistent with one another, as they lead to differing predictions of the response of tropopause temperature to surface warming. The former (water vapor) theory emphasize a fixed tropopause temperature irrespective of the warming agent. The latter theory permits a changing tropopause temperature if the warming agent perturbs Earth's TOA budget. The connections and differences between these theories should be made precise, which leads us to the third and final question in this thesis: *How does water vapor's thermodynamic and radiative properties conspire to constrain the depth of the tropospheric circulation?*

1.5 What lies ahead

We have now laid down the context for the three questions that will be pursued in this thesis. All three questions have their roots in the radiative and thermodynamic properties accompanying the presence of water and the following chapters will use these properties to decipher the connections between clouds, circulation, and climate sensitivity.

In the first question, we will focus on the interaction between climatological relative humidity maintained by the tropical circulation, the width of the water vapor window, and the longwave climate feedback. The effects of climatological anvil clouds will be accounted for with a simple model of their impact on TOA energy balance. In the second question, that model will be expanded to account for changes in anvil clouds with warming. The resulting feedback decomposition we develop will help bridge the gap between the changes in anvil cloud area expected from moist thermodynamics and continuity of the tropical circulation, and the resulting radiative feedbacks from such changes. In the the third question, ties between convection, eddies, and radiative cooling will be combined with water vapor thermodynamics and spectroscopy to constrain the response of the tropopause to surface warming. Ultimately, we hope to impart to the reader the profound influence water vapor has in coupling the smallest scales of spectroscopy to the general circulation and climate sensitivity.

Chapter 2

Longwave feedbacks

This chapter is published as McKim, B. A., Jeevanjee, N., & Vallis, G. K. (2021). *Joint dependence of longwave feedback on surface temperature and relative humidity.* Geophysical Research Letters, 48 (18), e2021GL094074. doi: https://doi.org/10.1029/2021GL094074

2.1 Abstract

Many studies have suggested that Earth's clear-sky outgoing longwave radiation (OLR) varies linearly with surface temperature, with a longwave clear-sky feedback that is independent of surface temperature and relative humidity. However, this uniformity conflicts with the notion that humidity controls tropical stability (e.g. the "furnace" and "radiator fins" of Pierrehumbert (1995)). Here, we use a column model to explore the dependence of longwave clear-sky feedback on both surface temperature and relative humidity. We find that a strong humidity dependence in the feedback emerges above 275 K, which stems from the closing of the H_2O window, and that the furnace and radiator fins are consequences of this dependence. We then clarify that radiator fins are better characterized by tropical variations in clear-sky feedback than OLR. Finally, we construct a simple model for estimating the all-sky feedback and find that although clouds lower the magnitude of longwave feedback, the humidity-dependence persists.

2.2 Introduction

The longwave clear-sky feedback parameter λ_{cs} relates a change in clear-sky outgoing longwave radiation OLR_{cs} to a change in surface temperature T_s,

$$\lambda_{cs} \equiv \frac{\mathrm{dOLR}_{cs}}{\mathrm{d}T_s} \quad (\mathrm{Wm^{-2}K^{-1}}). \tag{2.1}$$

It is a measure of the stability of the climate and thus is a well studied quantity, with a canonical value for its global mean of about $2.2 \pm 10\%$ $\mathrm{Wm^{-2}K^{-1}}$ (Allan et al. 1999; Bony et al. 1995; Budyko 1969; Cess et al. 1989, 1990; Chung et al. 2010; Dessler et al. 2008; Jeevanjee 2018; Koll and Cronin 2018; Raval et al. 1994; Zhang et al. 2020).

The convergence of the global mean value of λ_{cs} across both observations and the model hierarchy suggests robust physics that is insensitive to the idiosyncrasies of the individual studies. Recently, Koll and Cronin (2018) gave an explanation of this physics as a balance between increasing surface Planck feedback and decreasing surface transmissivity. They verified that $\lambda_{cs} \approx 2.2$ $\mathrm{Wm^{-1}K^{-1}}$ for a wide range of T_s in a column model. Zhang et al. (2020) then extended this analysis to GCMs and similarly found λ_{cs} to be independent of both T_s and free-tropospheric relative humidity (RH).

This work on the uniformity of feedback lies in tension with the notion that meridional variations in clear-sky relative humidity are important in controlling tropical stability. In particular, Pierrehumbert (1995) argued that the warm and moist deep tropics, with active deep convection (furnace) are close to a local runaway greenhouse, but are radiatively stabilized by the warm, yet dryer, and more quiescent subtropics (radiator fins). However, Pierrehumbert (1995) was equivocal on whether the furnace and radiator fins manifest as tropical variations in OLR_{cs}, or rather in λ_{cs}, which is the more relevant parameter for stability. Indeed, as we shall show later, the latitudinal variations in OLR_{cs} within the tropics are quite muted compared to OLR_{cs} variations over the globe. Here, then, we will pursue the idea that radiator fins manifest instead as tropical variations in λ_{cs}.

Clouds are another process that may play a role in controlling the structure of zonal-mean feedback. Pierrehumbert (1995) argued for the presence of tropical furnaces and radiator fins using only clear-sky physics. However, humid regions and cloudy regions often go hand-in-hand, and high clouds are known to have a robust influence on the longwave feedback (Zelinka and Hartmann 2010), so we might expect the longwave all-sky feedback parameter λ_{as} to look different from λ_{cs} in the zonal mean.

We lack clarity on whether the taxonomy of the furnace and radiator fins are better described by OLR_{cs} or by λ_{cs}. There is also a tension between the constancy of λ_{cs} observed across studies and the notion that humidity variations control tropical stability, and it is unclear how clouds might modulate this relationship. This state of affairs motivates us to ask the following questions:

1. Do furnaces and radiator fins indeed manifest as a contrast in the zonal-mean λ_{cs} as opposed to the zonal-mean OLR_{cs}?
2. How do we reconcile variations in λ_{cs} implied by furnaces and radiator fins when other studies suggest λ_{cs} is approximately constant?
3. How do clouds modify the meridional structure of longwave feedback?

To this end we first construct a "phase space", in which λ_{cs} is computed as a joint function of T_s and column RH. Below 275 K, we find that λ_{cs} stays within 10% of 2.2 $\mathrm{Wm^{-2}K^{-1}}$, even as RH varies. Above 275 K, however, a significant RH-dependence emerges, leading to much greater variations in λ_{cs}. We show that this RH-dependence stems from the closing of the H_2O window. The tropical contrast in zonal-mean λ_{cs} is, then, a consequence of this RH-dependence at high temperatures. Finally, we construct a simple model for evaluating the all-sky feedback and find that although clouds decrease the zonal-mean feedback, the RH-dependence remains significant.

2.3 Results

Exploring the state dependence of λ_{cs}

We first address Question 2 by exploring the state dependence of λ_{cs} as a function of both T_s and RH. We use RH as a state variable because RH-based feedbacks have certain advantages over specific humidity (q_v) based feedbacks both from a thermodynamic point of view (Held and Shell 2012) and from a radiative point of view (Jeevanjee et al. 2021b), as specific humidity already has a de facto strong temperature dependence through the Clausius-Clapeyron relation. To compute radiative transfer we use PyRADS, a validated line-by-line column model (Koll and Cronin 2019). We used the model in 1-D radiative-convective equilibrium, following Koll and Cronin (2018), in which a moist adiabat profile is assumed and allowed to extend to 150 K. We set the CO_2 concentration to 340 ppmv, the number of pressure levels to 30 from 0.1 to 1000 hPa (sensitivity experiments increasing the number of levels to 60 found no significant differences in the computed feedback), and consider a spectral

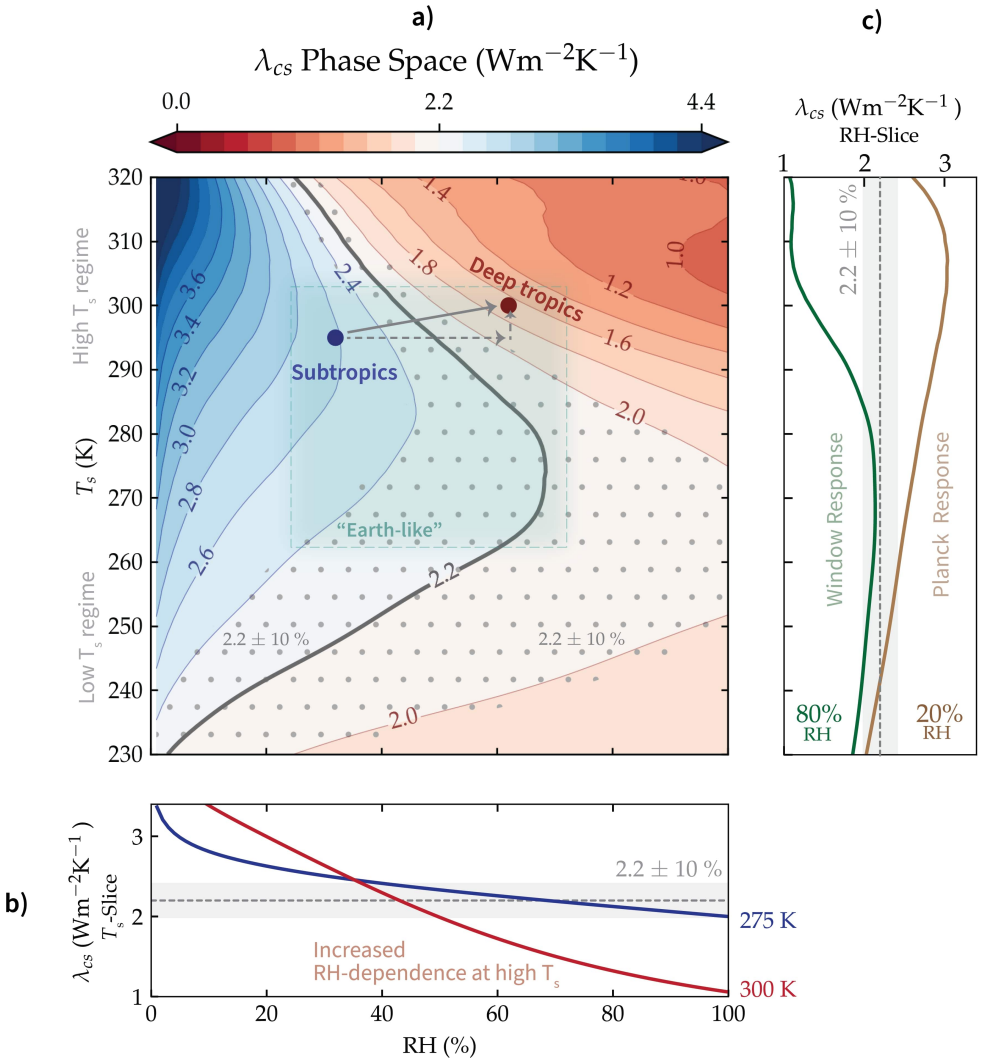

Figure 2.1: **Exploration of state dependence of longwave clear-sky feedback λ_{cs} in a column model**. (a) λ_{cs} phase space as a function of surface temperature T_s and column relative humidity RH, with contours indicating values of λ_{cs} and stipples indicating values between 2.2 ± 10% Wm^{-2}K^{-1}. See Equation (2.2) for details of the calculation. Typical temperatures and humidity ranges spanned by the Earth are shaded in green. The subtropics and deep tropics are noted as ∼295 K/30%, and ∼300 K/60%, respectively. The gray arrows indicate different pathways to move from the subtropics to the deep tropics. (b) Cross section of λ_{cs} phase space at 275 K and 300 K. (c) Cross section of λ_{cs} phase space at 20% and 80% relative humidity.

range between 0.1 and 3500 cm^{-1} at 0.01 cm^{-1} resolution. We only then need to specify the surface temperature and a vertically-uniform relative humidity to compute OLR_{cs} for the column. For more details of atmospheric structure and spectral databases, see "Materials and Methods" in Koll and Cronin (2018).

We calculate λ_{cs} in the following way. We first compute OLR_{cs} for some T_s and RH; we then perturb the surface temperature by an amount ΔT, and allow the moist-adiabatic atmosphere to respond while holding RH fixed; finally we calculate the perturbed outgoing longwave radiation and take the finite difference between the two states. In summary:

$$\lambda_{cs}(T_s, \mathrm{RH}) \approx \frac{\mathrm{OLR}_{cs}(T_s + \Delta T, \mathrm{RH}) - \mathrm{OLR}_{cs}(T_s, \mathrm{RH})}{\Delta T}, \tag{2.2}$$

where $\Delta T = 1$ K in our calculations. Note that the Planck, lapse rate, and water vapor feedbacks are included in λ_{cs}. The moist adiabat is not satisfied in the mid-latitudes, but we note that the lapse rate feedback is small when RH is fixed (Cess 1975; Held and Shell 2012; Jeevanjee et al. 2021b; Zelinka et al. 2020). We exclude the RH-feedback associated with a change in RH with surface warming for simplicity and because its value in the global mean is < 0.1 $Wm^{-2}K^{-1}$ (Held and Shell 2012; Zelinka et al. 2020). We also assume the atmosphere responds like a moist adiabat for simplicity, although in reality the atmospheric temperature change is not always due to a local T_s change (Mauritsen 2016). We give some perspective on our feedback analysis in Section 2.4.

Our results are summarized in Figure 2.1a) for surface temperatures between 230 K and 320 K and relative humidities between 0% and 100%. We identify 275 K as the de facto boundary between a low temperature regime and a high temperature regime because each region exhibits distinct behaviors for λ_{cs}. Below 275 K, there is a very small RH-dependence — for values of RH between 20% and 80%, λ_{cs} remains within 10% of 2.2 $Wm^{-2}K^{-1}$. Above 275 K, however, a significant RH-dependence emerges: the value of λ_{cs} differs from 2.2 $Wm^{-2}K^{-1}$ by much more than 10% over the same range of humidity. We explicitly plot the RH-dependence of λ_{cs} at 275K and 300K (Figure 2.1b) to highlight this difference in behaviour. The majority of "Earth-like" values of (T_s, RH) pairs fall within 10% of 2.2 $Wm^{-2}K^{-1}$ (indicated by the overlap between the boxed and stippled areas in Figure 2.1a). Thus, in response to Question 2, a λ_{cs} value of 2.2 $Wm^{-2}K^{-1}$ will occur over much of the globe, and in particular will manifest as the constant slope of an OLR_{cs} vs T_s regression, as in Figure 1 of Koll and Cronin (2018). Nonetheless, Figure 2.1 shows that λ_{cs} can still vary considerably at the higher temperatures of Earth's tropics.

Importance of the H_2O window

This section provides additional context about λ_{cs} by focusing on the underlying radiation physics that controls the climate response.

Since λ_{cs} is dominated by surface emission through the H_2O window (Koll and Cronin 2018), the wavenumbers at which H_2O absorption is negligible for surface emission, we expect the window to play an important role in the RH-dependence of λ_{cs} at high temperatures. To display the H_2O window, we plot the surface-to-space transmission $\mathcal{T}_\nu$, which measures the

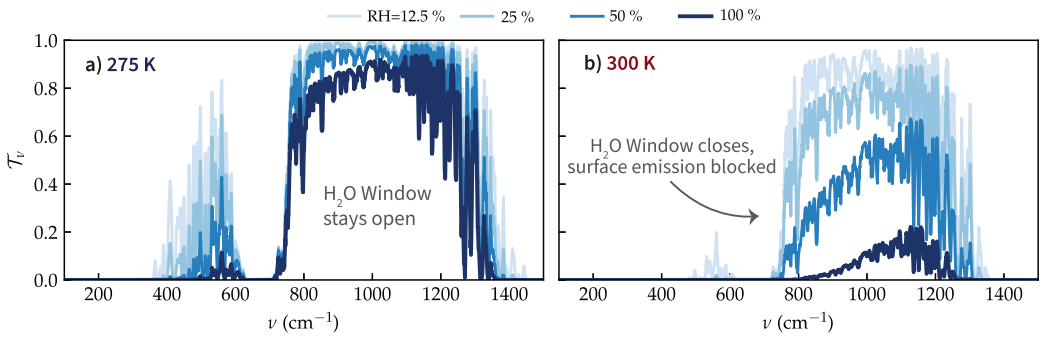

Figure 2.2: **The closing of the H_2O window is sensitive to relative humidity at high surface temperatures.** The surface-to-space transmission $\mathcal{T}_\nu$ is plotted as a function of wavenumber ν for a surface temperature of 275 K (a) and 300 K (b), and a relative humidity of 12.5%, 25%, 50%, and 100%. The H_2O window is where $\mathcal{T}_\nu \approx 1$ and surface emission escapes directly to space. We use a Savitzky–Golay filter with a 5 cm^{-1} width to smooth these plots.

portion of surface emission at wavenumber ν that escapes to space. At a surface temperature of 275 K (Figure 2.2a), the H_2O window remains open as the relative humidity is increased from 12.5% to 100%. At a surface temperature of 300 K (Figure 2.2b), however, the H_2O window closes rapidly as the relative humidity is increased from 12.5% to 100%. This is due to activation of H_2O continuum absorption (Koll and Cronin 2018). Thus relative humidity variations are sufficient to close the H_2O window, but only at high temperatures.

Koll and Cronin (2018) emphasized the robustness of $\lambda_{cs} \approx 2.2$ Wm^{-2}K^{-1} as arising from a balance between the closing of the H_2O window and the nonlinear $4\sigma T_s^3$ surface Planck feedback. However, at high temperatures this balance is not as robust, as evidenced by the decreasing width of the stippled area of the λ_{cs} phase space, which denotes $\lambda_{cs} = 2.2 \pm 10\%$ Wm^{-2}K^{-1}, with increasing temperature (Figure 2.1a). The balance is not as robust because the H_2O window closes much faster with temperature at 100% RH than at 20% RH (Figure 2.2b), leading to a "Planck-dominated" response at low RH, and a "window-dominated" response at high RH (Figure 2.1c).

Tropical variations in λ_{cs}

In Question 1 we asked whether the furnaces and radiator fins described in Pierrehumbert (1995) manifest as a contrast in the zonal-mean λ_{cs} as opposed to the zonal-mean OLR$_{cs}$. To answer this question we will first compute time- and zonal-mean T_s and RH from ERA5 reanalysis (Hersbach et al. 2020) and use these values to read off zonal-mean λ_{cs} from the phase space of Figure 2.1. We take hourly data sub-sampled every 6 hours from January 1 — December 31, 1981 and compute annual averages. Following Zhang et al. (2020), we calculate a free-tropospheric column RH as the water vapor mass between 850 hPa and 300 hPa, divided by the saturated water vapor mass within the column. We exclude the boundary layer RH and stratospheric water vapor because of their limited impact on the

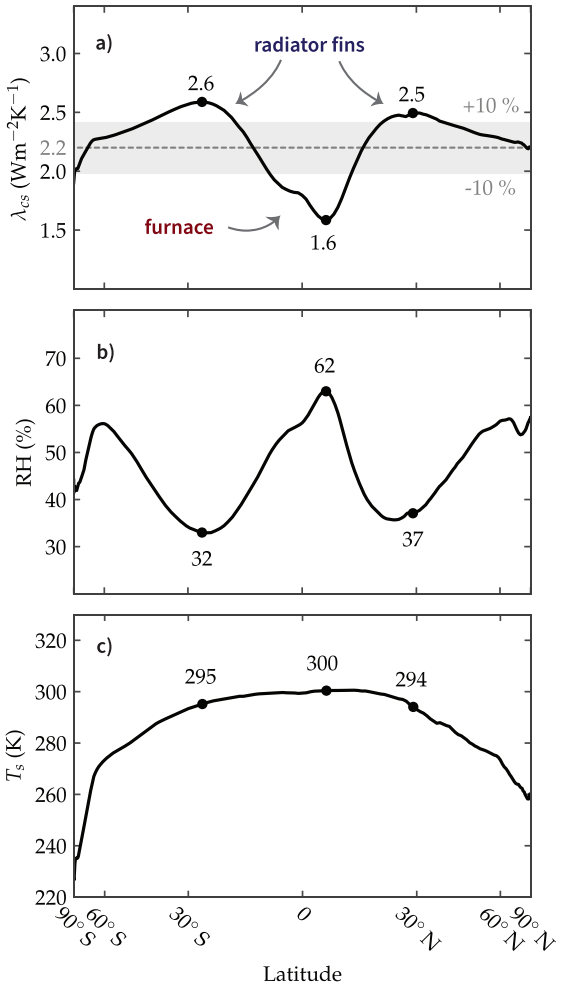

Figure 2.3: **Furnaces and radiator fins manifest as meridional variations in longwave clear-sky feedback** λ_{cs}. (a) Zonal-mean λ_{cs} is diagnosed from Figure 2.1, using the reanalysis zonal-mean RH (b) and the reanalysis zonal-mean T_s (c) as inputs (see text for details). The shaded region in (a) represents the global mean value of $2.2 \pm 10\%$ Wm^{-2}K^{-1} reported in other studies. We posit that the local maxima and minimum of λ_{cs} that lie outside this range should be considered the "radiator fins" and "furnace", respectively, of the tropics. Note the equal-area scaling of the x-axis.

OLR (Zhang et al. 2020).

We might expect a significant drop in λ_{cs} from the subtropics to the deep tropics by looking at representative values of T_s and RH in the λ_{cs}-phase space (Figure 2.1). Indeed, the meridional structure of zonal-mean λ_{cs} calculated as described above, shows λ_{cs} varying varies from 2.6 to 1.6 $\mathrm{Wm^{-2}K^{-1}}$ in the tropics, a 38% drop (Figure 2.3a). Both the subtropical maxima and deep tropical minimum lie outside the 2.2 $\pm$ 10% $\mathrm{Wm^{-2}K^{-1}}$ range. We posit that these extrema of λ_{cs} should be considered the true "radiator fins" and "furnace", respectively, of the tropics.

We can test whether the significant drop in λ_{cs} between the radiator fins and the furnace is due to the difference in humidity, as emphasized by Pierrehumbert (1995), or if the drop is due to the difference in temperature. If we look again at the phase space in Figure 2.1, we can take a path that goes from the subtropics to the deep tropics in two parts (the order does not matter): a first part with constant surface temperature, and a second part with constant relative humidity (see the dashed gray arrows). In this region of phase space, the doubling of relative humidity from 30% to 60% causes a much larger change in λ_{cs} than the increase in surface temperature from 295 K to 300 K does.

Our answer to the first part of Question 1 is then: zonal-mean λ_{cs} exhibits local extrema, which may be usefully viewed as the "furnace" and "radiator fins" of the tropics. Furthermore, these extrema are indeed due to RH variations, consistent with Pierrehumbert (1995). λ_{cs} exhibits a local maxima in the subtropics because they are hot and dry enough for the feedback to exhibit a Planck-dominated response, and λ_{cs} exhibits a local minimum in the deep tropics because they are hot and moist enough for the feedback to exhibit a window-dominated response (Figure 2.1c).

To answer the second part of Question 1, that is, why radiator fins should not be regarded as a contrast in the zonal-mean OLR_{cs}, we plot the annual- and zonal-mean OLR_{cs} and OLR_{as} from ERA5 reanalysis in gray in Figure 2.4c,d. Note the muted latitudinal variations of OLR_{cs} within the tropics ($\sim$ 10 $\mathrm{Wm^{-2}}$) compared to variations in OLR_{cs} throughout the rest of the globe ($\sim$ 100 $\mathrm{Wm^{-2}}$). This muted latitudinal dependence within the tropics is inconsistent with the notion of radiator fins as significant subtropical maxima in OLR_{cs}, which is why we focus on λ_{cs} instead. OLR_{as} does have more significant subtropical extrema, but these should not be interpreted as a furnace and radiator fins because the longwave warming effect of deep tropical clouds is approximately balanced by their shortwave cooling effect (Hartmann and Berry 2017; Pierrehumbert 1995).

Incorporating the effects of cloudiness

In Question 3, we asked whether clouds affect the meridional structure in zonal-mean longwave feedback in the tropics. Rather than explicitly compute cloud feedbacks, which is beyond the scope of this paper, we try to estimate them by constructing a simple model for how clouds modify longwave emission. To validate the approach, we first estimate the all-sky OLR, OLR_{as}, from a few inputs: OLR_{cs}, the cloud-top fraction f, and the cloud-top temperature T_{ct}. OLR_{cs} is taken directly from ERA5 reanalysis. f is diagnosed from ERA5

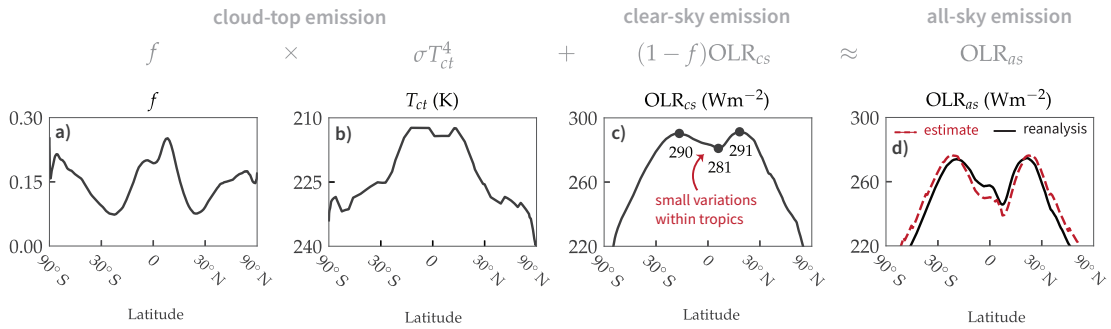

Figure 2.4: **A simple model for zonal-mean all-sky emission.** (a) cloud-top fraction f, (b) cloud-top temperature T_{ct}, (c) clear-sky emission OLR_{cs}, and (d) all-sky emission OLR_{as}. The black curves are from ERA5 reanalyis. The dashed-red curve in (d) is our simple estimate produced by the equation above the panels (see Equation 2.3). Note the equal-area scaling of the x-axis.

reanalysis as the local max of the zonal-mean cloud fraction profile above a 550 hPa threshold, which is used to avoid misidentifying cloud tops with boundary layer cloudiness. T_{ct} is the atmospheric temperature at which cloud fraction profile peaks. We smooth T_{ct} with a Savitzky-Golay filter with a 10° latitude width to account for sharp jumps in T_{ct} arising from the limited vertical resolution. This method of identifying cloud tops is similar to Thompson et al. (2017). We show our methodology in the SI.

To estimate OLR_{as}, we first consider the effect of high clouds, which block longwave emission from lower levels and replace it with their own longwave emission from cloud tops. We assume high cloud emission acts like a black body and occurs high enough in the atmosphere that emission travels directly to space (Siebesma et al. 2020). As for low clouds, we grossly assume the low clouds emit at a temperature close enough to T_s that they only negligibly alter the outgoing radiation (Hartmann 2015). Given these assumptions, we can now write down a simple expression for OLR_{as}:

$$\mathrm{OLR}_{as} \approx \sigma T_{ct}^4 f + \mathrm{OLR}_{cs}(1-f). \tag{2.3}$$

This model is similar in some ways to the conceptual model created in Soden et al. (2008) to examine cross-field correlations between clear-sky and cloud feedbacks.

To get a sense of what the inputs to Equation 2.3 look like, we plot annual- and zonal-mean f, T_{ct}, OLR_{cs}, and OLR_{as} from ERA5 reanalysis in gray in Figure 2.4. We test the approximate all-sky radiation from Equation 2.3 against OLR_{as} directly output from ERA5 analysis, which includes cloud opacities and comprehensive radiative transfer in its calculation. We find that our model does an acceptable job in replicating the reanalysis (Figure 2.4d), although there is a slight underestimate within the tropics and a slight overestimate outside the tropics. Overall, the relative accuracy and physical transparency of our estimate gives us enough confidence in this model to proceed.

We now use Equation 2.3 to compute the longwave all-sky feedback, λ_{as}. We aim to assess the order of magnitude impact of clouds on our findings, so we first assume high cloud temperatures do not change appreciably with warming, consistent with the fixed anvil temperature (FAT) hypothesis (Hartmann and Larson 2002b; Zelinka and Hartmann 2010) and how the convective top in the column model is imposed to a fixed temperature. We assume a FAT as opposed to a proportionally higher anvil temperature (PHAT) to explore a well-defined limit of the high cloud altitude feedback. Although f can change with warming (Bony et al. 2016; Saint-Lu et al. 2020), the high cloud area feedback is quite uncertain (Sherwood et al. 2020; Wing et al. 2020), so for simplicity we assume f is constant with warming (though we relax this assumption in the next chapter). Differentiating Equation 2.3 with respect to T_s yields:

$$\lambda_{as} = \lambda_{cs}(1 - f). \tag{2.4}$$

This equation makes it conceptually clear how clouds modify λ_{cs}: the longwave feedback over clouds is 0. Since f is positive definite (Figure 2.4), $\lambda_{as} \leq \lambda_{cs}$, which is well demonstrated in the in the zonal mean in Figure 2.5a. The all-sky feedback looks like a simple translation downward of the clear-sky feedback, and there is still a significant ($\sim$50%) variation in λ_{as} from the subtropics to the deep tropics. Our answer to Question 3 is then: Clouds have a destabilizing influence on the longwave feedback. However, the structure of all-sky feedback looks similar to clear-sky feedback, implying that the RH-dependence from clear-sky effects still dominates the meridional structure.

2.4 Discussion

Our work can be summarized as follows:

1. At high temperatures, variations in RH are sufficient to close the H_2O window, driving deviations in λ_{cs} from the typical value of 2.2 $\mathrm{Wm^{-2}K^{-1}}$ (Figure 2.1).

2. Furnaces and radiator fins can be interpreted as tropical extrema in zonal-mean λ_{cs} as a consequence of the RH-dependence (Figure 2.3). They should not be interpreted as significant tropical extrema in zonal-mean OLR_{cs} because tropical variations in OLR_{cs} are small compared to global variations in OLR_{cs} (Figure 2.4c).

3. Cloud radiative effects can be estimated with a simple equation to reconstruct the all-sky OLR (Figure 2.4), which we then use to estimate the all-sky feedback. Clouds lower the feedback relative to clear skies, but the RH-dependence of the feedback remains significant (Figure 2.5).

Comparison to other work

We have demonstrated a reason for why a large contrast in λ_{cs} emerges in the tropics, but our results for the zonal-mean feedback cannot be directly compared to most other studies

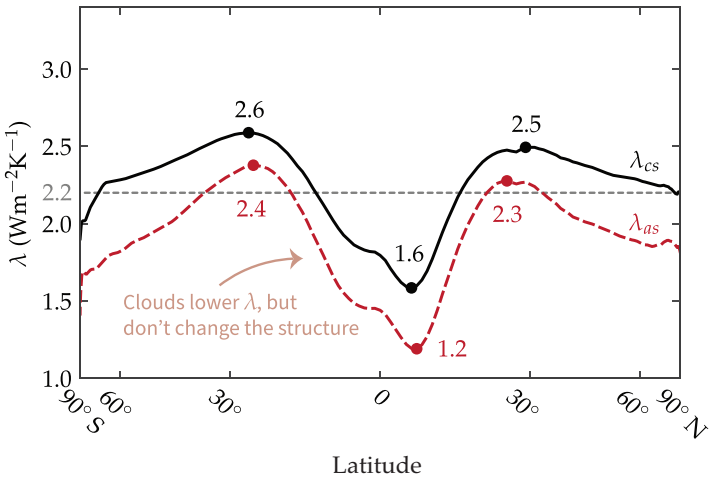

Figure 2.5: **Incorporating clouds into the longwave feedback.** Zonal-mean all-sky feedback (λ_{as}, dashed-red) is diagnosed from zonal-mean clear-sky feedback (λ_{cs}, solid-black) and zonal-mean cloud-top fraction f. See Equation 2.4 for details. Note the equal-area scaling of the x-axis.

of regional feedback (e.g. Armour et al. (2013), Feldl and Roe (2013a), and Feldl and Roe (2013b)). Our clear-sky feedback λ_{cs} is not equal to the sum of the Planck, lapse rate, and water vapor feedbacks, because these feedbacks include "cloud climatological effects" (Yoshimori et al. 2020), i.e. these feedbacks are calculated in the presence of clouds from the control simulation, which will affect the magnitude of the Planck Feedback, for instance, because clouds will still block a portion of the additional emission from imposed uniform warming, and this blocking will be different whether the clouds are held at fixed pressure or fixed temperature. Furthermore, our all-sky feedback λ_{as} is also not equal to this sum of conventional feedbacks, because those feedbacks fix the cloud pressure, whereas we fix the cloud temperature. These issues were discussed in detail by Yoshimori et al. (2020), and our λ_{as} should be comparable to their T-FRAT feedback in which the RH and cloud temperatures are fixed. Further work could explicitly explore such comparisons.

Our results can still be fruitfully compared to Zhang et al. (2020), who also analyzed the zonal-mean λ_{cs} in GCMs, but without the assumptions that column RH is fixed with warming and that the atmosphere follows a moist adiabat. We both find a drop in λ_{cs} of $\sim$1 $\mathrm{Wm^{-2}K^{-1}}$ from the subtropics to the deep tropics. However, Zhang et al. (2020) suggested that the drop in zonal mean λ_{cs} results from the RH-feedback due to local column RH increases with surface warming. Column RH is fixed in our study and yet we still get a significant tropical dip, although our λ_{cs} is offset by a constant $\sim$0.5 $\mathrm{Wm^{-2}K^{-1}}$ from their results. This comparison suggests that climatological RH causes the tropical variations in λ_{cs}, whereas the RH-feedback and deviations from a moist adiabat uniformly lowers λ_{cs}. The importance of climatological RH is further supported by Bourdin et al. (2021), who also finds that climatological RH influences climate sensitivity, even if the vertical distribution

of RH remains unchanged with warming.

Analyzing feedbacks locally or globally can give opposing impressions to the radiative response to warming. Local surface warming in the deep tropics yields a small, local OLR increase (as measured by λ_{cs} and λ_{as}) but a large, global OLR increase (Dong et al. 2019). The discrepancy between the weak, local and the strong, global radiative response from warming the deep tropics arises from atmospheric temperature changes not associated with a local T_s change, that is, the remote warming of the free troposphere (Ceppi and Gregory 2017; Mauritsen 2016). A local feedback analysis, by construction, cannot capture the effects of remote warming, which should be noted when comparing results across studies. The relative contributions of local surface warming versus non-local free-tropospheric warming to OLR change is relatively unexplored, so further study might alter our characterization of the tropical radiative response if one contribution can be shown to dominate over the other.

Our new understanding of the state dependence of λ_{cs} gives context to previous results. For example, Meraner et al. (2013) and Bloch-Johnson et al. (2021) attributed an increase in equilibrium climate sensitivity to the decrease in λ_{cs} with warming. We expect these variations in λ_{cs} to be enhanced in climates hotter than present-day Earth and conversely to be suppressed in climates cooler than present-day Earth. Our particular calculation of the λ_{cs} phase space assumed that the CO_2 concentration is fixed at 340 ppmv, which neglects the increasingly important role of CO_2 in stabilizing the climate at high CO_2 concentrations (Seeley and Jeevanjee 2020). However, the strength in our approach of studying the joint dependence of λ_{cs} on T_s and RH is its generality, for our approach can not only be applied to our present-day climate, but to past climates like the Eocene, Pliocene, and Last Glacial Maximum, and to future climates predicted from different climate change scenarios.

2.5 Acknowledgements

ERA5 data is available from https://doi.org/10.24381/cds.bd0915c6. Data from the PyRADS calculations are available from . This work was funded by CEMPS at the University of Exeter. We thank two anonymous reviewers for their constructive comments. We also thank Penelope Maher, Stephen Thomson, Hugo Lambert, and Mitchell Koerner for their helpful conversations on this project.

2.6 Supporting Information

Cloud top identification

We identify zonal-mean cloud-top properties using zonal-mean profiles of cloud-fraction and atmospheric temperature that are obtained from ERA5 reanalysis. We take hourly data subsampled every 6 hours from January 1 - December 31, 1981 and compute annual averages. Then, the cloud-top fraction f is the cloud fraction at which the cloud fraction profile is maximum. We use a 550 hPa cutoff to avoid misidentifying cloud-tops with low-level cloudiness. The cloud-top temperature T_{ct}, is the atmospheric temperature at which the cloud fraction

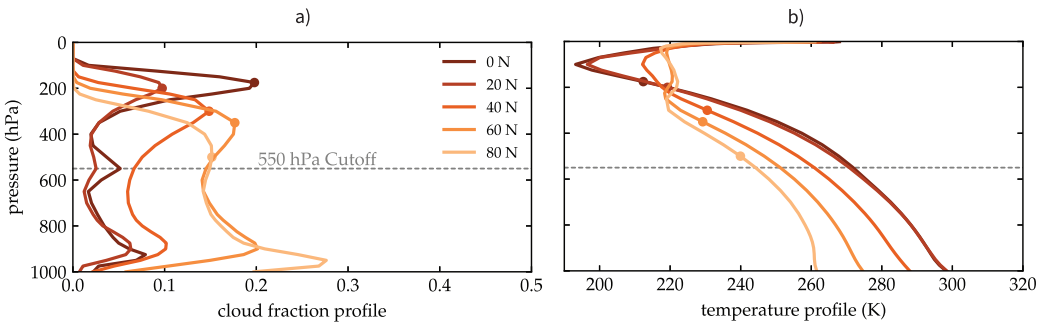

Figure 2.6: **Identifying zonal-mean cloud-top properties.** a) We identify the zonal-mean cloud-top fraction f by selecting the maximum of the zonal-mean cloud fraction profile above a 550 hPa cutoff. b) We identify the zonal-mean cloud-top temperature T_{ct} as the atmospheric temperature at which cloud fraction peaks. Data is shown for a select number of latitude bands.

profile is maximum. We smooth T_{ct} with a Savitzky-Golay filter of 10° width to account for sharp jumps in T_{ct} arising from the limited vertical resolution. This method of identifying cloud-top properties is similar to the one used in Thompson et al. (2017). We use ERA5 hourly data from 1981, which can be obtained from https://doi.org/10.24381/cds.bd0915c6.

Chapter 3

Anvil cloud feedbacks

This chapter is published as McKim, B. A., Bony, S., & Dufresne, J.L. (2024). *Weak anvil cloud area feedback suggested by physical and observational constraints.* Nature Geoscience, https://doi.org/10.1038/s41561-024-01414-4.

Note to Examiners
Most of the work in this chapter was completed during an interruption of my PhD, while receiving a Fulbright Scholarship at Laboratoire de Météorologie Dynamique under the supervision of Sandrine Bony and Jean-Louis Dufresne. I have been advised by the Postgraduate Research Administration that I am welcome to include this work because the interruptions system can be used to undertake a placement which involves research relevant to the rest of the thesis.

3.1 Abstract

Changes in anvil clouds with warming remain a leading source of uncertainty in estimating the Earth's climate sensitivity. Here, we develop a feedback analysis that decomposes changes in anvil clouds and creates testable hypotheses for refining their proposed uncertainty ranges with observations and theory. To carry out this storyline approach, we derive a simple but quantitative expression for the anvil area feedback, which is shown to depend on the present day, measurable cloud radiative effects and the fractional change in anvil area with warming. Satellite observations suggest an anvil cloud radiative effect of about ± 1 Wm^{-2}, which requires the fractional change in anvil area to be about $\pm 50\%$ K^{-1} to produce a feedback equal to the current best estimate of the anvil area feedback strength's lower bound. We use quantitative theory and observations to show that the change in anvil area is closer to about -4% K^{-1}. This constrains the area feedback and leads to our revised estimate of 0.02 ± 0.07 $\mathrm{Wm}^{-2}\mathrm{K}^{-1}$ for the area feedback, which is many times weaker and more constrained than the overall anvil cloud feedback. In comparison, we show the anvil cloud albedo feedback to be much less constrained, both theoretically and observationally, which poses an obstacle for bounding the Earth's climate sensitivity.

3.2 Introduction

Global warming depends on Earth's sensitivity to increased CO_2, but this sensitivity is tied to how clouds "feedback" on global warming (Ceppi and Nowack 2021). While recent progress has been made in constraining low cloud feedbacks (Myers et al. 2021; Vogel et al. 2022), anvil cloud feedbacks are still leading sources of uncertainty in quantifying climate sensitivity (Forster et al. 2021; Sherwood et al. 2020) despite decades of study (Hartmann 2016; Hartmann and Michelsen 2002; Lindzen et al. 2001; Mauritsen and Stevens 2015; Pierrehumbert 1995; Ramanathan and Collins 1991; Yoshimori et al. 2020). The question thus remains: How do anvil clouds respond to and affect warming?

Changes in anvils were once thought to produce a strong negative climate feedback by acting as a solar *thermostat* (Ramanathan and Collins 1991), but the observations that led to this conclusion are no longer considered evidence of such an effect (Pierrehumbert 1995). Then anvils were thought to act as an infrared *iris* (Lindzen et al. 2001). Criticisms of this study's methodology followed (Fu et al. 2002; Hartmann and Michelsen 2002; Lin et al. 2002), but recent comprehensive assessments still cannot rule out a modest anvil cloud feedback (Forster et al. 2021; Sherwood et al. 2020).

These assessments refer to an *anvil cloud area* (or *amount*) *feedback*, but it should be more precisely referred to as the *altitude-corrected anvil cloud feedback* (hereafter the *anvil cloud feedback*) since it results from changes in area and optical depth, but not changes in altitude which are considered in a separate feedback (Zelinka et al. 2022). Such decompositions are arbitrary because climate is unchanged by how it is analyzed, but the choice is important because it can simplify interpretations of uncertainty (Held and Shell 2012). Further decomposition may help constrain the anvil cloud feedback by answering which individual feedback—area or optical depth—truly embodies the uncertainty that obscures estimates of

climate sensitivity.

Anvil cloud area is controlled in part by unconstrained microphysics (Beydoun et al. 2021; Gasparini et al. 2019; Jeevanjee 2022), but also by robust thermodynamic principles (Bony et al. 2016; Zelinka and Hartmann 2010) which predict a decrease in anvil area with warming as atmospheric static stability increases (Bony et al. 2016). This is consistent with observed variability (Ito and Masunaga 2022; Saint-Lu et al. 2020, 2022) and most simulations (Stauffer and Wing 2022). The resulting area feedback *might* be small because anvils are radiatively neutral (Ceppi et al. 2017; Hartmann 2016; Pierrehumbert 1995). But how neutral must anvil clouds be for the area feedback to be insignificant? What if their radiative effect changes with warming? Or if more of the Earth is then exposed to the radiative effects of underlying low clouds? These questions limit our ability to constrain the anvil cloud area feebdack.

Less is known about how cloud optical depth changes with warming (Lutsko et al. 2023), but it will manifest in optical properties such as anvil cloud albedo. Changes in albedo might produce an even stronger feedback than changes in area because anvils have a much stronger effect in the shortwave than in the net (Hartmann 2016). But how much does cloud albedo change with warming? And by how much must it change to produce a substantial feedback? These questions call for more quantitative answers before we can conclude which feedback is more uncertain.

We need a physically-motivated decomposition that addresses confounding factors such as cloud overlap and distinguishes feedbacks from changes in anvil area and albedo. Since models must contend with representing unconstrained microphysics (Beydoun et al. 2021; Gasparini et al. 2019; Jeevanjee 2022), we primarily use observations. This rules out using purely model-based cloud feedback decompositions (Li et al. 2019; Zelinka et al. 2012). Cloud controlling factor analysis, an observational-based method mostly used for constraining low cloud feedbacks (Klein et al. 2017), requires further study before being suitable for confidently constraining anvil cloud feedbacks. The connection between anvil clouds and their cloud controlling factors are not as well understood as for low clouds.

Here, we derive an analytical cloud feedback decomposition based on the essential physics of cloud radiative effects. When it is combined with cloud observations, we can identify, understand, and constrain cloud feedbacks transparently. We adopt a *storyline approach* (Stevens et al. 2016) where we examine the driving factors that control a cloud feedback and judge the plausibility of these factors to produce a particular feedback value by comparing to observations and theory derived from process understanding. This approach shows which feedback is constrained and which obscures estimates of climate sensitivity.

3.3 Methods

For readers who want to quickly proceed to the main results of this chapter, they may skip this section and refer to it as necessary. Otherwise, we now proceed into the conceptual derivations that form the basis of this chapter, as well as the methodology.

Conceptualizing cloud radiative effects

We start with an idealized model of cloud radiative effects at the top of the atmosphere (TOA). Although tropical cloudiness is expected to be trimodal (Johnson et al. 1999), for simplicity we will consider a domain containing two cloud types: high clouds (h) and low clouds (ℓ). (Many assessments of cloud feedbacks also use this bi-modal decomposition (Sherwood et al. 2020).) Each type has an emission temperature T_h, T_ℓ; an optically thick cloud fraction f_h, f_ℓ; and an albedo α_h, α_ℓ (Figure 3.1). Mid-level clouds will be considered in our error analysis.

The TOA energy balance is $N = S - R$, where S is the absorbed shortwave radiation and R is the outgoing longwave radiation. The cloud radiative effect C is the difference in N between all-sky and clear-sky (cs) conditions, $C = N - N_{\text{cs}}$ (Coakley and Baldwin 1984). C can be decomposed into longwave and shortwave components: $C = C^{\text{sw}} + C^{\text{lw}}$.

In the longwave component, clear-sky regions with a surface temperature T_s will emit to space with an outgoing longwave radiation of $R_{\text{cs}}^{T_s}$, but a portion will be blocked by clouds. Longwave emissivity will not be considered because most clouds have an emissivity close to one (Fu and Liou 1993). Assuming random overlap between high clouds and low clouds (Oreopoulos et al. 2022), the domain-averaged clear-sky contribution is $R_{\text{cs}}^{T_s}(1-f_h)(1-f_\ell)$. Low clouds are so close to the surface that we treat their emission to space like clear-sky surface emission but at T_ℓ. Their domain-averaged contribution is $R_{\text{cs}}^{T_\ell} f_\ell (1-f_h)$. Since $R_{\text{cs}}^{T_s}$ is an approximately linear function of temperature (Koll and Cronin 2018), $R_{\text{cs}}^{T_\ell} \approx R_{\text{cs}}^{T_s} + \lambda_{\text{cs}}(T_s - T_\ell)$, where $\lambda_{\text{cs}} \equiv -dR_{\text{cs}}/dT_s \approx -2$ Wm^{-2}K^{-1} is a representative value for the longwave clear sky feedback (McKim et al. 2021). We assume that high clouds are so high that they emit directly to space (Siebesma et al. 2020) with a value $\sigma T_h^4 f_h$. Summing these contributions, the domain-averaged outgoing longwave radiation is

$$R = R_{\text{cs}}^{T_s}(1-f_h) + \sigma T_h^4 f_h + \lambda_{\text{cs}}(T_s - T_\ell)(1-f_h)f_\ell, \tag{3.1}$$

and the longwave cloud radiative effect $-(R - R_{\text{cs}})$ is

$$C^{\text{lw}} = R_{\text{cs}}^{T_s} f_h - \sigma T_h^4 f_h - \lambda_{\text{cs}}(T_s - T_\ell)(1-f_h)f_\ell. \tag{3.2}$$

In the shortwave component, there is an incoming solar radiation $S^{\downarrow}$, and we assume that there is no absorption except at the surface. High clouds reflect a portion $\alpha_h f_h$ back to space. The transmitted radiation then hits low clouds which reflect a portion $\alpha_\ell f_\ell$ back to space (ignoring secondary reflections with the anvils above). The transmitted radiation then hits the surface which reflects a portion α_s back out to space and absorbs the rest. Summing these contributions, the domain-averaged absorbed shortwave radiation at TOA is

$$S = S^{\downarrow}(1-\alpha_h f_h)(1-\alpha_\ell f_\ell)(1-\alpha_s). \tag{3.3}$$

The TOA absorbed shortwave in clear-skies is $S_{\text{cs}} = S^{\downarrow}(1-\alpha_s)$, so the shortwave cloud radiative effect $(S - S_{\text{cs}})$ is:

$$C^{\text{sw}} = S_{\text{cs}}\big(- \alpha_h f_h - \alpha_\ell f_\ell + \alpha_h \alpha_\ell f_h f_\ell \big). \tag{3.4}$$

It will prove helpful to separate the contribution of isolated high clouds and isolated low clouds to the net cloud radiative C. Setting $f_\ell = 0$ yields the isolated high cloud radiative effect:

$$C_h = \big(- S_{\text{cs}} \alpha_h + R_{\text{cs}}^{T_s} - \sigma T_h^4 \big) f_h. \tag{3.5}$$

Setting $f_h = 0$ yields the isolated low cloud radiative effect:

$$C_\ell = \big(- S_{\text{cs}} \alpha_\ell - \lambda_{\text{cs}} (T_s - T_\ell) \big) f_\ell. \tag{3.6}$$

The total cloud radiative effect C in terms of each cloud is:

$$C = C_h + C_\ell + m_{\ell h}, \tag{3.7}$$

where

$$m_{\ell h} = \big(S_{\text{cs}} \alpha_\ell \alpha_h + \lambda_{\text{cs}} (T_s - T_\ell) \big) f_\ell f_h, \tag{3.8}$$

represents the cloud overlap masking effect. Note that $C_h \propto f_h$, $C_\ell \propto f_\ell$, and $m_{\ell h} \propto f_\ell f_h$.

Feedback decomposition

We will now derive various cloud feedbacks from these equations and assume a fixed relative humidity. The lapse rate feedback has been shown to be small when using this reference response (Held and Shell 2012; Zelinka et al. 2020), so it will be ignored here.

$$
\begin{aligned}
\lambda &\equiv \frac{dN}{dT_s} \\
&= \frac{S_{\rm cs}}{dT_s} - \frac{dR_{\rm cs}^{T_s}}{dT_s} + \frac{dC}{dT_s} \\
&= \lambda_{\rm cs}(1-f_h) \\
&\quad + (R_{\rm cs}^{T_s} - \sigma T_h^4 + \lambda_{\rm cs}(T_s - T_\ell) f_\ell - S_{\rm cs}\alpha_h + S_{\rm cs}\alpha_h\alpha_\ell f_\ell)\frac{df_h}{dT_s} \\
&\quad + (-\lambda_{\rm cs}(T_s - T_\ell)(1-f_h) - S_{\rm cs}\alpha_\ell + S_{\rm cs}\alpha_h f_h \alpha_\ell)\frac{df_\ell}{dT_s} \\
&\quad + -4\sigma T_h^3 f_h \frac{dT_h}{dT_s} \\
&\quad + -\lambda_{\rm cs}(1-f_h) f_\ell \frac{d(T_s - T_\ell)}{dT_s} \\
&\quad + (-S_{\rm cs} f_h + S_{\rm cs} f_h \alpha_\ell f_\ell)\frac{d\alpha_h}{dT_s} \\
&\quad + (-S_{\rm cs} f_\ell + S_{\rm cs}\alpha_h f_h f_\ell)\frac{d\alpha_\ell}{dT_s} \\
&\quad - S^{\downarrow}(1-\alpha_h f_h)(1-\alpha_\ell f_\ell)\frac{d\alpha_s}{dT_s} \\
&\quad - (T_s - T_\ell)(1-f_h) f_\ell \frac{d\lambda_{\rm cs}}{dT_s}.
\end{aligned}
\tag{3.9}
$$

Recognizing that many of these terms can be rewritten as cloud radiative effects, we get:

$$
\begin{aligned}
\lambda &= \lambda_{\rm cs}(1-f_h) \\
&\quad + \Big(C_h + m_{\ell h}\Big)\frac{d\ln f_h}{dT_s} \\
&\quad + \Big(C_\ell + m_{\ell h}\Big)\frac{d\ln f_\ell}{dT_s} \\
&\quad - 4\sigma T_h^3 f_h \frac{dT_h}{dT_s} \\
&\quad - \lambda_{\rm cs}(1-f_h) f_\ell \frac{d(T_s - T_\ell)}{dT_s} \\
&\quad + \Big(C_h^{\rm sw} + m_{\ell h}^{\rm sw}\Big)\frac{d\ln \alpha_h}{dT_s} \\
&\quad + \Big(C_\ell^{\rm sw} + m_{\ell h}^{\rm sw}\Big)\frac{d\ln \alpha_\ell}{dT_s} \\
&\quad + C_s \frac{d\ln \alpha_s}{dT_s},
\end{aligned}
\tag{3.10}
$$

where we have assumed that $d\lambda_{\rm cs}/dT_s$ is negligible, and $C_s = -S^{\downarrow}(1-\alpha_h f_h)(1-\alpha_\ell)\alpha_s$ is the surface albedo radiative effect, which is equivalent to the "cryosphere radiative forcing" (Flanner et al. 2011).

Now we name and then describe each term:

$$\lambda = \lambda_0 + \lambda_h^{\rm area} + \lambda_\ell^{\rm area} + \lambda_h^{\rm temp} + \lambda_\ell^{\rm temp} + \lambda_h^{\rm albedo} + \lambda_\ell^{\rm albedo} + \lambda_s^{\rm albedo} \tag{3.11}$$

λ_0 is the anvil cloud-masked longwave clear-sky feedback. It is our null hypothesis for the climate response to warming because it assumes fixed relative humidity; fixed anvil temperature, area, and albedo; fixed low cloud temperature difference, area, and albedo; and fixed surface albedo. $\lambda_h^{\rm area}$ and $\lambda_\ell^{\rm area}$ are the feedbacks from a changing anvil cloud and low cloud area, respectively. $\lambda_h^{\rm temp}$ is the feedback from a changing anvil cloud temperature. $\lambda_\ell^{\rm temp}$ is the feedback from a changing temperature difference between low clouds and the surface. $\lambda_h^{\rm albedo}$, $\lambda_\ell^{\rm albedo}$, and $\lambda_s^{\rm albedo}$ are the feedbacks from a changing albedo of anvil clouds, low clouds, and surface, respectively. We omit the surface albedo feedback from Equation 3.16 because we are interested in tropical climate.

For simplicity, we have assumed that cloud emissivities of high clouds and low clouds $(\varepsilon_h, \varepsilon_\ell)$ are equal to one (Fu and Liou 1993). However, if we relax this assumption for completeness, one can show this leads to a high- and low-cloud emissivity feedback with the following form:

$$\begin{aligned} \lambda_h^{\rm emissivity} &= \left(C_h^{\rm lw} + m_{\ell h}^{\rm lw}\right)\frac{d\ln\varepsilon_h}{dT_s}, \\ \lambda_\ell^{\rm emissivity} &= \left(C_\ell^{\rm lw} + m_{\ell h}^{\rm lw}\right)\frac{d\ln\varepsilon_\ell}{dT_s}, \end{aligned} \tag{3.12}$$

which closely resemble the form of the cloud albedo feedback. Some of the other feedbacks will have small modifications, but they are unimportant here.

Climatology

We combine monthly-mean satellite observations, surface temperature measurements, and reanalysis and re-grid all datasets onto a common 2° latitude × 2.5° longitude grid over the tropical belt (30°N−30°S) from June 2006 to December 2016. Although anvil clouds populate the globe (Thompson et al. 2017), it is less clear how extratropical anvils change with warming. Most cloud feedback assessments only consider tropical anvil clouds, so we will follow this convention.

From the CALIPSO lidar satellite dataset (Winker et al. 2010), we obtain vertical profiles of cloud fraction for optical depths between $0.3 \leq \tau \leq 5$. This range excludes both deep convective cores and optically thin cirrus unconnected to deep convection (Saint-Lu et al. 2020). We then vertically smooth the native vertical 60 m resolution profiles with a 480 m running mean. For anvil detection, we consider ice cloud data above 8 km. For shallower clouds, we consider the sum of ice and liquid cloud fraction data below 8 km. The diagnosed cloud fractions are the absolute maximum of the profile in their respective domains, but if

the identified maximum does not exceed a cutoff ($f_{\text{cut}} = 0.03$), then that region is considered to be clear-sky ($f = 0$). This algorithm is applied to every grid point and then tropically-averaged. Our approach thus far resembles Saint-Lu et al. (2020), just extended to include low clouds.

To match the inferred cloud radiative effects with the observed, we consider an effective cloud fraction $f_h = n \cdot \text{Max}(f(z))$ for high clouds, where n is a single tuned parameter to account for collapsing the high cloud profile into one level. This accounting is more important for high clouds, as their profile's full width-half maximum is $\approx$ 5 km (Figure 3.5), whereas low clouds are already localized with a full width-half maximum of $\approx$ 1 km (Figure]reffig: profiles). While n could be more rigorously derived from detailed considerations of cloud overlap (Oreopoulos et al. 2022), we opt to determine n by fitting the predicted tropical- and time-averaged longwave cloud radiative effect C^{lw} to its observed counterpart $C^{\text{lw}}_{\text{obs}}$ from CERES (see **Cloud fraction** subsection of section 3.3). Doing so yields a spatially and temporally constant value of $n = 1.7$. This value lies between that from assuming maximum overlap between each layer of the anvil cloud, which yields $n = 1$ and random overlap, which yields $n \approx 5$.

The height of the diagnosed maximum cloud fraction is then used to diagnose the cloud temperatures T_h, T_ℓ at each space and time by selecting the corresponding atmospheric temperature in ERA5 reanalysis (Hersbach et al. 2020). We use the HadCRUT5 dataset (Morice et al. 2021) to diagnose the surface temperature T_s.

We use monthly mean TOA radiative fluxes, both clear-sky and all-sky, from the CERES satellite EBAF Ed4.1 product (Loeb et al. 2018, 2020). We diagnose the surface albedo α_s as the ratio of upwelling clear-sky shortwave radiation $S^{\uparrow}_{\text{cs}}$ to incoming shortwave radiation $S^{\downarrow}$. However, because shortwave absorption and scattering occurs in the real atmosphere, our surface albedo is more accurately characterized as the planetary clear-sky albedo (Chen and Ohring 1984). We diagnose the cloud albedos by assuming that they are constant in space, and by fitting the predicted tropical- and time-averaged shortwave cloud radiative effect C^{sw} to its observed counterpart $C^{\text{sw}}_{\text{obs}}$ from CERES. With two unknowns (α_h and α_ℓ), we must provide two constraints. We do this by splitting the tropics into two distinct dynamical regimes based on threshold of 500 hPa midtropospheric velocity $\omega_{500} = 25$ hPa day^{-1} obtained from monthly ERA5 reanalysis data. These regions are treated as independent so that they provide two constraints. The regime-averaged shortwave radiative effect is then fitted to its observed counterpart by using the `fsolve` function from the `scipy.optimize` python module. (The precise threshold of 25 hPa day^{-1} was chosen because it resulted in the smallest root mean square error between C^{sw} and $C^{\text{sw}}_{\text{obs}}$.)

Cloud fraction

We use the CALIPSO Lidar Satellite CAL_LID_L3_Cloud_Occurence-Standard-V1-00 data product (NASA/LARC/SD/ASDC 2018), the same dataset used in Saint-Lu et al. (2020). While the high cloud fraction could simply be diagnosed as the maximum cloud fraction of the profile (i.e. $f_h = \text{Max}(f(z))$), the calculated longwave cloud radiative effect C^{lw} will not match with observations. To rectify this, we will consider using a single tuning parameter,

n. That is, we have an effective cloud fraction $f_h = n \cdot \text{Max}(f(z))$ which accounts for representing a cloud profile with a single level.

We first demand that n be constant with space and time to ensure that areal changes (changes in f_h) are not artificially convolved with vertical changes which relate to optical depth and albedo (α). This decision projects the spatio-temporal variability in the vertical extent of anvils more onto α than f_h.

We then fit the predicted tropically- and temporally-averaged longwave radiative effect C^{lw} to its observed counterpart $C^{\text{lw}}_{\text{obs}}$ from CERES. Given these constraints, and the inputs to Equation 3.2, n can be solved for as

$$n = \frac{\langle C^{\text{lw}}_{\text{obs}} + \lambda_{\text{cs}}(T_s - T_\ell) f_\ell \rangle}{\langle R_{\text{cs}} \text{max}(f(z)) - \sigma T_h^4 \text{max}(f(z)) + \lambda_{\text{cs}}(T_s - T_\ell) f_\ell \text{max}(f(z)) \rangle}, \tag{3.13}$$

where $\langle \cdot \rangle$ denotes a tropical- and temporal-average.

When plotting the scatter of $\ln f_h$ against T_s in Figure 3.4, grid cells with $f_h = 0$ are excluded to avoid logarithmic divergences.

Uncertainty analysis for area feedback

Uncertainty in our estimates of $d \ln f_h / dT_s$ and $C_h + m_{\ell h}$ translate to uncertainty in λ_h^{area}. As stated in the main text, we estimate $d \ln f_h / dT_s = -4 \pm 2$ % K^{-1}. For the anvil cloud radiative effect, we found $C_h + m_{\ell h} = -1.5$ Wm^{-2}. However, other observational studies have found it to be -4 Wm^{-2} (Hartmann and Berry 2017), 0.6 Wm^{-2} (Gasparini et al. 2019), and 2 Wm^{-2} (L'Ecuyer et al. 2019). These differences are probably due to methodological differences and the fact that anvil clouds have no precise definition. Furthermore, CERES TOA monthly fluxes have a stated uncertainty of 2.5 Wm^{-2} (Loeb et al. 2018).

Another source of error comes from neglecting mid-level clouds, a fairly common cloud type (Johnson et al. 1999), as their own identities. Let's assume that emission from mid level congestus clouds (c) experience a clear-sky greenhouse effect. By symmetry with low clouds, they should contribute an additional cloud overlap masking term that appears in our expression for λ_{area}: $m_{ch} = (S_{\text{cs}} \alpha_c \alpha_h + \lambda_{\text{cs}}(T_s - T_c)) f_c f_h$. Assuming that $f_c = 0.1$, $f_h = 0.17$, $\alpha_c = \alpha_h = 0.45$, $T_c = 250$ K, $T_s = 298$ K, $S_{\text{cs}} = 347$ Wm^{-2}, $\lambda_{\text{cs}} = -2$ Wm^{-1}K^{-1} yields $m_{ch} \approx -0.5$ Wm^{-2}.

We therefore estimate $C_h + m_{\ell h} = -1 \pm 3$ Wm^{-2}. This results in our best estimate of the anvil cloud area feedback:

$$\begin{aligned} \langle \lambda_h^{\text{area}} \rangle &= 1/2 \cdot (-4 \pm 2 \text{ \% K}^{-1}) \cdot (-1 \pm 3 \text{ Wm}^{-2}) \\ &= 0.02 \pm 0.07 \text{ Wm}^{-2}\text{K}^{-1}. \end{aligned} \tag{3.14}$$

3.4 Conceptualizing cloud radiative effects

Clouds are complex, but for simplicity we divide them into two types: high (h) and low (ℓ), and subsume their properties into a few parameters obtainable from observations and reanalysis (Table 3.1). They include area fractions f_h, f_ℓ, emission temperatures T_h, T_ℓ, and albedos α_h, α_ℓ. Longwave emissivities are not considered because most clouds have an emissivity close to one (Fu and Liou 1993). Clear-sky radiation is distilled to the incoming solar radiation $S^{\downarrow}$, surface albedo α_s, and outgoing longwave radiation for a given surface temperature $R_{\text{cs}}^{T_s}$. Neglecting atmospheric absorption will bias the surface and cloud albedos to be higher, but this permits the derivation of analytical expressions for cloud radiative effects from high clouds and low clouds C_h, C_ℓ; cloud overlap effects $m_{\ell h}$; and the TOA energy balance N. See Figure 3.1 for an illustration and Section 3.12 for the derivation.

3.5 Analytic feedbacks and the storyline approach

Feedbacks are computed by differentiating Earth's TOA energy balance (Equation 3.3 minus Equation 3.1, see section 3.3) with respect to the surface temperature T_s (Siebesma et al. 2020). To start, we have:

$$\lambda \equiv \frac{dN}{dT_s} = \frac{dN_{\text{cs}}}{dT_s} + \frac{dC}{dT_s}, \tag{3.15}$$

where N_{cs} is the clear-sky TOA energy balance and $C = C_h + C_\ell + m_{\ell h}$ is the net cloud radiative effect from all clouds. Plugging in the expressions for C (Equation 3.2 and 3.4, see section 3.3), we arrive at an equation for tropical climate feedbacks:

$$\lambda = \lambda_0 + \sum_{i=h,\ell} \Big(\lambda_i^{\text{area}} + \lambda_i^{\text{temp}} + \lambda_i^{\text{albedo}} \Big), \tag{3.16}$$

where λ_0 is the reference response assuming a fixed anvil temperature and fixed relative humidity (McKim et al. 2021; Yoshimori et al. 2020); and λ_i^{area}, λ_i^{temp}, $\lambda_i^{\text{albedo}}$ are the feedbacks from changes in cloud area, cloud temperature, and cloud albedo. See section 3.3 for the derivation.

These analytic expressions serve our storyline approach by transparently and quantitatively relating changes in cloud properties to their radiative feedbacks. A more formal Bayesian framework of hypothesis testing (used in Sherwood et al. (2020) and Stevens et al. (2016) to constrain climate sensitivity by reconciling diverse lines of evidence) will not be necessary here because we only consider a process perspective on anvil changes.

The anvil cloud area feedback, λ_h^{area}, comes from collecting terms from Equation 3.15 (see Equation 3.10 for fully expanded form) that involve changes in anvil area df_h/dT_s:

$$\lambda_h^{\text{area}} = \frac{d \ln f_h}{dT_s} \Big(C_h + m_{\ell h} \Big). \tag{3.17}$$

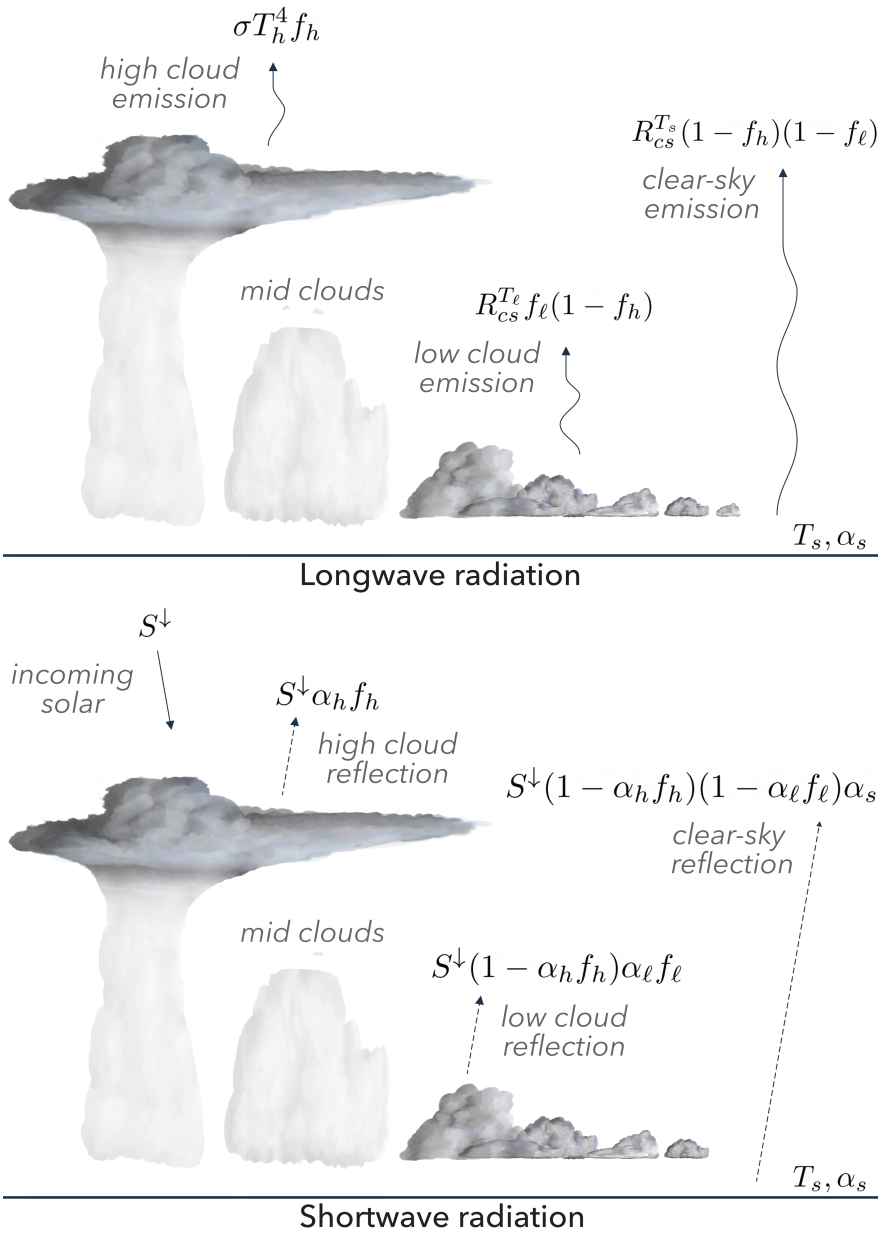

Figure 3.1: **Conceptualizing cloud radiative effects.** We idealize the vertical cloud profile into two distinct layers that represent anvil clouds and low clouds with random overlap, a reasonable assumption for clouds separated by more (Oreopoulos et al. 2022). Equations indicate the domain-averaged contribution of high clouds, low clouds, and the surface to TOA energy balance. Their sum in the longwave and shortwave is given by Equation 3.1 and 3.3, respectively. See Table 3.1 for symbol meanings and values.

This physically-based derivation shows that λ_h^{area} depends on the *fractional* change in anvil area with warming $d \ln f_h / dT_s$ and the sum of the *present day* anvil cloud radiative effect C_h and cloud overlap effect $m_{\ell h}$. This aids our storyline approach in two ways. Fractional changes in cloud area are easier to interpret and bound than absolute changes. And though we computed the change in cloud radiative effect with warming, our derivation reveals the area feedback *does not* depend on the change in radiative effect, but its present-day value.

This means it can be quantified and used to constrain the feedback—the smaller $C_h + m_{\ell h}$ is, the larger $d \ln f_h / dT_s$ has to be to produce a given λ_h^{area} bound. We can probe the plausibility of a given bound by quantifying the observed anvil cloud radiative effect, calculating the change in anvil area required to produce the bound, and then comparing the required change in anvil area to the amount expected from theory, simulations, and observations. If the expected change in anvil area is much smaller than the required change, then that bound can be refined.

3.6 Climatology

Bounding the area feedback requires quantifying the tropically averaged anvil cloud radiative effect and cloud overlap effect ($C_h + m_{\ell h}$). These quantities are not directly observed and must be inferred from our simple model of cloud radiative effects.

We do this by inputting observations of cloud fraction from CALIPSO (Winker et al. 2010), clear-sky radiation from CERES (Loeb et al. 2018), surface temperature from HadCRUT5 (Morice et al. 2021), and atmospheric temperature from ERA5 reanalysis (Hersbach et al. 2020) into our expression for the net cloud radiative effect (Equations 3.2 and 3.4), see section 3.3. Similar to Saint-Lu et al. (2020), f_h and f_ℓ are identified as the maximum of the observed cloud fraction profile above and below 8 km, respectively, and for an optical depth range between 0.3 and 5. This excludes the thickest and thinnest portion of anvil clouds, but the relationship between cloud area and surface warming is robust to the optical depth range considered (Saint-Lu et al. 2020). T_h and T_ℓ are the atmospheric temperature at the height of f_h and f_ℓ.

We ensure goodness of fit between the inferred and observed cloud radiative effects by adding a single scaling factor n to the anvil cloud fraction, which accounts for collapsing the anvil cloud fraction profile into a single level (Section 3.3 and Figure 3.5). We treat n as a constant because spatio-temporal variations in the *vertical* profile of anvil clouds affect the optical depth and hence α_h and α_ℓ, which already capture this variability as they are allowed to vary from year-to-year. In summary, n, α_h, and α_ℓ are tuneable parameters to ensure consistency with observations at TOA (see section 3.3 for further details).

We test our idealizations by comparing the observed net, shortwave, and longwave cloud radiative effects (C_{obs}, $C_{\text{obs}}^{\text{sw}}$, $C_{\text{obs}}^{\text{lw}}$) with their counterparts from the simple model (Figure 3.2), which take the spatial fields of cloud fraction, temperature, albedo, and clear-sky radiation as inputs. Our model can reproduce spatial patterns of longwave and shortwave cloud radiative effects, although there are small deviations throughout the tropics: an underestimate of C

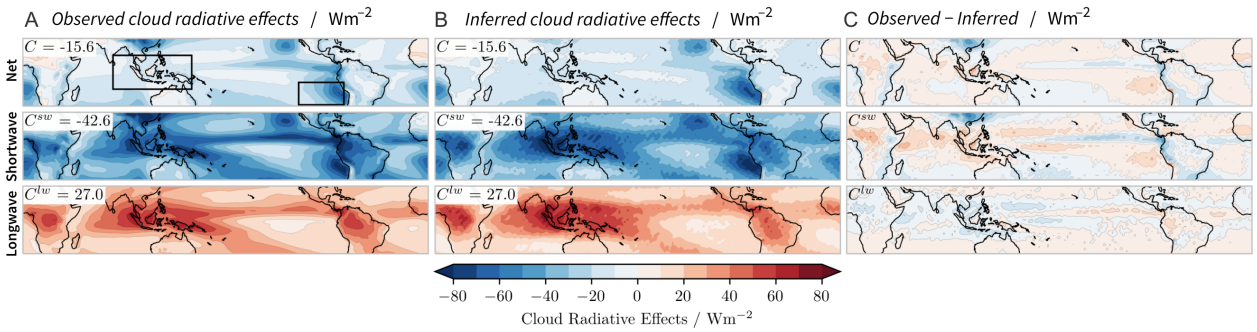

Figure 3.2: **Observed net, shortwave, and longwave cloud radiative effects (C, $C^{\mathbf{sw}}$, $C^{\mathbf{lw}}$) from CERES compared to their inferred counterparts.** Tropical mean values are shown in the upper left of each panel. The West Pacific Warm Pool and East Pacific regions are boxed in (a). The colorbar is the same for all plots.

in the south east of China and an overestimate of C in the eastern Pacific, next to South America (Figure 3.2c). Given the overall close agreement, we consider our model fit for evaluating the tropical anvil cloud area feedback.

The climatological values of tropical quantities used in our calculations are summarized in Table 3.1 and the cloud properties of interest are plotted in Figure 3.3. f_h is maximum in the West Pacific Warm Pool and f_ℓ is maximum along the East Pacific. Decomposing C into its contributions from different layers reveals that the net C is dominated by C_ℓ. By comparison, the overlap effect $m_{\ell h}$ is much smaller and varies less. The same is true for the high cloud radiative effect C_h, which exhibits strong cancellation between its shortwave and longwave components not just in the warm pool (Hartmann and Berry 2017; Ito and Masunaga 2022; Kiehl 1994), but across the tropics.

3.7 Constraining the anvil cloud area feedback

We can now constrain the tropical anvil cloud area feedback. To scale our estimate of λ_h^{area} to the global average, we multiply by the area ratio of the tropics and the globe, 1/2.

$$\langle \lambda_h^{\text{area}} \rangle = \frac{1}{2} \frac{d \ln f_h}{dT_s} \Big(C_h + m_{\ell h} \Big). \tag{3.18}$$

The plausible lower bound of $\langle \lambda_h^{\text{area}} \rangle > -0.4$ Wm^{-2}K^{-1} comes from assuming the anvil cloud feedback in Sherwood et al. (2020) is due to area changes alone. This bound allows the possibility of an overall negative cloud feedback, a necessary ingredient for a climate sensitivity below 1.5 K (Stevens et al. 2016). Our inferred value tropical mean value of $C_h + m_{\ell h} \approx -1.5$ Wm^{-2} implies that $d \ln f_h / dT_s$ must be $\approx 50\%$ K^{-1} to achieve this bound. Following our storyline approach, we assess how plausible these cloud changes are by comparing them to

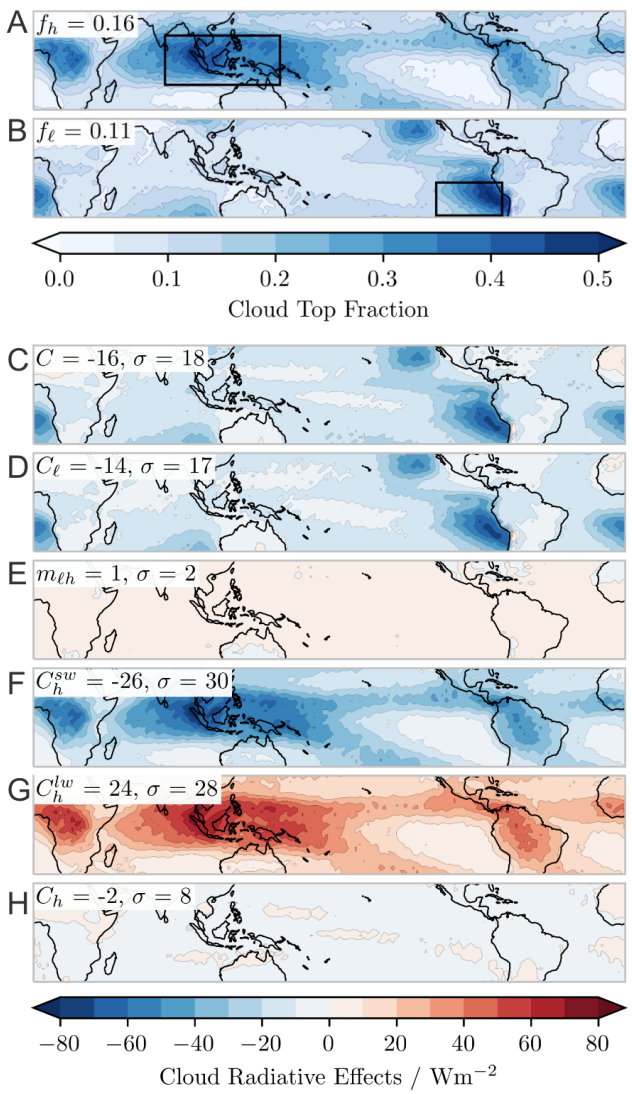

Figure 3.3: **Climatological values of tropical quantities.** Effective anvil cloud fraction (a) and low cloud fraction from CALIPSO (b). The West Pacific Warm Pool and East Pacific regions are boxed to indicate regions of maximum anvil and low cloud coverage, respectively. (c–h) Inferred cloud radiative effects from Equations 3.5, 3.6, 3.8. Tropical mean values and standard deviations are shown in the upper left of each panel. Refer to Figure 3.6 to see $m_{\ell h}$ and C_h plotted with a finer color scale.

the changes expected from theory (Bony et al. 2016) and observed interranual variability (Saint-Lu et al. 2020).

The stability iris hypothesis (Bony et al. 2016) states that anvil cloud fraction f_h is proportional to detrainment from deep convection. Owing to mass conservation, this detrainment is equal to the clear-sky convergence, $\partial_p \omega$, where ω is the subsidence vertical velocity [hPa day^{-1}]. If we make the ansatz that $\partial_p \omega$ is proportional to ω at the level of detrainment (h), then the fractional change in anvil area is equal to the fractional change in subsidence velocity at the anvil level:

$$\frac{d \ln f_h}{dT_s} = \frac{d \ln \omega_h}{dT_s}. \tag{3.19}$$

This ansatz can be justified by geometrical considerations: if the convective top height (where $\omega = 0$ by definition) is fixed, and if the height of detrainment is fixed, then increasing ω at the level of detrainment should necessarily increase the average $\partial_p \omega$ beginning from the level of detrainment and ending at the convective top.

The subsidence velocity can be written as the quotient of the clear-sky radiative flux divergence in temperature coordinates ($-\partial_T F$) and the difference between actual and dry lapse rates (Jeevanjee 2022):

$$\omega = \frac{-\partial_T F}{1/\Gamma - 1/\Gamma_d}. \tag{3.20}$$

Given that $\partial_T F$ does not vary with surface temperature (Jeevanjee and Romps 2018), if we further assume that Γ_h, the lapse rate at the anvil level, is moist adiabatic, then the change in cloud area can be computed with a few representative numbers. Assuming the surface warms from $T_s = 298$ K to 299 K and the anvil cloud warms from $T_h = 221$ K to anywhere between 221 and 221.4 K (a typical range of anvil warming (Wing et al. 2020), which affects the static stability the anvil finds itself in (Bony et al. 2016)), then we expect that anvils change in area at about

$$\begin{aligned} \frac{d \ln f_h}{dT_s} &= -\frac{d \ln(1/\Gamma_h - 1/\Gamma_d)}{dT_s} \quad \text{(stability iris)} \\ &\approx -1 \text{ to } -4\% \text{ K}^{-1}, \end{aligned} \tag{3.21}$$

depending on anvil warming. Despite the simplifications, the result is similar to the mean and standard deviation of large-domain models in RCEMIP ($-2 \pm 5\%$ K^{-1} for cloud resolving models, $-2 \pm 4\%$ K^{-1} for all models, Table S5 of Wing et al. (2020)).

Now turning to ENSO-driven interannual variability, we compute annual averages of $\ln f_h$ and T_s (tropical mean surface temperature) from July to June, similar to Saint-Lu et al.

(2020) (who uses the same dataset as we do) and plot their scatter in Figure 3.4. The line of best fit for this relation gives

$$\frac{d\ln f_h}{dT_s} \approx -7 \text{ to } -11\% \text{ K}^{-1}. \quad \text{(interannual variability)} \tag{3.22}$$

This change is larger than our simple estimate and from RCEMIP; it is also larger than the change of -5% K^{-1} inferred from interannual variability in AMIP runs with the IPSL, MPI, and NCAR models (see Figure S3 of Bony et al. (2016)). However, since *all* of these estimates of anvil cloud changes are still much smaller than what is required to achieve the lower bound of $\langle \lambda_h^{\text{area}} \rangle = -0.4$ Wm^{-2}K^{-1}, the bounds of the area feedback can be refined.

Care should be taken when inferring the long term anvil cloud area change from present day observations. Anvil area is better correlated with upper tropospheric stability than surface temperature (Saint-Lu et al. 2020, 2022), and surface- and upper-tropospheric warming (and thus changes in stability) do not always go hand-in-hand on interannual timescales (Fueglistaler 2019; Saint-Lu et al. 2022). ENSO-driven variability is associated with reorganization of deep convection (Deser and Wallace 1990), which may further alter anvil area's sensitivity to surface temperature. Anvil clouds are about half as sensitive to surface temperature for long term warming as compared to interannual variability in the IPSL general circulation model (Saint-Lu et al. 2022), the only model where such analysis has been done.

Given the evidence from theory (Equation 3.21), observations (Equation 3.22), and simulations (Bony et al. 2016; Hartmann and Larson 2002b; Saint-Lu et al. 2022; Stauffer and Wing 2022), we estimate that anvil cloud area changes at about

$$\frac{d\ln f_h}{dT_s} = -4 \ \pm \ 2 \ \% \text{ K}^{-1}. \quad \text{(best estimate)} \tag{3.23}$$

We found $C_h + m_{\ell h} = -1.5$ Wm^{-2}, but other studies have estimated -4 Wm^{-2} (Hartmann and Berry 2017), 0.6 Wm^{-2} (Gasparini et al. 2019), and 2 Wm^{-2} (L'Ecuyer et al. 2019). This is probably due to methodological differences and because anvil clouds have no precise definition. CERES TOA fluxes have their own small uncertainties (Loeb et al. 2018) and considering mid-level clouds as distinct entities from low clouds adds an additional uncertainty of 0.5 Wm^{-2} (see section 3.3). Therefore, we estimate the anvil cloud radiative effect and cloud overlap effect to be,

$$C_h + m_{\ell h} = -1 \pm 3 \text{ Wm}^{-2}. \quad \text{(best estimate)} \tag{3.24}$$

Using these best estimates in Equation 3.18, we get our best estimate of the anvil area feedback to within one standard deviation:

$$\langle \lambda_h^{\text{area}} \rangle = 0.02 \ \pm \ 0.07 \text{ Wm}^{-2}\text{K}^{-1}. \quad \text{(best estimate)} \tag{3.25}$$

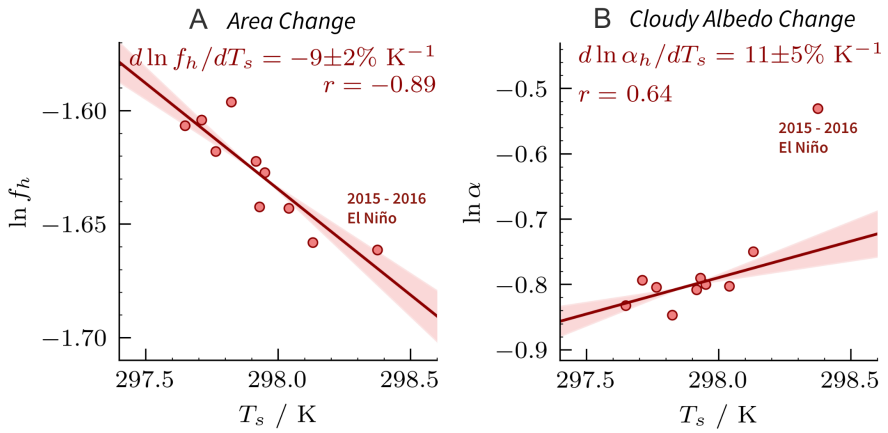

Figure 3.4: **Interannual changes in tropical mean anvil cloud area (a) and anvil cloud albedo (b) as a function of surface temperature.** Each point represents one year from 2006–2016. In each subplot, the slope, correlation of the best fit line and its standard error are shown. Standard error in the slope due to limited sampling is indicated by shading. In (b), the regression is calculated excluding the 2015–2016 El Niño. See Figure 3.8 for regression calculated including the El Niño and the regression calculated for low cloud albedo.

Overlap effects with low-level clouds are accounted for ($m_{\ell h} = 0.5\ \mathrm{Wm}^{-2}$): they dampen the anvil cloud area feedback by about 25%. Our estimate for the anvil cloud area feedback is positive but ten times smaller in magnitude and three times more constrained than the WCRP estimate of $-0.2 \pm 0.2\ \mathrm{Wm}^{-2}\mathrm{K}^{-1}$ for the anvil cloud feedback (Sherwood et al. 2020). We deem the area feedback is now well constrained because its uncertainty is comparable to other assessed cloud feedbacks (Forster et al. 2021; Sherwood et al. 2020). Our results provide a rigorous basis to qualitative arguments for a small area feedback (Ceppi et al. 2017; Hartmann 2016; Pierrehumbert 1995). What about the anvil cloud albedo feedback?

3.8 Uncertainty in the anvil cloud albedo feedback

A significant feedback could be produced without any change in anvil area (Hartmann 2016; Li et al. 2019). To see why, consider the anvil cloud albedo feedback,

$$\lambda_h^{\text{albedo}} = \frac{1}{2}\frac{d\ln\alpha_h}{dT_s}\left(C_h^{\text{sw}} + m_{\ell h}^{\text{sw}}\right). \tag{3.26}$$

It follows a similar form to the area feedback but depends on the fractional change in cloud albedo with warming $d\ln\alpha_h/dT_s$, the shortwave anvil cloud radiative effect C_h^{sw}, and the shortwave cloud overlap effect $m_{\ell h}^{\text{sw}}$ (see section 3.3 for derivation).

Given that $C_h^{\text{sw}} + m_{\ell h}^{\text{sw}} \approx -25\ \mathrm{Wm}^{-2}$ (Table 3.1), producing $\lambda_h^{\text{albedo}} = -0.2\ \mathrm{Wm}^{-2}\mathrm{K}^{-1}$ requires a fractional change in cloud albedo of only 1 to 2% K^{-1}. How plausible is such a change?

Computing the anvil cloud albedos for each year (see section 3.3), we find $d \ln \alpha_h / dT_s \approx 6$ to 16 % K^{-1}, with significant increases during the 2015–2016 El Niño (Figure 3.4b) for reasons that are unclear—anvil height and temperature are not as sensitive to El Niño (Figure 3.7); and changes in low cloud albedo are more ambiguous than anvil cloud albedo (Figure 3.8). Such a change implies $\lambda_h^{\text{albedo}} \approx 1/2 \cdot 10\%\ \mathrm{K}^{-1} \cdot -25\ \mathrm{Wm}^{-2} \sim \mathcal{O}(-1)\ \mathrm{Wm}^{-2}\mathrm{K}^{-1}$, a large negative feedback, but this should be interpreted carefully.

First, our diagnosed values of cloud albedo may be biased by ignoring clear-sky atmospheric absorption, assuming a spatially uniform cloud albedo, excluding the thickest ($\tau > 5$) and thinnest ($\tau < 0.3$) portions of anvil clouds, and assuming a cloud emissivity of 1. We have shown an increase in anvil cloud albedo with warming, whereas another observational study showed anvil cloud thinning with warming and thus a decrease in cloud albedo (Kubar and Jiang 2019). Yet another observational study showed ice water path, a proxy for optical depth, to be non-monotonic with sea surface temperatures (Igel et al. 2014).

Second, there is no guarantee that long term warming will follow interannual warming.

Third, there is no compelling, quantitative understanding of cloud condensate or albedo changes. The cloud albedo response in simulations warrant caution because of large inter-model spreads in climatology of cloud condensate and cloud radiative effects (Wing et al. 2020). A precise answer may depend on disentangling the uncertain response of precipitation efficiency with warming (Ito and Masunaga 2022; Lutsko et al. 2023).

Fourth, if anvil cloud optical depth is increasing, then longwave emissivity ε_h will increase too and produce a countervailing positive longwave feedback,

$$\lambda_h^{\text{emissivity}} = \frac{1}{2} \frac{d \ln \varepsilon_h}{dT_s} \left(C_h^{\text{lw}} + m_{\ell h}^{\text{lw}} \right), \tag{3.27}$$

but with an uncertain magnitude (see section 3.3 for further discussion). The net result of these competing components of the optical depth feedback are unclear, though they might account for the negative anvil cloud feedback found in the observation study Williams and Pierrehumbert (2017) that forms the basis of estimates in comprehensive assessments (Forster et al. 2021; Sherwood et al. 2020).

Given the lack of understanding of albedo changes, conflicting observational evidence, and a potentially countervailing longwave anvil emissivity feedback, we conclude the magnitude and uncertainty of the anvil cloud feedback in these previous assessments is primarily embodied by optical depth changes. Convective aggregation may also contribute some uncertainty if it changes anvil optical depth (Bony et al. 2020).

3.9 Implications of uncertainty

A rigorous assessment of the anvil cloud area feedback was lacking because the confounding factors of cloud overlap and a changing cloud radiative effect on the feedback could not be accounted for. We leveraged the arbitrary nature of feedback decompositions to derive a physically-based decomposition that could address these challenges. With it, we constrained

the bounds on the anvil cloud area feedback by creating a physical storyline for its prior bounds and then refuting that storyline with observations and theory.

Much attention has been devoted to changes in anvil cloud area, but optical depth changes are now the most uncertain aspect of the anvil cloud response to warming. Focusing on them will promise enhanced returns for constraining climate sensitivity, but doing so with observations alone will be hard because detecting fractional change in cloud albedo at the precision of 1% K^{-1} nears the limit of active sensor global cloud observing systems (Kotarba and Solecki 2021).

Constraining these feedbacks will require a mechanistic understanding of how anvil clouds partition themselves into their convective and stratiform components (Gasparini et al. 2019; Hartmann 2016). Pursuing such an understanding would benefit other approaches to constraining anvil cloud optical depth feedbacks, including emergent constraints, model intercomparisons, cloud-controlling factor analysis, process studies, and climatological predictors, because confidence in these methods ultimately derives from understanding the physical relationships between environmental changes, cloud changes, and the TOA response.

Such a physically transparent approach has even broader implications. Communicating with the public about our confidence (or lack thereof) in clouds and climate change is hard. However, a physical theory of cloud feedbacks that can constrain, quantify, and interpret models and observations, like the one proposed here, could help clear the cloud of uncertainty.

3.10 Further uses of our framework

Our feedback expressions might also provide a quick, quantitative, and physically transparent way to interpret how model biases influence feedbacks. For instance, if members of a GCM ensemble simulate C_h between ± 10 $\mathrm{Wm^{-2}}$, but they all simulate the same $d \ln f_h / dT_s = -4\%$ $\mathrm{K^{-1}}$, then their area feedbacks will range between ∓ 0.2 $\mathrm{Wm^{-2}K^{-1}}$. If all ensemble members simulate $C_h = 1$ $\mathrm{Wm^{-2}}$, but simulate $d \ln f_h / dT_s = \pm 5\%$ $\mathrm{K^{-1}}$, then their area feedbacks will range between ± 0.03 $\mathrm{Wm^{-2}K^{-1}}$. This quantitative yet clear diagnostic could provide testable hypothesis that advance our understanding and development of models.

Revisiting the iris effect

The notion of a large negative anvil cloud area feedback originated from Lindzen et al (Lindzen et al. 2001), who argued that it would approximately halve the predicted climate sensitivity. Such a change corresponds to $\langle \lambda_h^{\mathrm{iris}} \rangle \sim -1$ $\mathrm{Wm^{-2}K^{-1}}$. We will attempt to reproduce this estimate.

Using their values: $S^{\downarrow} = 400$ $\mathrm{Wm^{-2}}$, $\alpha_s = 0.13$, $\alpha_h = 0.24$, $f_h = 0.44$, we get $C_h^{sw} = -S^{\downarrow}(1 - \alpha_s)\alpha_h f_h \approx -37$ $\mathrm{Wm^{-2}}$. Using their "clearmoist" emission temperature $T_{\mathrm{clear}} = 261$ K, and "cloudymoist" emission temperature $T_{\mathrm{cloud}} = 222$ K, we get $C_h^{lw} = -\sigma(T_{\mathrm{cloud}}^4 - T_{\mathrm{clear}}^4) f_h \approx 55$ $\mathrm{Wm^{-2}}$. Combining the two,

$$C_h \approx 18 \text{ } \mathrm{Wm^{-2}}, \quad \text{(Lindzen et al, 2001)} \tag{3.28}$$

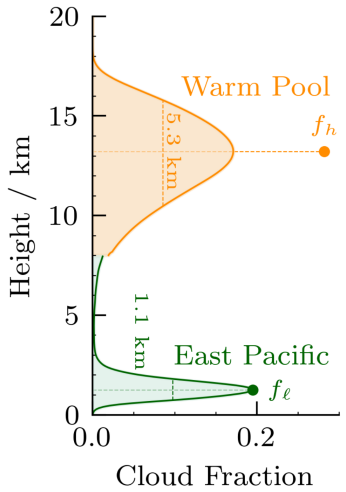

Figure 3.5: **Illustration of effective cloud fraction.** The high cloud fraction profile in the Warm Pool and low cloud fraction profile in the East Pacific are from CALIPSO. The full width-half maximum and effective cloud fraction of each profile are shown. The high cloud and low cloud profiles are clipped below 8 km and above 4 km, respectively, in accordance with our detection method.

which implies the greenhouse warming of anvils is *much* stronger than their reflective cooling. Using their change in anvil area with warming, $d\ln f_h/dT_s \approx -22\%\ \mathrm{K}^{-1}$ and their idealized model configuration that confined anvil clouds to a portion, $A_h = 25\%$ of the globe, we estimate their globally averaged area feedback to be:

$$\begin{aligned}\langle \lambda_h^{\text{iris}} \rangle &= A_h \frac{d\ln f_h}{dT_s} C_h \\ &\approx -1.0\ \mathrm{Wm}^{-2}\mathrm{K}^{-1}. \quad \text{(Lindzen et al, 2001)}\end{aligned} \tag{3.29}$$

Our calculation suggests that they inferred a large feedback because their inferred cloud changes are much larger than what is now expected and because their assumed parameters, primarily the anvil cloud albedo, resulted in an unrealistically strong greenhouse warming from anvil clouds. Our findings are consistent with Fu et al. (2002) and Lin et al. (2002).

3.11 Acknowledgements

We thank Geet George for illustrating the clouds in Figure 3.1, and Adam Sokol, Dennis Hartmann, Marion Saint-Lu, Blaž Gasparini, Isla Simpson, David Randall, and Bjorn Stevens for helpful conversations. We also thank Stephen Klein and two other anonymous reviewers whose comments have greatly improved this paper. The Franco-American Fulbright Commission (B.A.M.) and EU Horizon 2020 grant agreement 820829 "CONSTRAIN" (S.B. and J.L.D.) supported this work.

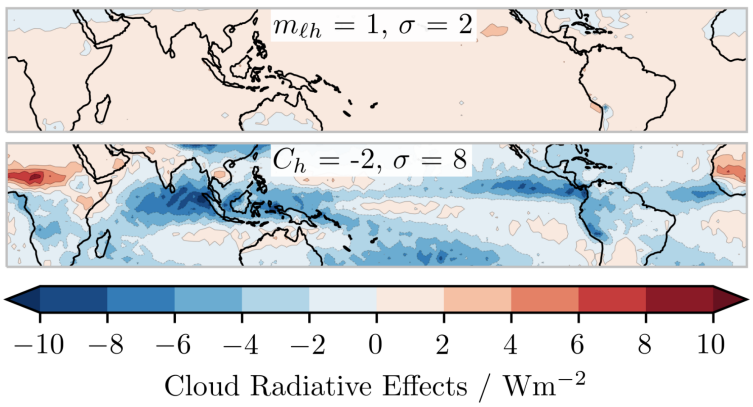

Figure 3.6: **Climatological values of tropical quantities.** Top) Inferred cloud overlap effect from Equation 3.8. Bottom) Inferred anvil cloud radiative effect from Equation 3.5. Tropical mean values and standard deviations are shown in the upper middle of each panel. Refer to Figure 3.3 to see $m_{\ell h}$ and C_h and other quantities plotted with a broader color scale.

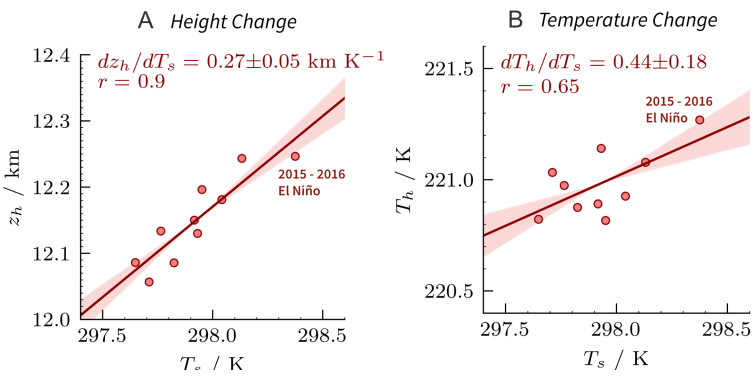

Figure 3.7: **Interannual changes in tropical mean anvil cloud height (a) and temperature (b).** In each subplot, the slope, correlation for the best fit line and its standard error are shown. Standard error in the slope due to limited sampling is indicated by shading.

Table 3.1: **Climatological values of tropical quantities (30°S – 30°N) used in this study**. All radiative quantities are evaluated at the top of atmosphere. $C^{\mathrm{lw}}_{\mathrm{obs}}$ and $C^{\mathrm{sw}}_{\mathrm{obs}}$ refer to the observed longwave and shortwave cloud radiative effects from CERES. See Climatology section for details.

Quantity	Description	Tropical mean value	Derivation
f_h	Anvil cloud area fraction	0.16	CALIPSO
f_ℓ	Low cloud area fraction	0.11	CALIPSO
T_h	Anvil temperature	221 K	ERA5
T_ℓ	Low cloud temperature	287 K	ERA5
T_s	Surface temperature	298 K	HadCRUT5
α_s	Planetary surface albedo	0.13	CERES
$S^{\downarrow}$	Incoming shortwave radiation	398 $\mathrm{Wm^{-2}}$	CERES
S_{cs}	Clear-sky absorbed shortwave	347 $\mathrm{Wm^{-2}}$	CERES
R_{cs}	Clear-sky outgoing longwave	287 $\mathrm{Wm^{-2}}$	CERES
n	Effective cloud fraction scaling	1.7	Fitted from $C^{\mathrm{lw}}_{\mathrm{obs}}$
α_h	Anvil albedo	0.45	Fitted from $C^{\mathrm{sw}}_{\mathrm{obs}}$
α_ℓ	Low cloud albedo	0.45	Fitted from $C^{\mathrm{sw}}_{\mathrm{obs}}$
C	Net cloud radiative effect	-15.6 $\mathrm{Wm^{-2}}$	Inferred
C^{sw}	Shortwave cloud radiative effect	-42.6 $\mathrm{Wm^{-2}}$	Inferred
C^{lw}	Longwave cloud radiative effect	27.0 $\mathrm{Wm^{-2}}$	Inferred
C_h	Anvil cloud radiative effect	-2.0 $\mathrm{Wm^{-2}}$	Inferred
C^{sw}_h	Shortwave anvil cloud radiative effect	-26.1 $\mathrm{Wm^{-2}}$	Inferred
C^{lw}_h	Longwave anvil cloud radiative effect	24.1 $\mathrm{Wm^{-2}}$	Inferred
C_ℓ	Low cloud radiative effect	-14.3 $\mathrm{Wm^{-2}}$	Inferred
C^{sw}_ℓ	Shortwave low cloud radiative effect	-17.3 $\mathrm{Wm^{-2}}$	Inferred
C^{lw}_ℓ	Longwave low cloud radiative effect	3.1 $\mathrm{Wm^{-2}}$	Inferred
$m_{\ell h}$	Cloud overlap effect	0.6 $\mathrm{Wm^{-2}}$	Inferred
$m^{\mathrm{sw}}_{\ell h}$	Shortwave cloud overlap effect	1.1 $\mathrm{Wm^{-2}}$	Inferred
$m^{\mathrm{lw}}_{\ell h}$	Longwave cloud overlap effect	-0.5 $\mathrm{Wm^{-2}}$	Inferred

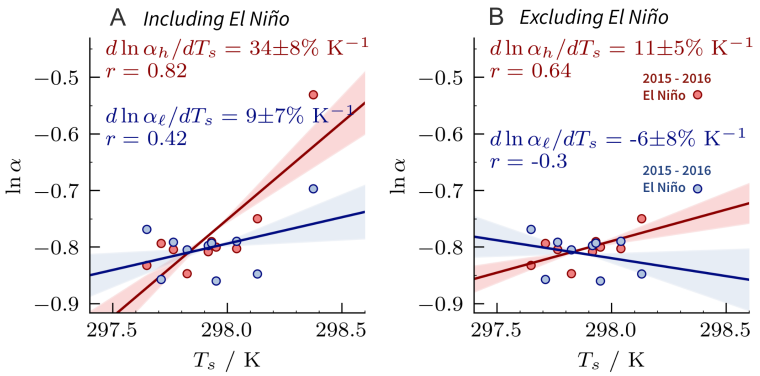

Figure 3.8: **Interannual changes in tropical mean anvil cloud albedo (red) and low cloud albedo (blue).** (a) The line of best fit is calculated with the 2015–2016 El Niño included. (b) The line of best of fit is calculated without the El Niño.

3.12 Data

Data availability

CERES data were obtained from the NASA Langley Research Center (https://ceres.larc.nasa.gov/data/). CALIPSO / CLOUDSAT data were obtained from NASA Atmospheric Science Data Center (https://asdc.larc.nasa.gov/project/CALIPSO/CAL_LID_L3_Cloud_Occurrence-Standard-V1-00_V1-00). ERA5 reanalysis data were obtained from the Copernicus Climate Change Service (https://cds.climate.copernicus.eu/). HadCRUT5 data were obtained from the Met Office Hadley Centre (https://www.metoffice.gov.uk/hadobs/hadcrut5/data/current/download.html).

Code availability

Scripts used to support the analysis of satellite and reanalysis data are available at https://github.com/mckimb/anvil-area-feedback and https://nbviewer.org/github/mckimb/anvil-area-feedback/blob/main/github_plotting.ipynb.

Chapter 4

Tropopause temperature

This chapter is submitted as McKim, B. A., Jeevanjee, N., Vallis, G. K., & Lewis, N. T. (2024). *Water vapor spectroscopy and thermodynamics constrain Earth's Tropopause Temperature*. Submitted to AGU Advances: DOI:10.22541/essoar.170904795.55675140/v1.

4.1 Abstract

As Earth warms, the tropopause is expected to rise, but predictions of its temperature change are less certain. One theory ties tropopause temperature to outgoing longwave radiation (OLR), but this contradicts simulations that exhibit a Fixed Tropopause Temperature (FiTT) even as OLR increases. Another theory ties tropopause temperature to upper tropospheric moisture, but is not precise enough to make quantitative predictions. Here, we argue that tropopause temperature, defined by where radiative cooling becomes negligible, is set by water vapor's maximum spectroscopic absorption and Clausius-Clapeyron scaling. This "thermospectric constraint" makes quantitative predictions for tropopause temperature that are borne out in single column and general circulation model experiments where the spectroscopy is modified and the tropopause changes in response. This constraint underpins the FiTT hypothesis, shows how tropopause temperature can decouple from OLR, suggests a way to relate the temperatures of anvil clouds and the tropopause, and shows how spectroscopy manifests in Earth's general circulation.

4.2 Introduction

The tropopause separates the strong surface-driven overturning troposphere from a more gently overturning stratosphere. Understanding the mechanisms setting tropopause temperature and height remains a fundamental and important unsolved problem in climate science (Phillips 1956) — fundamental because it depends on how two branches of climate, dynamics and radiation, interact (Schneider 2008; Vallis 2017); important because the tropopause is a boundary condition in hurricane intensity (Emanuel 2006; Emanuel et al. 2013), convectively available potential energy (Romps 2016), CO_2 forcing (Jeevanjee et al. 2021a), the water vapor feedback (Feng et al. 2023; Koll et al. 2023; Meraner et al. 2013), stratospheric water vapor (Mote et al. 1996), and ozone destruction (Match and Gerber 2022).

The dynamically active troposphere is thought to extend upwards until the radiative equilibrium temperature profile of the stratosphere becomes stable to convection and eddies (Held 1982; Thuburn and Craig 2000), a condition known as the *radiative constraint* that defines a radiative tropopause as the lowest level at which the atmosphere attains radiative equilibrium. We focus on this radiative definition, but note that the tropopause can also be diagnosed with a lapse-rate criterion, and the two measures will often but not always be similar (Highwood and Hoskins 1998), a point we return to later.

One way to understand the radiative tropopause temperature is in terms of top-of-atmosphere energy balance (Held 1982; Thuburn and Craig 2000; Vallis 2017; Vallis et al. 2015). In this theory, *gray* radiative transfer (independent of wavenumber) and an optically thin stratosphere and upper troposphere are often assumed for conceptual simplicity. This lets tropopause temperature (T_{tp}) be regarded as a skin-like temperature (Pierrehumbert 2010; Schneider 2008) dictated by the outgoing longwave radiation (OLR):

$$T_{\mathrm{tp}} = (\mathrm{OLR}/2\sigma)^{1/4} \quad \text{(OLR constraint)}, \tag{4.1}$$

where σ is the Stefan-Boltzmann constant. Note, though, that the source of the outgoing radiation still lies within the troposphere. This suggests a direct coupling between T_{tp} and OLR and makes no direct reference to the properties of Earth's greenhouse gasses. It predicts an unchanging tropopause temperature with CO_2-driven global warming, which is generally consistent with comprehensive climate models (Hu and Vallis 2019; Vallis et al. 2015). It also suggests a sensitivity of T_{tp} to warming agents that increase OLR (such as an increase in insolation).

However, a fixed tropopause temperature (FiTT) has been shown in simulations of warming *without* fixed OLR (Seeley et al. 2019), which may be at odds with the OLR constraint. The expectation of a FiTT *independent* of the warming agent originates from an entirely different branch of research focused on the fixed temperature of anvil clouds in response to surface warming (Hartmann and Larson 2002b). In this theory, water vapor, the primary source of radiative cooling in the troposphere (Manabe and Strickler 1964), is thought to control T_{tp}. Harrop and Hartmann (2012) and Hartmann and Larson (2002b) showed that tropical convection is tied to water vapor-driven radiative cooling. Moisture declines exponentially with temperature, until there is so little water vapor that it can no longer radiatively cool, thereby limiting the vertical extent of convection. These results were generalized and shown to apply to extratropical high clouds (Thompson et al. 2017, 2019), and Seeley et al. (2019) suggested that a similar hypothesis may be even more apt for the radiative tropopause. As evidence of this potential connection, Seidel and Yang (2022) showed that anvil clouds and the radiative tropopause covary with surface warming.

If this is all true, then the temperature dependence of water vapor and its radiative cooling imposes a *moist thermodynamic constraint* on the tropopause. This is consistent with observations and models (Thompson et al. 2017, 2019) and helps explain the FiTT response to surface warming and its relation to Fixed Anvil Temperatures (FAT) (Hartmann and Larson 2002b; Seeley et al. 2019; Seidel and Yang 2022). However, it makes no reference to OLR and it remains unclear what sets the temperature at which water vapor is unable to radiatively cool. The moist constraint cannot predict T_{tp}, and thus the FiTT hypothesis lacks a quantitative basis.

These limitations and contradictions may be resolved by noting that OLR *is* coupled to moist thermodynamics (Jeevanjee et al. 2021b; Koll and Cronin 2018; Nakajima et al. 1992; Simpson 1928), and that spectral (wavenumber-dependent) theories of radiation can yield quantitative insights into this coupling (Feng et al. 2023; Koll et al. 2023). This approach led to a moist radiative theory for anvil cloud temperatures (Jeevanjee and Fueglistaler 2020b) and we will follow suit to derive a more precise theory of the radiative tropopause temperature and of FiTT. Like Held (1982) and Thuburn and Craig (2000), we study the radiative tropopause (henceforth "the tropopause"), but we will inspect the lapse rate tropopause and the role of dynamical constraints (Held 1982; O'Gorman 2011; Schneider 2004, 2008; Schneider and O'Gorman 2008; Stone and Carlson 1979; Vallis 2017; Zurita-Gotor and Vallis 2011) later on. Stratospheric dynamics and ozone affect tropopause structure (Birner 2010; Dacie et al. 2019; Fueglistaler et al. 2009; Highwood and Hoskins 1998; Lin et al. 2017; Thuburn and Craig 2000, 2002) and their inclusion is necessary to capture the full complexity

of the tropopause response to climate change (Randel and Jensen 2013). However, here we focus on more basic mechanisms that should be embedded in most climate models.

4.3 Formulating the thermospectric constraint

Qualitative overview

Understanding clear-sky radiative cooling is key to constraining the tropopause. The cooling profile is controlled by the wavenumber-dependence of water vapor spectroscopy (Jeevanjee and Fueglistaler 2020b). At each temperature (or height), there are only a few wavenumbers that cool (Jeevanjee and Fueglistaler 2020a,b), with colder temperatures (higher heights) cooling at wavenumbers with stronger spectroscopic absorption. We demonstrate this in a moist-adiabatic (to 150 K) single column model at $T_s = 300$ K with line-by-line radiative transfer, PyRADS (Koll and Cronin 2018). Plotting the spectrally-resolved cooling reveals that at any given height, most cooling is contained within a roughly 200 cm^{-1} width band whose contours mimic the V-shape of water vapor spectroscopy (Figure 4.1a,c).

Following this logic, water vapor's maximum spectroscopic absorption strength around 150 cm^{-1} (Figure 4.1a) suggests there is a minimum temperature (maximum height) to which water vapor can radiatively cool (Figure 4.1c). We argue that the *combination* of water vapor spectroscopy and Clausius-Clapeyron scaling constrains tropopause temperature. This *thermospectric constraint* refines the moist constraint with a more fundamental explanation for where and why water vapor's radiative cooling declines in the upper troposphere. It refines the OLR constraint into a spectral emission constraint that relates particular features of the radiative cooling profile to their corresponding emission temperatures.

Making the constraint quantitative

Small amounts of upper tropospheric water vapor can cool because of its strong radiative absorption in the rotational band (Figure 4.1a and Clough et al. (1992)). Consider water vapor's optical depth:

$$\tau_{\text{H}_2\text{O}}(\nu, z) = \int_z^\infty \kappa_{\text{H}_2\text{O}}(\nu) \frac{p}{p_{\text{ref}}} \rho_{\text{H}_2\text{O}} dz', \tag{4.2}$$

where $\kappa_{\text{H}_2\text{O}}(\nu)$ is the spectroscopic absorption strength of water vapor ($\text{m}^2\ \text{kg}^{-1}$) at wavenumber ν (cm^{-1}), p/p_{ref} accounts for pressure broadening at wavenumbers more than about 0.1 cm^{-1} away from line centers (Fu 2006), p is the pressure, $p_{\text{ref}} = 500$ hPa is a reference pressure, and $\rho_{\text{H}_2\text{O}}$ is the density of water vapor. Infrared emission from water vapor peaks around $\tau_{\text{H}_2\text{O}} \approx 1$ (Jeevanjee 2023; Jeevanjee and Fueglistaler 2020a). For $\tau_{\text{H}_2\text{O}}$ to remain close to 1, changes in $\kappa_{\text{H}_2\text{O}}$ must be compsensated by the integral of $\rho_{\text{H}_2\text{O}}$. $\kappa_{\text{H}_2\text{O}}$ varies by many orders of magnitude across the infrared (Figure 4.1a), so many possible values of z can result in the product of $\kappa_{\text{H}_2\text{O}}$ and the integral of $\rho_{\text{H}_2\text{O}}$ being close to one. In other words, many atmospheric levels emit to space (Figure 4.1c,d). However, a maximum in $\kappa_{\text{H}_2\text{O}}$ implies a minimum integral of $\rho_{\text{H}_2\text{O}}$, and hence a maximum height z_{max}, above which the atmosphere that can no longer effectively cool to space. Owing to the Clausius-Clapeyron scaling of $\rho_{\text{H}_2\text{O}}$, this can be formulated more easily as a minimum temperature.

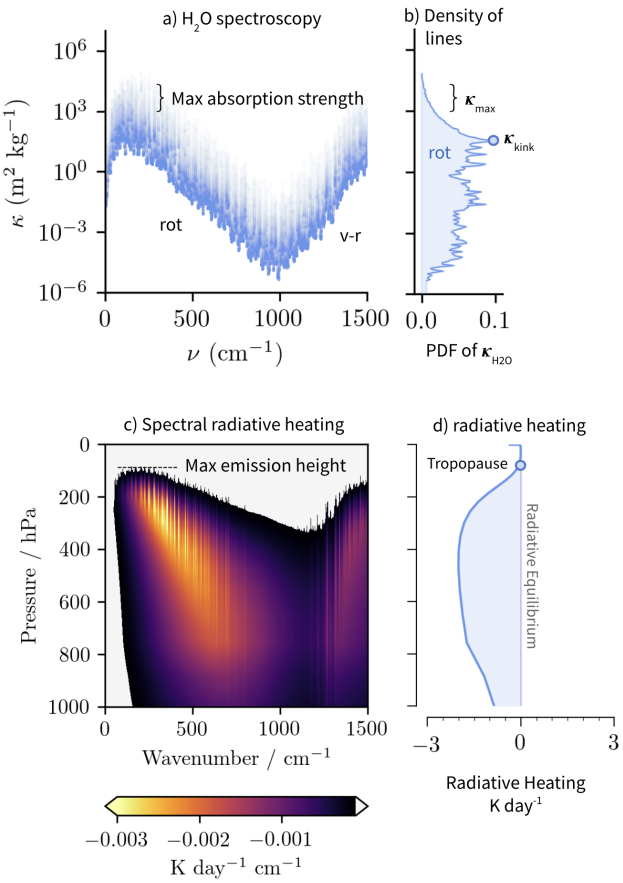

Figure 4.1: **The max absorption strength of water vapor spectroscopic absorption is hypothesized to constrain Earth's tropopause.** (a) Water vapor absorption strength as a function of wavenumber. (b) The rotational branch (150 to 1000 cm^{-1}) of absorption strength as a normalized histogram (plotted vertically), with units of $\ln \kappa_{\text{H}_2\text{O}}$. (c) Spectrally-resolved radiative cooling from a single column model with line-by-line radiative transfer, PyRADS. (d) Spectrally-integrated radiative cooling. We make a rough estimate of the maximum absorption coefficient as $\kappa_{\text{max}} \sim 10^3 - 10^4$ m^2kg^{-1}, which we hypothesize relates to the tropopause. $\kappa_{\text{kink}} = 40$ m^2 kg^{-1} refers to where the density of lines begins to decline rapidly, which has been hypothesized to relate to anvil clouds (Jeevanjee and Fueglistaler 2020b). Spectral data plotted at a resolution of 0.1 cm^{-1} using PyRADS (Koll and Cronin 2018).

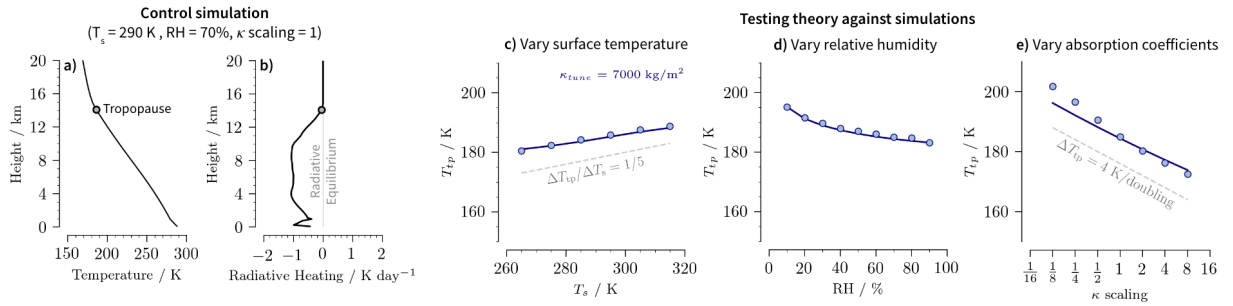

Figure 4.2: **The thermospectric constraint, Equation 4.5 and 4.6, can quantitatively capture the change in tropopause temperature ($T_{\mathbf{tp}}$).** (a) Isca's single column model control simulation's temperature profile. (b) Control simulation's radiative cooling profile. (c) The surface temperature is varied and RH kept fixed at 0.7. Simulations (dots), theory (solid lines). (d) The relative humidity is varied and T_s fixed at 290 K. (e) The absorption coefficients of water vapor are scaled uniformly and T_s and RH fixed at 290 K and 0.7, respectively. Water vapor and CO_2 (280 ppmv) are the only greenhouse gases present in these simulations.

To formulate this statement quantitatively, we assume that all emission occurs at $\tau_{\mathrm{H_2O}} = 1$, which defines an emitting temperature T_{em} at wavenumber ν by the relation

$$\tau_{\mathrm{H_2O}}(\nu, T_{\mathrm{em}}) = 1. \tag{4.3}$$

It is more accurate to invert this equation numerically, but more informative to do so analytically, as shown in Jeevanjee (2023) and Jeevanjee and Fueglistaler (2020b). We reproduce some of their steps for clarity.

The variable of integration in optical depth can be changed from height to temperature, and though water vapor spectroscopy varies due to pressure broadening, it varies much less than water vapor density does across the troposphere, so it can be pulled out of the integral. Optical depth is then proportional to water vapor path, which can be computed analytically (Koll and Cronin 2018), resulting in a simplified expression:

$$\tau_{\mathrm{H_2O}}(\kappa_{\mathrm{H_2O}}, T) \approx \underbrace{\kappa_{\mathrm{H_2O}} \frac{p}{p_{\mathrm{ref}}}}_{\text{spectroscopy}} \underbrace{M_{\mathrm{v}} \mathrm{RH} \exp\left(-\frac{L}{R_{\mathrm{v}} T}\right)}_{\text{water vapor path}}, \tag{4.4}$$

where p is the atmosphere pressure, $p_{\mathrm{ref}} = 500$ hPa is the reference pressure at which $\kappa_{\mathrm{H_2O}}$ is evaluated at to account for pressure broadening, $M_{\mathrm{v}} \equiv p_v^{\mathrm{ref}} T_{\mathrm{av}} / \Gamma L$ is a characteristic column water vapor mass (kg m^{-2}), where $T_{\mathrm{av}} \equiv (T_s + T_{\mathrm{tp}})/2$, which we set to a constant of 250 K for simplicity (results are not sensitive to this approximation), $p_v^{\mathrm{ref}} = 2.5 \times 10^9$ hPa is a reference pressure from Clausius-Clapeyron scaling, $L = 2.5 \times 10^6$ J kg^{-1} is water's latent

heat of vaporization ,and $M_\mathrm{v}\mathrm{RH}\exp(-L/R_\mathrm{v}T)$ is the column mass of water vapor above the isotherm with temperature T.

Setting $\tau_{\mathrm{H_2O}} = 1$, writing $p = p_\mathrm{ref}(T/T_\mathrm{ref})^{g/\Gamma R_d}$, where T_ref is the temperature at p_ref, and solving for T_em results in the emission temperatures as a function of absorption coefficients:

$$T_\mathrm{em}(\kappa_{\mathrm{H_2O}}) = \frac{T^*}{W\left(\frac{T^*}{T_\mathrm{ref}}(D \cdot \mathrm{RH} \cdot M_\mathrm{v} \cdot \kappa_{\mathrm{H_2O}})^{R_\mathrm{d}\Gamma/g}\right)}, \tag{4.5}$$

where T^* is a characteristic temperature for water vapor, W is the Lambert-W function, T_ref is the temperature , $D = 1.5$ is a scaling factor that accounts for the two stream approximation in radiative transfer theory, $R_\mathrm{d} = 287$ J kg^{-1} K^{-1} is the specific gas constant for dry air, $\Gamma = 7$ K km^{-1} is the globally-averaged lapse rate of the troposphere in the general circulation model used later on (Figure S1b), and g is the gravitational acceleration (see Table 1 in Methods for values and meanings of the variables and constants). The Lambert-W function appears because of inverting an expression with the form $y = x\exp(x)$.

The thermospectric constraint posits that tropopause temperature T_tp is the emission temperature determined by a combination of Clausius-Clapeyron scaling (as embodied by RH and M_v) and the maximum absorption coefficient of water vapor, κ_max. That is,

$$T_\mathrm{tp} = T_\mathrm{em}(\kappa_\mathrm{max}). \quad \text{(Thermospectric constraint)} \tag{4.6}$$

The presence of thousands of absorption lines across the infrared (Figure 4.1a) makes it difficult to select an appropriate value of κ_max. It helps that the strength of spectrally integrated radiative cooling is roughly proportional to the density of absorption lines at a given strength (Figure 4.1b,d and Jeevanjee and Fueglistaler (2020b)). For values of $\kappa_{\mathrm{H_2O}} \in (10^{-4}, 10^{1})$ m^2 kg^{-1}, which correspond to tropospheric emission and a typical value of -2 K day^{-1} of radiative cooling (Jeevanjee and Fueglistaler 2020b), the density of absorption lines in the rotational band (150 to 1000 cm^{-1}) has a characteristic value of $0.07 \ln \kappa_{\mathrm{H_2O}}$ (Figure 4.1b). The vibrational-rotational band (1000 to 1500 cm^{-1}) is not as important because its Planck emission is about 1/6 of the rotational band's emission (Jeevanjee and Fueglistaler 2020b).

The proportionality between the density of lines and the strength of cooling provides a heuristic way to determine κ_max: look for where the density of lines drops between a tenth and a hundredth of its density for tropospheric emission, as this would roughly correspond to where cooling drops to between a tenth and a hundredth of its tropospheric value (thereby achieving radiative equilibrium) (Figure 4.1b,d). Other factors influence the strength of cooling, such as the change in optical depth with height and the strength of the Planck function at a given wavenumber and temperature, but Jeevanjee and Fueglistaler (2020b) showed that these cannot explain the declining strength of cooling in the upper troposphere.

We plot the density of absorption lines in the rotational band in Figure 4.1b. The density drops to between a tenth and a hundredth of its typical value at $\kappa_{\mathrm{H_2O}} \in (4 \cdot 10^3, 4 \cdot 10^4)$ m^2 kg^{-1}. Taking the geometric average of the upper and lower bounds, we arrive at our estimate

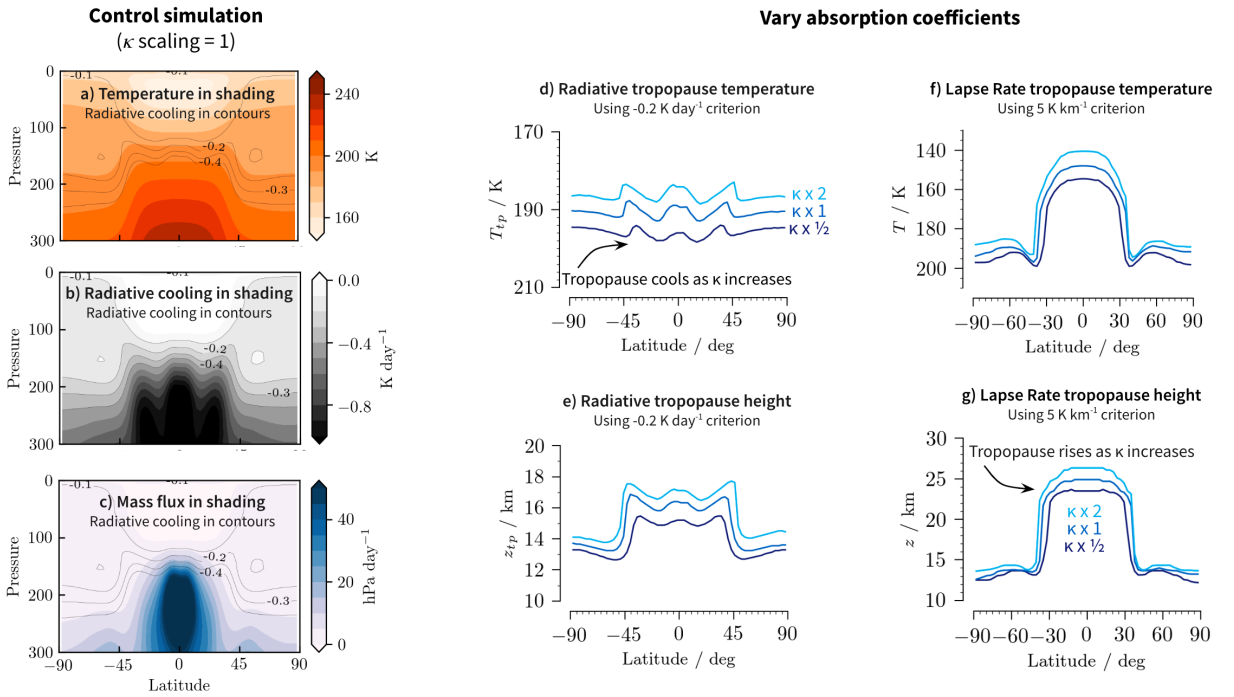

Figure 4.3: **Water vapor spectroscopy affects the radiative and lapse rate tropopauses.** (a) Zonal-mean temperature profile of the control Isca aquaplanet simulation. (b) Zonal-mean radiative cooling profile of the control. (c) Zonal-mean mass flux profile of the control. (d-g) Water vapor absorption coefficients are increased geometrically by [1/2, 1, 2] and the resulting changes in radiative- and lapse rate-tropopause temperature and height are recorded. The lack of ozone in these simulations accounts for the high (25 km) lapse rate tropopause.

of $\kappa_{\text{max}} \approx 13000$ m^2 kg^{-1}. Plugging into Equation 4.6, our prediction for the tropopause temperature is $T_{\text{tp}} \approx 180$ K.

4.4 Testing the thermospectric constraint

To test the thermospectric constraint (Equation 4.6), we run simulations using a clear-sky single column model (SCM) configuration of the Isca modeling framework (Vallis et al. 2018). The SCM is configured with the correlated-k radiative transfer code RRTM (Mlawer et al. 1997), and a simplified representation of moist convection (the simple Betts-Miller code of Frierson (2007) and O'Gorman and Schneider (2008)). In a single model context, the simple Betts-Miller essentially constrains the atmosphere to a moist adiabat, but in a GCM, where horizontal transfers of energy can occur, means that deviations from the moist adiabat should be expected, particularly when looking at the extratropics. Nevertheless, configuring the SCM using Isca lets us compare to general circulation model (GCM) simulations with identical column-wise physics later in the paper. Further description of our model set-up

can be found in the Supporting Information.

To begin, we consider an SCM control run with a prescribed surface temperature of T_s = 290 K, relative humidity RH= 0.7, and CO_2 concentration of 280 ppmv. The diagnosed tropopause temperature obtained in this simulation (the lowest level to which radiative equilibrium is achieved, which we identify as -0.05 K day^{-1} to avoid sensitivity issues related to the cooling profile's asymptotic approach to 0 K day^{-1}, see Figure 4.2a,b and Supporting Information), is 184 K, close to our prediction. Physically, the asymptotic approach to 0 K day^{-1} might be expected from the fact that the density of lines of water vapor's absorption spectrum also asymptotically approaches 0 (Figure 4.1a), and therefore its radiative cooling profile might exhibit this behavior too.

The maximum absorption coefficient of water vapour, $\kappa_{\max}$, can also be considered a free parameter to match the predicted tropopause temperature with the value diagnosed from a climate model. Tuning $\kappa_{\max}$ results in a value of 7000 m^2 kg^{-1}, which is within our identified range for $\kappa_{\max}$ based on the density of absorption lines. This tuned value is used henceforth and will not be retuned, except where explicitly scaled. Regarding this climate as our base state, we can test the thermospectric constraint by varying the prescribed surface temperature, column relative humidity, and absorption coefficients of water vapor in the SCM and see how well theory compares with the numerical simulations.

Surface temperature

As surface temperature increases, the thermospectric constraint (Equation 4.6) predicts a small but nonzero warming of the tropopause of about $\Delta T_{tp}/\Delta T_s = 1/5$ (Figure 4.2c, solid line) due to the change in T_{ref}, the temperature at p_{ref} = 500 hPa, which appears from accounting for pressure broadening effects (Equation 4.5 and Feng et al. (2023) and Koll et al. (2023). The slight warming can be understood as follows. The tropopause temperature is fixed, to first order, which implies a rising tropopause as surface temperature increases. As pressure decreases, the effective water vapor absorption coefficients ($\kappa_{H_2O} \cdot p/p_{ref}$) also decreases, which implies a larger ρ_{H_2O} is needed to achieve $\tau_{H_2O} = 1$, and thus a slightly warmer tropopause temperature. A simple calculation shows that the change in water vapor emission temperatures (including at the tropopause) should be about 1/4 to 1/5 of the warming at the surface (Equation B4 of Jeevanjee (2023) and Equation 46 of Koll et al. (2023)).

In an SCM experiment where surface temperature is increased (Figure 4.2c, dots), the tropopause warms almost exactly as predicted. The relatively fixed tropopause temperature (FiTT) has been noted before (Seeley et al. 2019) and explained qualitatively by Thompson et al. (2019) with the thermodynamic constraint. However, the thermospectric constraint provides a quantitative understanding of how T_{tp} should change with warming. The pressure broadening explanation differs from Hu and Vallis (2019), who explains the slight warming as a consequence of increased longwave radiation from outside the water vapor window.

Relative humidity

Variations in column relative humidity (RH) may influence T_{tp}. A larger RH implies a smaller saturation water vapor density $\rho^{\mathrm{sat}}_{\mathrm{H_2O}}$ to reach $\tau_{\mathrm{H_2O}} = 1$, and thus a cooler temperature. We vary RH in the SCM but keep surface temperature fixed and find the tropopause cools as RH increases (Figure 4.2d), in excellent agreement with predictions from inputting RH into the thermospectric constraint (Equation 4.5).

Water vapor absorption

Modifying the $\rho_{\mathrm{H_2O}}$ passed to the radiation code of a climate model alters the temperature of anvil clouds and the tropopause (Harrop and Hartmann 2012; Spaulding-Astudillo and Mitchell 2023; Thompson et al. 2019). The thermospectric constraint suggests that modifying $\kappa_{\mathrm{H_2O}}$ should have a similar effect. A geometrically larger κ_{max} implies a geometrically smaller minimum $\rho_{\mathrm{H_2O}}$ to achieve $\tau_{\mathrm{H_2O}} = 1$ and hence an arithmetically colder T_{tp} due to Clausius-Clapeyron scaling: $d \ln \rho_{\mathrm{H_2O}} / dT|_{T_{\mathrm{tp}}} = L/(R_{\mathrm{v}} T^2_{\mathrm{tp}}) = 16\%\ \mathrm{K}^{-1}$ or roughly 4 K of cooling to halve $\rho_{\mathrm{H_2O}}$. These predictions are borne out quantitatively by the simulations, where T_{tp} cools arithmetically as κ_{max} is scaled geometrically over many octaves while T_{s} and RH are fixed, at a rate of roughly 4 K per doubling (Figure 4.2e). This is the most direct test of the thermospectric constraint and it confirms spectroscopy's key role in constraining T_{tp}.

4.5 From spectroscopy to the general circulation

The previous tests were done in a single column model, but the tropopause is a feature of Earth's general circulation and will be influenced by other factors (Birner 2010; Thuburn and Craig 2000). We test whether modifying $\kappa_{\mathrm{H_2O}}$ influences T_{tp} and z_{tp} (tropopause height) in a general circulation model configured as an idealized aquaplanet with a standard fixed sea surface temperature distribution (Neale and Hoskins 2000):

$$T_s(\phi) = \begin{cases} 300\big(1 - \sin^2(3\phi/2)\big)\ \mathrm{K}, & \text{for } -\pi/3 < \phi < \pi/3 \\ 273\ \mathrm{K}, & \text{otherwise,} \end{cases} \tag{4.7}$$

where ϕ is the latitude. The GCM is configured to use the same column-wise physics routines (e.g., RRTM radiative transfer, simplified Betts-Miller moist convection) as the SCM. See the Supporting Information for further details. When analysing the GCM, we diagnose the radiative tropopause with a -0.2 K day^{-1} threshold instead of the -0.05 K day^{-1} used for the SCM. The updated threshold more closely aligns with relevant dynamical features such the mass flux profile (Figure 4.3c) while still using a threshold value $\ll$ typical tropospheric cooling (Figure 4.3b). If one were to keep using the -0.05 K day^{-1} threshold, then the radiative tropopause would be very high in the atmosphere where there is coarse resolution, and it would no longer align with the dynamical features of the atmosphere (Figure 4.3b,c).

Spectroscopic control of the tropopause

We vary κ_{H_2O} geometrically and find the tropopause cools and rises across all latitudes, again at $\approx 4-5$ K and $0.5-1$ km per doubling of κ_{H_2O} (Figure 4.3d,e). This cooling confirms the quantitative predictions of thermospectric constraint (Figure 4.2e) in a more comprehensive and Earth-like setting. The spectroscopic control on the radiative tropopause has implications for the general circulation because infrared cooling constrains the residual motion of the atmosphere, the amplitude of tropospheric wave breaking, and the depth of its diabatic mixing (Thompson et al. 2017, 2019).

T_{tp} varies by only 5 K across latitude in these simulations, consistent with FiTT and the idea of a fairly insensitive radiative tropopause temperature to surface temperature and the large-scale circulation. However, radiative tropopause *height* is not uniform due to its strong dependence on surface temperature and vertically averaged lapse rate (Γ), $z_{tp} \approx (T_{tp} - T_s)/\Gamma$. It has a top-hat meridional structure because T_s varies from equator to poles and because Γ varies as the dominant control on stratification changes from moist convection in the tropics to baroclinic eddies in the extratropics (Held 1982; Schneider 2008; Stone and Carlson 1979; Vallis 2017).

This dynamical control extends to the lapse-rate tropopause, diagnosed here as where the lapse rate exceeds -5 K km^{-1}. It has a much more pronounced top-hat structure in *both* its height and temperature (Figure 4.3f,g). FiTT does not apply to all definitions of the tropopause because each definition respects different physical constraints (Birner 2010; Fueglistaler et al. 2009; Highwood and Hoskins 1998; Hu and Vallis 2019). The lapse rate tropopause, for instance, depends on the profile of stratification, which is primarily determined by dynamics (Schneider 2008). Nevertheless, the lapse rate tropopause still cools and rises as κ_{H_2O} is increased (Figure 4.3f,g), particularly in the tropics, hinting at a broader role of spectroscopy in the interaction between upper tropospheric radiative cooling, dynamics, and stratification which future work could make more precise.

Other controls of the tropopause

Meridional variations in radiative tropopause temperature may be due to surface temperature, which varies between 300 K and 273 K from equator to poles and can change T_{tp} with pressure-broadening effects. It may also be due to tropospheric relative humidity, which varies from 20 to 70 % (Figure S1a). The SCM and Equation 4.5 shows varying column relative humidity by a similar amount changes T_{tp} by about 5 K (Figure 4.2d). The lapse rate (Figure S1b) could also change T_{tp}; changing Γ from 4 K km^{-1} to 7 K km^{-1} in Equation 4.5 changes T_{tp} by 3 K.

Column-wise physics and water vapor may not be the only source of variations in T_{tp}. Stratospheric dynamics may influence z_{tp} and T_{tp} by altering the location of zero radiative cooling (Birner 2010; Hu and Vallis 2019; Thuburn and Craig 2000). CO_2-driven radiative cooling, which primarily emanates from the stratosphere (Jeevanjee and Fueglistaler 2020b), may also drive changes in T_{tp}. Future work could address these questions and lead to a more comprehensive theory, but our goal here is to provide a first order picture of moist

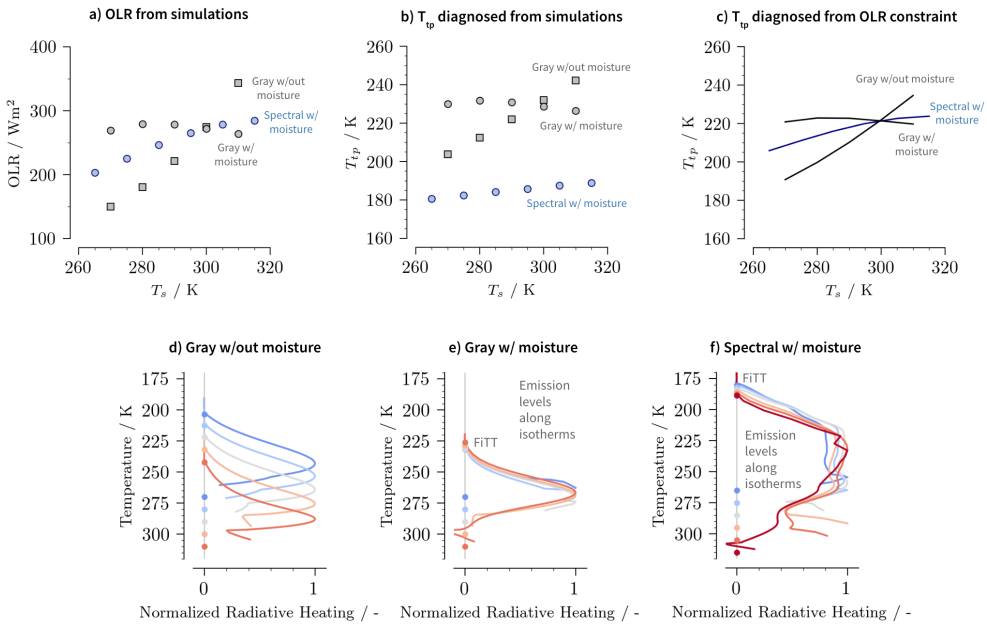

Figure 4.4: **Moisture is essential to capturing a fixed tropopause temperature and spectral radiative transfer decouples tropopause temperature from outgoing longwave radiation.** (a) Outgoing longwave radiation (OLR) of Isca single column model with various types of radiative transfer. (b) Tropopause temperature for the same simulations. (c) Predicted tropopause temperature from the OLR constraint (Equation 4.1). (d-f) The radiative cooling profile plotted in temperature coordinates for $T_s = 270, 280, 290, 300, 310$ K for each model setup. Each profile has been normalized by its maximum tropospheric value and is plotted starting at the lifting condensation level for clarity. See Supporting Information for details.

thermodynamics interact with spectroscopy to set T_{tp}.

4.6 Reconciling different constraints

Previous theories of tropopause temperature have either emphasized outgoing radiation (Held 1982; Thuburn and Craig 2000; Vallis et al. 2015) *or* moist thermodynamics and upper tropospheric radiative cooling (Hartmann and Larson 2002b; Thompson et al. 2017). Combining moisture with a spectral perspective of radiative cooling can make more precise predictions for T_{tp} and FiTT (Figure 4.2c). Now we combine the OLR constraint (Equation 4.1) with moisture to make better predictions of FiTT, and consider how adding bands to gray radiative transfer theory morphs the OLR constraint into an upper tropospheric radiative emission constraint.

The OLR constraint was derived with gray radiative transfer uncoupled to moisture (Held 1982; Thuburn and Craig 2000; Vallis et al. 2015). This "dry" constraint predicts a FiTT with respect to CO_2-driven global warming because OLR remains fixed (Vallis et al. 2015).

By this logic, a warming that changes OLR would change T_{tp}, which stands in contrast to simulations that exhibit a FiTT even as OLR increases (Seeley et al. 2019; Seidel and Yang 2022). For both gray and spectral atmospheres, the amount of OLR increase for a prescribed surface warming depends on the presence of radiatively active moisture and its optical thickness (Feng et al. 2023; Ingram 2010; Jeevanjee et al. 2021b; Koll et al. 2023; Koll and Cronin 2018; Nakajima et al. 1992; Simpson 1928; Stevens and Kluft 2023). Changes in T_{tp} may be similarly constrained.

We test the role of moisture and choice of radiative transfer in controlling OLR and T_{tp} by varying surface temperature in different configurations of Isca's SCM: a model with gray radiation uncoupled to moisture, similar to Frierson et al. (2006); with gray radiation coupled to moisture, similar to Byrne and O'Gorman (2013); and with spectral radiation coupled to moisture, as already described. In these experiments, OLR and T_{tp} change much more in the dry gray model than the moist gray and spectral models (Figure 4.4a,b).

In dry simulations, the greenhouse gas is assumed to be well mixed and so optical depth is a single valued function of pressure, $\tau = \tau(p)$. As T_{s} increases, isobars warm and radiative cooling at $\tau = 1$ emanates from a warmer layer of atmosphere that can emit more radiation to space (Figure 4.4d). In contrast, moisture constrains the optical depth to be a single valued function of temperature, $\tau = \tau(T)$ (in the absence of pressure broadening). As T_{s} increases, radiative cooling at $\tau = 1$ emanates from nearly the same temperature (Figure 4.4e,f and Figure S1a of Seeley et al. (2019) and thus OLR is constrained to increase less than in the dry case. (Radiative cooling can increase for other reasons, see, e.g., Jeevanjee and Romps (2018), but less so if there is moisture.) Therefore, the OLR constraint, when combined with a notion of how moisture constrains changes in OLR, is more consistent with FiTT for a wider variety of warming scenarios such as in Seeley et al. (2019) and Seidel and Yang (2022).

However, this explanation still does not address a motivating question of this study: How can T_{tp} decouple from OLR (compare Figure 4.4b,c)? The answer lies in the role of additional bands of radiative transfer. Hu and Vallis (2019) showed that adding a window band decouples the radiative equilibrium temperature of the planet, T_{re}, from total OLR and couples it instead to outgoing radiation from the optically thick band ($\mathrm{OLR}_{\mathrm{thick}}$):

$$T_{\mathrm{re}} = \left[\frac{\tau_{\mathrm{thick}} + 1}{2\sigma}\mathrm{OLR}_{\mathrm{thick}}\right]^{1/4}. \tag{4.8}$$

The window band becomes optically thin at the surface, so its emission does not contribute to radiative balance at the stratosphere (Hu and Vallis 2019). If a third, even thicker band were introduced, then this logic implies that the thickest band's emission would determine the radiative balance at the stratosphere and constrain T_{re}, rather than the emission from the thinner bands. If we take the spectral limit of an infinite number of bands that vary by orders of magnitude in their optical depth, which is the case for Earth's atmosphere, then T_{re} would be determined primarily by the optically thickest band and constrained by its spectral emission. T_{re} (and hence T_{tp}) would be related to the brightness temperature of that spectral emission. This is essentially what we have calculated in the thermospectric

constraint (Equations 4.5 and 4.6), though framed in a different way. The OLR constraint is only strictly true for a gray atmosphere, and the thermospectric constraint is the generalization of that idea to a spectral, moist atmosphere. Hence, T_{tp} can decouple from OLR, as seen in simulations of FiTT (Figure 4.4c and Seeley et al. (2019) and Seidel and Yang (2022)).

4.7 Discussion

Summary

Spectral radiative transfer decouples Earth's radiative tropopause temperature from the total outgoing radiation and constrains it instead to where water vapor becomes optically thin across *all* wavenumbers and stops radiative cooling. This is set by water vapor's maximum spectroscopic absorption and Clausius-Clapeyron scaling. The thermospectric constraint implies a relatively fixed radiative tropopause temperature (FiTT) with warming because isopleths of water vapor path follows isotherms. However, pressure broadening modifies the strength of spectroscopic absorption as the tropopause rises with surface warming, causing it to warm slightly. FiTT also constrains the meridional distribution of the radiative tropopause, but not the lapse rate tropopause, which is more strongly controlled by dynamics than by radiation. The thermospectric constraint does not rule out a role for processes such as the Brewer-Dobson circulation (which is relatively weak in an aquaplanet, but can affect the tropopause height Birner (2010), Hu and Vallis (2019), and Thuburn and Craig (2000) and ozone (which is not present in our simulations but can affect stratospheric temperature Dacie et al. (2019), Lin et al. (2017), and Thuburn and Craig (2000, 2002), but it does suggest a previously unnoticed mechanism grounded in robust physics is important in controlling tropopause temperature.

Anvil clouds and the tropopause

The temperature of anvil clouds and the tropopause respond similarly to surface warming (Seidel and Yang 2022), despite their ≈ 5 km difference in height (Seeley et al. 2019). The thermospectric constraint offers an explanation. Anvil clouds and the tropopause share a thermodynamic control by water vapor, which is why they respond similarly to warming, but they depend on distinct features of water vapor spectroscopy, so they occur at different temperatures. The radiative tropopause occurs where radiative cooling goes to zero, which is controlled by the maximum spectroscopic absorption ($\kappa_{\mathrm{max}} \approx 13000$ m^2 kg^{-1}): $T_{\mathrm{tp}} = T_{\mathrm{em}}(\kappa_{\mathrm{max}}) \approx 180$ K. Anvil clouds predominantly occur near the max vertical derivative of radiative cooling (Hartmann and Larson 2002b), which is controlled by the *sharp decline* in water vapor's emission line density at $\kappa_{\mathrm{kink}} = 40$ m^2 kg^{-1}: $T_{\mathrm{anvil}} = T_{\mathrm{em}}(\kappa_{\mathrm{kink}}) \approx 214$ K (Jeevanjee and Fueglistaler 2020b). These thermodynamic and spectroscopic ingredients are embedded in most climate models, which could be why the relationship between anvil clouds and the tropopause are robust with respect to modeling configuration (Seidel and Yang 2022). It is possible that the distribution of anvil temperatures/heights is related to the distribution of water vapor absorption coefficients, with the mode of the distribution of anvil

heights at roughly 200 hPa / 215 K aligning with κ_{kink} and the wing of the distbrution at roughly 125 hPa / 190 K (Figure 3.5) aligning with κ_{max}. One question that arises from this work is whether the proportionally higher anvil temperatures (PHAT) seen with warming, which has been explained with changes in static stability Zelinka and Hartmann 2010, might also be due to pressure broadening of water vapor's absorption spectra. Future work could verify the relative contributions of each mechanism.

A role for gray radiative transfer in studying climate?

Water vapor's thermodynamic and radiative properties have distinct but equally profound influences on Earth's climate (Held and Soden 2006; Stevens and Bony 2013), but are gray models of radiative transfer fit for understanding these influences? Gray climate models can capture the interplay of latent heat release and the general circulation (Frierson et al. 2006; Schneider et al. 2010; Vallis 2020), some of the interaction between radiation and moisture necessary for water vapor feedbacks (Byrne and O'Gorman 2013) and the runaway greenhouse effect (Nakajima et al. 1992), and can offer a qualitative understanding of Earth's greenhouse effect (Pierrehumbert 2010).

However, many circulation responses to warming depend sensitively on the radiative response to warming (Ceppi and Hartmann 2016; Kang et al. 2009; Tan et al. 2019; Voigt and Shaw 2015), which stresses the need for more nuanced understanding of radiation. For the problems where a quantitative answer is desired, such as the forcing from CO_2 (He et al. 2023; Jeevanjee et al. 2021a), water vapor feedback (Feng et al. 2023; Koll et al. 2023), and equilibrium climate sensitivity (Jeevanjee 2023; Stevens and Kluft 2023); or for the problems involving vertical gradients in radiative cooling, such as the temperature of anvil clouds (Hartmann and Larson 2002b; Jeevanjee and Fueglistaler 2020b), radiation's wavenumber dependence matters. Spectral theories promise to be the more powerful approach to identifying, studying, and potentially resolving them.

4.8 Supporting Information

Isca Framework

For all simulations, we use Isca, a modeling framework that makes it easy to vary between configurations (Vallis et al. 2018). We use Isca configured as a clear-sky general circulation model (GCM) and a clear-sky single column model (SCM). There is no sea ice, land, or topography. The GCM and SCM configurations use the same column-wise physics routines (e.g., radiative transfer, convective adjustment).

In the GCM, we run at T42 resolution with 40 vertical levels, distributed according to $\sigma = \exp[-7(0.25\tilde{z} + 0.75\tilde{z}^7)]$, where $\tilde{z}$ is evenly spaced on the unit interval. This distribution produces levels that are roughly evenly spaced in the troposphere, and spaced more closely in the stratosphere to mitigate the increasingly coarse resolution that results from distributing levels along even intervals of p. We use a slab mixed-layer ocean with a standard specified

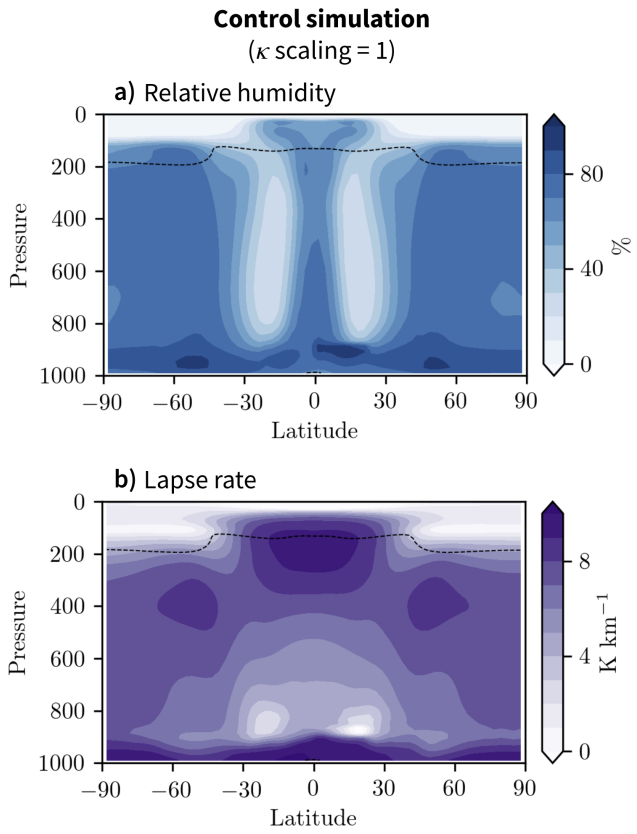

Figure 4.5: **Zonal-mean profiles from control Isca aquaplanet simulation.** (a) Relative humidity. (b) Lapse rate. The dashed line indicates the radiative tropopause. The globally averaged tropospheric lapse rate is 7 K km^{-1}, defined here as the region between the average lifting condensation level ($\approx$ 950 hPa) and the average tropopause height ($\approx$ 150 hPa).

meridional profile of sea surface temperatures (Neale and Hoskins 2000):

$$T_s(\phi) = \begin{cases} 300\big(1 - \sin^2(3\phi/2)\big) \text{ K}, & \text{for } -\pi/3 < \phi < \pi/3 \\ 273 \text{ K}, & \text{otherwise}, \end{cases} \tag{4.9}$$

where ϕ is the latitude.

In the SCM, we run at 80 vertical levels, necessarily omit the dynamical core, and constrain stratospheric water vapor so that it cannot increase with height. We prescribe surface temperature in increments of 10 K by setting the mixed-layer temperature and then setting its depth to 10^9 m.

In both models, we use the simple Betts-Miller convection scheme (Frierson 2007; O'Gorman and Schneider 2008), which drives the free troposphere to a prescribed relative humidity of 70%. Large scale condensation is included to prevent supersaturation, following (Frierson et al. 2006), and all condensed water returns immediately to the surface. Boundary layer

turbulence is parameterized using a k-profile scheme similar to Troen and Mahrt (1986), and diffusion coefficients are obtained from Monin-Obukhov similarity theory (in the column model, this computation uses a prescribed surface wind of $5\,\mathrm{m\,s^{-1}}$). In the SCM, we set the boundary layer depth to the lifting condensation level. For consistency, we also use this method to determine the boundary layer depth in the GCM.

In both the GCM and the SCM, we compute radiative transfer primarily with RRTM (Mlawer et al. 1997). The incoming solar radiation meridional profile resembles Earth's seasonally-averaged profile with a Second Legendre Polynomial. The surface albedo is set to 0.2. CO_2 and water vapor are the only greenhouse gasses (unless specified otherwise). In the SCM, we also run experiments with gray radiative transfer configured to resemble the setup of (Frierson et al. 2006), in which water vapor has no effect on radiative fluxes. That is, the gray optical depth is

$$\tau = \tau_0 \left[f_\ell \left(\frac{p}{p_s} \right) + (1 - f_\ell) \left(\frac{p}{p_s} \right)^4 \right], \tag{4.10}$$

where $\tau_0 = 6$ is the surface optical depth and $f_\ell = 0.1$ is a constant. See Frierson et al. (2006) and the Isca documentation (https://execlim.github.io/Isca/index.html) for details. Atmospheric shortwave absorption is turned off, the surface albedo is still set to 0.2 and the stellar constant is set to 342.5 Wm^2 unless stated otherwise.

When water vapor is coupled to the gray radiative transfer scheme, our approach resembles Byrne and O'Gorman (2013). That is, the optical depth is calculated as a function of specific humidity q (kg kg^{-1}),

$$\frac{d\tau}{d\sigma} = bq, \tag{4.11}$$

where $b = 1997.9$ and $\sigma = p/p_0$, the pressure normalized by a constant (10^5 Pa). See Byrne and O'Gorman (2013) and Vallis et al. (2018) for details.

Diagnosing the tropopause

The radiative tropopause is diagnosed as the lowest layer of atmosphere where radiative cooling goes to zero. In the absence of radiative heating from ozone, the radiative cooling profile asymptotes to zero in the upper troposphere and so a threshold of -0.05 K day^{-1} is used for the SCM and -0.2 K day^{-1} for the GCM. To make the diagnostic less sensitive to model's vertical resolution, the vertical profiles of temperature, pressure, and radiative cooling are linearly interpolated from 40 (GCM) or 80 (SCM) levels to 800.

The lapse rate tropopause is diagnosed as where the lapse rate is smaller than 5 K km^{-1}. This nonstandard threshold is used because there is no ozone present in our simulations, and because the standard choice of 2 K km^{-1} is idiosyncratic to Earth's present day climate (Vallis 2017). Again, the vertical profile is linearly interpolated.

Table 4.1: **Definition of symbols used**. See main text for details on computing $\kappa_{\max}$. See Jeevanjee and Fueglistaler (2020b) for more details and derivations of many of these quantities.

Symbol	Type	Description	Value/Units
ν	Variable	Wavenumber	cm^{-1}
τ_{H_2O}	Variable	Optical depth of water vapor at a given wavenumber	—
κ_{H_2O}	Variable	Spectroscopic absorption of water vapor at a given wavenumber	$\mathrm{m}^2\ \mathrm{kg}^{-1}$
ρ_{H_2O}	Variable	Density of water vapor	$\mathrm{kg\ m}^{-3}$
p_{ref}	Constant	Reference atmospheric pressure	500 hPa
T_{em}	Variable	Emission temperature at a given wavenumber	K
T^*	Constant	Characteristic temperature of water vapor	$LR_d\Gamma/(gR_v) \approx 635$ K
T_{ref}	Variable	Characteristic tropospheric temperature	260 K
T_{tp}	Variable	Tropopause temperature	K
M_v^{ref}	Constant	Characteristic column water vapor mass	$T_{\mathrm{ref}}p_v^\infty/(\Gamma L) \approx 6 \cdot 10^9\ \mathrm{kg\ m}^{-2}$
p_v^∞	Constant	Reference value for the saturation vapor pressure	$2.5 \cdot 10^{11}$ Pa
$\kappa_{\max}$	Constant	Maximum absorption of water vapor	$\approx 13000\ \mathrm{m}^2\ \mathrm{kg}^{-1}$
OLR	Variable	Outgoing longwave radiation	Wm^{-2}

Water vapor spectroscopy

We use PyRADS, a validated line-by-line column model (Koll and Cronin 2018), to plot the spectral line absorption coefficients of water vapor. These data are sourced from the HITRAN 2016 database (Gordon et al. 2017), with a Lorenz line profile assumed for all lines. Data is plotted with 0.1 cm^{-1} spectral resolution.

Table of constants and their values

See Table S1.

Chapter 5

Conclusions, reflections, and outlook

Inspired by *The Blue Marble*, we sought to better understand the coupling between clouds, circulation, and climate sensitivity by studying water vapor's thermospectric properties. What have we learned from our efforts? In this chapter, we review the questions asked in the introduction, the answers we came to in each chapter, the shortcomings of our efforts, and the immediate outlook for future work. We then take away broader insights from our work and why our approach was successful. We use these insights to suggest improvements on formal methods of feedback analysis used in community efforts like CMIP in order to quicken the pace of constraining climate sensitivity and learning about Earth's climate. We conclude with a reflection of how the author's background in physics influenced the research undertaken in this thesis.

5.1 Reinterpreting radiator fins with the longwave clear-sky feedback

The question of how water vapor and atmospheric circulation couple to influence climate stability has been analyzed in a number of idealized contexts so as to better understand Earth's response to increased CO_2. The prototypical example is that of radiative convective equilibrium and the water vapor feedback that ensues from the constraint of fixed relative humidity. This feedback was first captured accurately in the single column model experiments of Manabe and Wetherald (1967). Sixty years on, this water vapor feedback can now be quantitatively understood in terms of an emergent property of water vapor known as *Simpson's Law* (Jeevanjee et al. 2021b), which states that when relative humidity is held fixed, the emission from optically thick water vapor is constant with warming. With this principle, and with the notion of a spectral emitting temperature, one can calculate the strength of the water vapor feedback with pencil and paper (Jeevanjee 2023) and arrive at a nuanced understanding of Earth's radiative response to warming (Feng et al. 2023; Jeevanjee et al. 2021b; Kluft et al. 2021; Koll et al. 2023; Koll and Cronin 2018; Seeley and Jeevanjee 2020; Stevens and Kluft 2023) that is increasingly consistent with observations (Raghuraman et al. 2023; Roemer et al. 2023).

A more complicated example arises from considering the effect of meridional variations in climatological relative humidity on the water vapor feedback. This problem originated from considering how the tropics are stabilized as a whole, especially when the hot and humid tropics are seemingly close to a runaway greenhouse state. The dry subtropics were argued to act as "radiator fins" because they can emit more radiation to space (Pierrehumbert 1995). However, climate stability is more directly related to the change in emission with warming, i.e. the feedback, which leads to the question: do subtropical radiator fins in fact produce a more stabilizing feedback?

We demonstrate that yes, as one moves from the deep tropics to the subtropics, the feedback becomes more stabilizing. At the high surface temperature of the tropics, continuum effects introduce a quadratic dependence of spectroscopic absorption and vapor pressure, which allows variations in tropospheric relative humidity governed by the large scale circulation to have significant control over the width of the water vapor window. From Simpson's law, a

wider window region implies more of the surface's infrared emission spectrum can respond to warming and stabilize the climate more readily than when the window has closed. One immediate take away from this work is that the spectral perspective, though derived in the context of single column physics, can explicate the water vapor feedback in this more complex situation.

Another complication on the water vapor feedback is whether tropospheric relative humidity remains constant with global warming. Chapter 2 does not address this, but another study the author was involved in has shown that a moistening of the subtropics could impact Earth's climate sensitivity when considering large perturbations from its present day climate (Henry et al. 2023). For present-day and near future conditions, analyses based on the assumption of fixed climatological relative humidity seem appropriate (Zhang et al. 2020).

Our analysis extended the increasingly sophisticated clear-sky picture of radiative feedbacks by accounting for the role of optically thick high clouds (anvils). We built a simple model of the longwave anvil cloud radiative effect by assuming that anvils act like a broadband absorber which replaces clear-sky upwelling emission from below with their own infrared emission. This "cloud masking" of clear-sky emission is proportional to anvil cloud fraction and makes the climate less stable overall because anvil cloud infrared emission does not change much with warming due to a thermospectric constraint known as the Fixed Anvil Temperature (FAT) hypothesis (Harrop and Hartmann 2012; Hartmann and Larson 2002b; Jeevanjee and Fueglistaler 2020b).

A challenge that arose in our research was the difficulty in making quantitative comparisons with other studies that use different feedback decompositions. This decomposition of Earth's net feedback into sub-components is arbitrary, in the sense that climate is unchanged how it is analyzed, but it is important because decompositions are quantitatively sensitive to the choice of reference response. Consequently, results using different decompositions cannot be quantitatively compared. The choice is also important because it can simplify interpretations of uncertainty and lead to improved understanding and concordance with observations, a point we revisit later.

5.2 Constraining the radiative response of anvil clouds to warming

In the previous section, we assumed that anvil temperature and area remain fixed with warming, but in reality both of these quantities are expected to change (Bony et al. 2016; Zelinka and Hartmann 2010). The latter change has long been a topic of controversy and confusion (Lindzen et al. 2001; Ramanathan and Collins 1991) and leads to one of the largest sources of uncertainty in estimating Earth's climate sensitivity (Forster et al. 2021; Sherwood et al. 2020). Though this uncertainty is usually attributed to something called the "anvil cloud area feedback", it is more precise to refer to it as the "anvil cloud area-optical depth feedback". This distinction matters because the source of uncertainty in the radiative feedback may be due to changes in area, or it might in fact be due to changes in optical

depth.

To determine whether most of the uncertainty sourced from anvil cloud changes is from their area or their optical depth response to warming, we build upon the simple model of cloud radiative effects used to in the last section. We relax the assumption of fixed cloud properties with warming, we consider shortwave radiation, and we incorporate low clouds to quantify cloud overlap effects. The advantage of this framework is that it transparently relates cloud feedbacks to their present day radiative effects and the change in the cloud property of interest with with warming. The present day radiative effects can be inferred from observations with our simple model, which means that cloud feedbacks can be constrained by examining how plausible a given cloud change is.

In the case of the anvil cloud area feedback, we infer an anvil cloud radiative of -2 Wm^{-2}, which implies that anvil area would have to change by about 50 % K^{-1} to induce a significant feedback. However, this is not physically consistent with the stability iris hypothesis (i.e. changes in the large scale circulation), observations of interannual variability, or the overwhelming majority of climate models. We estimate the area feedback to be nearly neutral. In contrast, the anvil cloud albedo feedback, which is one consequence of a changing optical depth, depends on the shortwave anvil cloud radiative effect. We infer this to be -26 Wm^{-2}, which implies that only a 2 % K^{-1} change in albedo is required to induce a significant feedback. At present, it is unknown how plausible such a change is, and whether the albedo feedback will be nullified by a compensating cloud emissivity feedback. Evidently, changes in anvil cloud optical depth, which have been studied much less than changes in anvil cloud area, are the larger source of uncertainty in estimating Earth's climate sensitivity. Recent studies based on GCM and cloud-resolving models come to a similar conclusion (Stauffer and Wing 2023) and Sokol and Hartmann (in-review).

Our framework used a number of approximations to come to this conclusion and each line of evidence for changes in anvil cloud area has their own biases. Observations are limited by the short satellite record, theories are necessarily simplistic, and even the most detailed simulations of clouds must contend with representing unconstrained microphysics. Like in Stevens et al. 2016, an immediate takeaway from this work is the power of a simple framework that can reconcile different lines of evidence to refute a feedback value and to point out where understanding is fuzzy.

We are hopeful that the uncertain changes in optical depth with warming will be constrained in the near future. There are upcoming opportunities to observe anvil cloud optical thickness from new satellites (EarthCARE and MTG) and unprecedented in-situ measurement campaigns (MAESTRO, PERCUSSION, and PICCOLLO). These independent datasets will allow their cross referencing and validation. To confidently relate these high quality process-level observations to long-term climate change, it would help to relate optical depth changes to large scale constraints, much like how the stability iris hypothesis relates anvil cloud area to large scale subsidence. This recipe of striving for high quality observations and attempting to formulate a theory of how macroscopic cloud properties relates to the large scale circulation is perhaps the best way forward, given the Russian doll-like complexity of cloud microphysics (Morrison et al. 2020).

The philosophy of this approach has precedence, for instance, in understanding changes in anvil cloud area. Compare the progress gained from stability iris theory to the polemical debates surrounding microphysics that preceded it. A similar philosophy operates in geophysical fluid dynamics, where the focus is on constructing theories of emergent phenomena, such as the Gulf Stream, in terms of large scale parameters rather than the properties of individual fluid parcels (Stommel 1948; Vallis 2016). It is the de-facto approach in condensed matter physics, where microscopic degrees of freedom are absorbed into a small number of empirically-determined parameters, and the attention is focused on understanding the macroscopic scales of interest (Goldenfeld et al. 1989; Kardar 2007). These macroscopic theories are not only valued for their necessity in solving difficult problems, they are regarded for being *as fundamental as* the underlying microscopic theories (Anderson 1972). Macroscopic theories are consistent with the underlying microscopic physics, but they are not, in general, conceptually consequent from it. As Philip Anderson put it, *more is different*. When it comes to anvil clouds, microphysics should still be studied, because it is interesting in its own right and because it can lead to better observations and representations in climate models. However, when it comes to inferring the impacts of anvil clouds on climate change, a more "macroscopic" approach may well be the best way forward.

5.3 Water vapor's role in constraining the radiative tropopause temperature

Water vapor's thermodynamic and radiative physics is embedded in much of the behavior of Earth's climate system, as outlined in the introductory chapter. This physics has been argued to constrain the temperature of anvil clouds (Hartmann and Larson 2002b) and may be even more applicable for the radiative tropopause (Seeley et al. 2019). However, longstanding arguments based on TOA energy balance and gray radiative transfer theory suggest that tropopause temperature is directly coupled to OLR (Thuburn and Craig 2000; Vallis et al. 2015), which lies in tension with modeling results suggesting a fixed tropopause temperature independent of OLR (Jeevanjee and Romps 2018; Seeley et al. 2019; Seidel and Yang 2022).

We inspect each of these arguments and find that spectral radiative transfer decouples radiative tropopause temperature from OLR and couples it instead to emission from the most optically thick wavenumber. We show this emission temperature to be constrained by a thermospectric constraint: a combination of Clausius-Clapeyron scaling and water vapor's maximum effective spectroscopic absorption coefficient. We demonstrate this explicitly in both a single column and general circulation model, where varying water vapor's radiative absorption leads to changes in tropopause temperature quantitatively consistent with our theory. A spectral perspective is again able to provide new and quantitative insights into how water vapor interacts with the general circulation. This time, it focuses on the most optically thick wavenumbers, rather than the thinnest ones. That being said, there are limitations to this thermospectric constraint: it is most apt for the radiative tropopause and less so for the lapse rate tropopause, which can vary in temperature significantly with latitude.

Our analysis is necessarily idealized and incomplete to address the full complexity of the tropical tropopause layer (Fueglistaler et al. 2009; Randel and Jensen 2013). There is no ozone (neither interactive nor prescribed), nor are there significant stratospheric dynamics or overshooting convection, and nor is there detailed analysis of the role of CO_2, all of which have been shown to affect the upper troposphere and lower stratosphere (Dacie et al. 2019; Thuburn and Craig 2002). Despite this neglect, or perhaps because of it, the takeaway is that there is a previously unnoticed mechanism (the thermospectric constraint) that constrains tropopause temperature, one that should be embedded within most climate models.

Although we showed that spectroscopy influences tropopause height, the thermospectric constraint is not enough to predict it because the lapse rate must be prescribed. Dynamical considerations can constrain the tropospheric lapse rate to be neutral to convective instability within the tropics (Held 1982; Stone and Carlson 1979), but the constraint is less clear in the extratropics (Schneider 2008; Vallis 2017). The lapse rate may be neutral to baroclinic instability (Held 1982; Stone and Carlson 1979; Zurita-Gotor and Lindzen 2008), slantwise moist convection (Emanuel 1988), or moist convection embedded within baroclinic waves (Emanuel et al. 1987; Juckes 2000), but progress in advancing these theories have been limited by the inability of climate models to simultaneously resolve deep convection and baroclinic eddies. The advent of km-scale models that can resolve both (Stevens et al. 2019) will enable the testing of these constraints and hopefully lead to an even more predictive theory of the tropopause.

Looking further afield, most planets within our solar system appear to have a tropopause at $\mathcal{O}$(100 hPa) (Robinson and Catling 2014). Does the thermospectric constraint extend to other worlds? All greenhouse gasses necessarily have finite spectroscopic absorption (Pierrehumbert 2010), which suggests that the answer might be yes. However, spectroscopy differs from one species to another (Pierrehumbert 2010), and the thermodynamics of exoplanets differ from one another (Ingersoll 2013). These differences may limit the applicability of the cooling to space and emission level approximations employed here to derive an analytical formula for the spectral emitting level (Jeevanjee and Fueglistaler 2020a). Even Titan, with its condensible methane atmosphere complete with a vapor window (McKay et al. 1991), may behave differently because its methane is non-dilute, which may lead to unique and potentially confounding dynamics (Pierrehumbert and Ding 2016). It thus remains to be explored whether greenhouse gas spectroscopy provides the same level of constraint for other worlds as it does for Earth.

5.4 Takeaways

By regarding water vapor as a key intermediary between clouds, circulation, and climate sensitivity, we were able to make progress on the questions posed in this thesis, questions that touch upon grand challenges in climate science (Bony et al. 2015). Here, we would like to reflect on why our physically-based approach was successful and how it could be useful for the climate community in further constraining climate sensitivity.

Appreciate water vapor's thermospectric properties

Some of the key ingredients of Manabe and Wetherald (1967)'s success in estimating climate sensitivity included assuming fixed relative humidity and using a spectral representation of water vapor absorption (Jeevanjee et al. 2022). Chapter 1 showed that such an atmosphere would mask most surface emission and its increase with warming from escaping to space. A simple model of this emergent property could quantitatively estimate the water vapor feedback, thus demonstrating the importance of combining water vapor's thermodynamic and spectroscopic properties in theories of climate change. In this thesis, we embraced these combined thermospectric constraints and were able to add specificity to previous arguments about subtropical radiator fins and the radiative tropopause. Most climate models implicitly have these thermospectric constraints, but most *theories* of climate change appreciate the thermodynamic component far more than the spectroscopic one. It is likely then that there are many more problems that could benefit from a deeper study of water vapor spectroscopy. While the following quote by Johann Wolfgang von Goethe is over dramatic, it captures our message that a fuller appreciation of water vapor's thermospectric properties may lead to deeper insights into Earth's climate: *"Nature understands no jesting [...] The man incapable of appreciating her, she despises; and only to the apt, the pure, and the true, does she resign herself and reveal her secrets."*

Rethinking how to constrain climate sensitivity

Now we would like to argue how a fuller appreciation of water vapor and clouds' physical nature may lead to better methods of constraining climate sensitivity.

The net climate feedback is one of the two relevant parameters for quantifying climate sensitivity (the other being the net forcing). However, understanding the net climate feedback is difficult, so it is often decomposed into easier sub-problems with a "feedback analysis", a framework for quantifying coupled interactions in systems (Roe 2009). Ideally, a feedback decomposition should respect the underlying physics of the climate system and isolate independent feedbacks to facilitate their understanding (Held and Shell 2012; Roe 2009).

In the early days of feedback analysis in climate science, e.g. Hansen et al. (1984), when less was known about how the Earth would respond to warming, the net feedback was decomposed into a "Planck" feedback (p) quantifying the radiative response to vertically uniform tropospheric warming, deviations in the response due to non-vertically uniform warming (lr for Lapse Rate), to changes in specific humidity (q), to changes in surface albedo (α_s), and to changes in clouds (c):

$$\lambda_{\text{net}} = \lambda_{\text{p}} + \lambda_{\text{lr}} + \lambda_{\text{q}} + \lambda_{\alpha_s} + \lambda_{\text{c}}. \tag{5.1}$$

Although this decomposition is still often used today (Forster et al. 2021; Sherwood et al. 2020), it may not provide the best way of understanding Earth's climate sensitivity and isolating sources of uncertainty. For instance, the Planck response assumes that specific humidity is fixed with tropospheric temperature change, but this is physically unrealizable in

Earth's climate (Held and Shell 2012). It also differs from the Stefan-Boltzmann feedback inferred from observations ($\lambda_{\text{sb}} = 4\sigma T_{\text{e}}^3$), where $T_e = (\text{OLR}/\sigma)^{1/4}$, by -0.5 $\text{Wm}^{-2}\text{K}^{-1}$ (Cronin and Dutta 2023). Furthermore, this decomposition exhibits strong correlations between the water vapor (q), and lapse rate feedbacks (Soden and Held 2006; Soden et al. 2008), so they are often summed, thus negating the purpose of the feedback decomposition. There are also correlations between these "clear-sky" feedbacks and the anvil cloud height feedbacks (Soden et al. 2004; Yoshimori et al. 2020), because anvil clouds are kept at fixed height and artificially warmed in calculations of the Planck feedback. This leads to a strongly positive anvil cloud height feedback when their height is allowed to adjust (Zelinka and Hartmann 2010) that compensates the negative contribution from anvil clouds in the Planck feedback. As a result of these correlations, the spread in estimates of individual feedbacks largely cancel in their sum (Held and Shell 2012; Ingram 2012) and are unrepresentative of uncertainty in λ_{net}, which complicates their interpretation.

These deficiencies motivated Held and Shell (2012) and Ingram (2012) to propose using a fixed RH as part of the reference response, which is more concordant with theory, models, and observations (Held and Soden 2000; Romps 2014; Zhang et al. 2020). As a result, the correlations and cancellations in individual feedbacks are reduced between models (Caldwell et al. 2016; Held and Shell 2012; Ingram 2012; Jeevanjee and Fueglistaler 2020b) which simplifies their interpretation. Furthermore, the longwave component of this reference response can now be constrained with observations (Raghuraman et al. 2023; Roemer et al. 2023) and calculated directly from theory (Feng et al. 2023; Koll et al. 2023). Yoshimori et al. (2020) took this one step further and argued that the fixed temperature of anvil clouds should be included in the reference response. Using anvil cloud temperature, rather than pressure as a state variable helps to remove the correlation between the anvil cloud height and Planck feedbacks (Yoshimori et al. 2020) and reveals how clouds "mask" the clear-sky radiative response to warming (McKim et al. 2021; Stevens and Kluft 2023).

By aligning the feedback analysis with the physics of the problem (i.e. using a fixed relative humidity and fixed anvil temperature reference response), uncertainty in individual feedbacks are more representative of the uncertainty in the net feedback. This means that the weakest links in our understanding of climate change can be identified more quickly and addressed more directly. However, it is worth pondering whether feedback analysis can be refined further. The insights gained from clear-sky spectral decompositions (Bourdin et al. 2021; Feng et al. 2023; Jeevanjee 2023; Jeevanjee et al. 2021b; Kluft et al. 2021; Koll et al. 2023; Koll and Cronin 2018; McKim et al. 2021; Seeley and Jeevanjee 2020; Stevens and Kluft 2023) and physically-based cloud feedback decompositions (McKim et al. 2023; McKim et al. 2021; Stevens and Kluft 2023) suggests the answer is probably yes. What would this refined approach look like?

One approach would be to use the physically-based decomposition and storyline-approach of McKim et al. (2023) (Chapter 3) to constrain other feedbacks with hypothesis testing and incorporating multiple lines of evidence. Additionally, the equations that make up each feedback in the decomposition could be used to diagnose intermodel spread and answer whether the spread is due to errors in cloud climatology or cloud changes with warming.

Another approach would be combining spectral insights with a simple model of cloud masking and cloud feedbacks to come up with new hypotheses about how clouds affect the climate system. For instance Stevens and Kluft (2023) raised the possibility that low cloud masking over warm surface temperatures could stabilize the climate by replacing surface emission from a warm surface with a nearly closed water vapor window with emission from a 10 to 15 K cooler "surface" with a much more open water vapor window. They also point to how clouds can mask CO_2 forcing, making their net effect on climate sensitivity more ambiguous. The importance of cloud climatology in masking clear-sky forcings and feedbacks is becoming more apparent. It could be better quantified with theory and observations in the future and potentially lead to an observationally- and physically-informed estimate or "prior" of climate sensitivity with minimal inputs from a climate model (Jeevanjee 2023; Stevens and Kluft 2023), which would be useful for Bayesian reasoning (Sherwood et al. 2020).

We have seen how feedback analyses that do not align with the physics of Earth's climate can lead to misleading notions of strongly stabilizing feedbacks and make it harder to isolate sources of uncertainty. In contrast, a more physically consistent feedback analysis can make better use of theories and observations to constrain individual feedbacks, forcings, and climate sensitivity. The opportunity to constrain climate sensitivity and understand climate change more quickly stresses the need to continually refine feedback analyses as knowledge of the climate system improves. To accelerate this transition to new feedback decompositions, systematic comparisons with the traditional decomposition should be made. This will help to establish continuity with previous work and serve as a "translation tool" that can help ensure confusion and misinterpretations are minimized.

5.5 Personal reflections

When I first became interested in climate science as an undergraduate studying physics, my advisor cautioned me; he worried about the politics that surrounds climate science and how it might influence a young scientist's career. My friends in environmental science were surprised at my interest: despite years of studying the subject, they had never heard that physics has deep roots in climate science. My friends in physics were supportive but were similarly ignorant of these roots. This was understandable. Condensed matter physics, astronomy, and biophysics are all extensions of fundamental physics and were taught in our physics department. Climate science, on the other hand, could only be found in the geography department and there was not a single equation in any of the classes offered on the subject.

I too shared this perception of climate science as an important but non-technical science. As a physicist, someone who is interested not just in the *what* but in the *why*, climate science did not seem so interesting. But that changed when I found opinion pieces and pedagogical articles emphasizing the fundamental role of physics in climate science, the challenges and mysteries that remained, and the impact physicists could make on the field (Marston 2011; Pierrehumbert 2011; Schiermeier 2015; Stevens and Bony 2013; Wettlaufer 2016; Wettlaufer 2011). Here was the chance, I realized, to study something important and relevant to our daily lives, but also something that could offer compelling mysteries. I could still be a

physicist—just one that studies the climate.

I have tried to maintain this identity as a physicist who studies the climate, rather than think of myself as "climate scientist". I do this because the physicist's approach—of chiseling a problem down to the heart of the uncertainty, then proceeding from first principles, piece by piece, question by question, to ultimately arrive at its solution—is the most satisfying approach to understanding the natural world. Physics, then, is the art of perception; of building an awareness of what is essential, and most importantly, asking the right questions. Does a heavy object dropped at the at the same time as a light object hit the Earth first? Does a radiatively neutral anvil cloud's change in area impact climate sensitivity? These simple yes or no questions lead to the next question: *Why?* And that is where the learning begins.

As Lewis Epstein writes (Epstein 2002), "Most people study physics to satisfy some requirement. Some study physics to learn the tricks of Nature so they may find out how to make things bigger or smaller or faster or stronger or more sensitive. But a few, a very few, study physics because they wonder - not how things work, but why they work. They wonder what is at the bottom of things - the very bottom, if there is a bottom". I hope that this thesis gives a flavor not just of how Earth's climate works, but why it works the way it does. I hope it shows there is plenty of physics in climate science and space to wonder. In studying climate science the past few years, my sense of wonder has only grown.

Chapter 6

References

Allan, R. P. et al. (1999). "The dependence of clear-sky outgoing long-wave radiation on surface temperature and relative humidity". In: *Quarterly Journal of the Royal Meteorological Society* 125.558, pp. 2103–2126. DOI: https://doi.org/10.1002/qj.49712555809.

Anderson, P. W. (1972). "More Is Different". In: *Science* 177.4047, pp. 393–396. DOI: 10.1126/science.177.4047.393.

Arakawa, Akio and Wayne Howard Schubert (1974). "Interaction of a Cumulus Cloud Ensemble with the Large-Scale Environment, Part I". In: *Journal of Atmospheric Sciences* 31.3, pp. 674–701. DOI: 10.1175/1520-0469(1974)031<0674:IOACCE>2.0.CO;2.

Armour, Kyle C., Cecilia M. Bitz, and Gerard H. Roe (2013). "Time-Varying Climate Sensitivity from Regional Feedbacks". In: *Journal of Climate* 26.13, pp. 4518–4534. DOI: 10.1175/JCLI-D-12-00544.1.

Bao, Jiawei, Vishal Dixit, and Steven C. Sherwood (2022). "Zonal Temperature Gradients in the Tropical Free Troposphere". In: *Journal of Climate* 35.24, pp. 7937–7948. DOI: 10.1175/JCLI-D-22-0145.1.

Betts, Alan K. (May 1998). "Climate-Convection Feedbacks: Some Further Issues". In: *Climatic Change* 39.1, pp. 35–38. DOI: 10.1023/A:1005323805826.

Betts, Alan K. and W. Ridgway (1989). "Climatic Equilibrium of the Atmospheric Convective Boundary Layer over a Tropical Ocean". In: *Journal of Atmospheric Sciences* 46.17, pp. 2621–2641. DOI: 10.1175/1520-0469(1989)046<2621:CEOTAC>2.0.CO;2.

Beydoun, Hassan et al. (2021). "Dissecting Anvil Cloud Response to Sea Surface Warming". In: *Geophysical Research Letters* 48.15, e2021GL094049. DOI: https://doi.org/10.1029/2021GL094049.

Birner, Thomas (2010). "Residual Circulation and Tropopause Structure". In: *Journal of the Atmospheric Sciences* 67.8, pp. 2582–2600. DOI: https://doi.org/10.1175/2010JAS3287.1.

Bloch-Johnson, Jonah et al. (2021). "Climate Sensitivity Increases Under Higher CO2 Levels Due to Feedback Temperature Dependence". In: *Geophysical Research Letters* 48.4, e2020GL089074. DOI: https://doi.org/10.1029/2020GL089074.

Bony, S et al. (2004). "On dynamic and thermodynamic components of cloud changes". In: *Climate Dynamics* 22.2, pp. 71–86. ISSN: 1432-0894. DOI: 10.1007/s00382-003-0369-6.

Bony, S. et al. (2020). "Observed Modulation of the Tropical Radiation Budget by Deep Convective Organization and Lower-Tropospheric Stability". In: *AGU Advances* 1.3, e2019AV000155. DOI: https://doi.org/10.1029/2019AV000155.

Bony, Sandrine, J.P Duvel, and H. Le Trent (1995). "Observed dependence of the water vapor and clear-sky greenhouse effect on sea surface temperature: comparison with climate warming experiments." In: *Climate Dynamics* 11, pp. 307–320. DOI: https://doi.org/10.1007/BF00211682.

Bony, Sandrine et al. (2015). "Clouds, circulation and climate sensitivity". In: *Nature Geoscience* 8.4, pp. 261–268. DOI: 10.1038/ngeo2398.

Bony, Sandrine et al. (2016). "Thermodynamic control of anvil cloud amount". In: *Proceedings of the National Academy of Sciences* 113.32, pp. 8927–8932. DOI: 10.1073/pnas.1601472113.

Bourdin, Stella, Lukas Kluft, and Bjorn Stevens (2021). "Dependence of Climate Sensitivity on the Given Distribution of Relative Humidity". In: *Geophysical Research Letters* 48.8, e2021GL092462. DOI: https://doi.org/10.1029/2021GL092462.

Bretherton, Christopher S. and Piotr K. Smolarkiewicz (1989). "Gravity Waves, Compensating Subsidence and Detrainment around Cumulus Clouds". In: *Journal of Atmospheric Sciences* 46.6, pp. 740–759. DOI: 10.1175/1520-0469(1989)046<0740:GWCSAD>2.0.CO;2.

Budyko, Mikhail I (1969). "The effect of solar radiation variations on the climate of the Earth". In: *Tellus* 21.5, pp. 611–619.

Byrne, Michael P. and Paul A. O'Gorman (2013). "Land–Ocean Warming Contrast over a Wide Range of Climates: Convective Quasi-Equilibrium Theory and Idealized Simulations". In: *Journal of Climate* 26.12, pp. 4000–4016. DOI: https://doi.org/10.1175/JCLI-D-12-00262.1.

Caldwell, Peter M. et al. (2016). "Quantifying the Sources of Intermodel Spread in Equilibrium Climate Sensitivity". In: *Journal of Climate* 29.2, pp. 513–524. DOI: 10.1175/JCLI-D-15-0352.1.

Ceppi, Paulo and Jonathan M. Gregory (2017). "Relationship of tropospheric stability to climate sensitivity and Earth's observed radiation budget". In: *Proceedings of the National Academy of Sciences* 114.50, pp. 13126–13131. DOI: 10.1073/pnas.1714308114.

Ceppi, Paulo and Dennis L. Hartmann (2016). "Clouds and the Atmospheric Circulation Response to Warming". In: *Journal of Climate* 29.2, pp. 783–799. DOI: 10.1175/JCLI-D-15-0394.1.

Ceppi, Paulo and Peer Nowack (2021). "Observational evidence that cloud feedback amplifies global warming". In: *Proceedings of the National Academy of Sciences* 118.30, e2026290118. DOI: 10.1073/pnas.2026290118.

Ceppi, Paulo et al. (2017). "Cloud feedback mechanisms and their representation in global climate models". In: *WIREs Climate Change* 8.4, e465. DOI: https://doi.org/10.1002/wcc.465.

Cess, R. D. et al. (1989). "Interpretation of Cloud-Climate Feedback as Produced by 14 Atmospheric General Circulation Models". In: *Science* 245.4917, pp. 513–516. ISSN: 0036-8075. DOI: 10.1126/science.245.4917.513.

Cess, R. D. et al. (1990). "Intercomparison and interpretation of climate feedback processes in 19 atmospheric general circulation models". In: *Journal of Geophysical Research: Atmospheres* 95.D10, pp. 16601–16615. DOI: https://doi.org/10.1029/JD095iD10p16601.

Cess, Robert (1975). "Global climate change: an investigation of atmospheric feedback mechanisms". In: *Tellus* 27.3, pp. 193–198. DOI: https://doi.org/10.1111/j.2153-3490.1975.tb01672.x.

Chadwick, Robin, Ian Boutle, and Gill Martin (2013). "Spatial Patterns of Precipitation Change in CMIP5: Why the Rich Do Not Get Richer in the Tropics". In: *Journal of Climate* 26.11, pp. 3803–3822. DOI: 10.1175/JCLI-D-12-00543.1.

Charney, J. et al. (1979). *Carbon Dioxide and Climate: A Scientific Assessment*. Washington, DC: The National Academies Press. DOI: 10.17226/12181.

Charney, Jule G. (1963). "A Note on Large-Scale Motions in the Tropics". In: *Journal of Atmospheric Sciences* 20.6, pp. 607–609. DOI: 10.1175/1520-0469(1963)020<0607:ANOLSM>2.0.CO;2.

Chen, T. S. and George Ohring (1984). "On the Relationship between Clear-Sky Planetary and Surfae Albedos". In: *Journal of Atmospheric Sciences* 41.1, pp. 156–158. DOI: 10.1175/1520-0469(1984)041<0156:OTRBCS>2.0.CO;2.

Chung, Eui-Seok, David Yeomans, and Brian J. Soden (2010). "An assessment of climate feedback processes using satellite observations of clear-sky OLR". In: *Geophysical Research Letters* 37.2. DOI: https://doi.org/10.1029/2009GL041889.

Clough, Shepard A., Michael J. Iacono, and Jean-Luc Moncet (1992). "Line-by-line calculations of atmospheric fluxes and cooling rates: Application to water vapor". In: *Journal of Geophysical Research: Atmospheres* 97.D14, pp. 15761–15785. DOI: https://doi.org/10.1029/92JD01419.

Coakley, J. A. and D. G. Baldwin (1984). "Towards the Objective Analysis of Clouds from Satellite Imagery Data". In: *Journal of Applied Meteorology and Climatology* 23.7, pp. 1065–1099. DOI: 10.1175/1520-0450(1984)023<1065:TTOAOC>2.0.CO;2.

Cronin, Timothy W. and Ishir Dutta (2023). "How Well do We Understand the Planck Feedback?" In: *Journal of Advances in Modeling Earth Systems* 15.7, e2023MS003729. DOI: https://doi.org/10.1029/2023MS003729.

Dacie, Sally et al. (2019). "A 1D RCE Study of Factors Affecting the Tropical Tropopause Layer and Surface Climate". In: *Journal of Climate* 32.20, pp. 6769–6782. DOI: https://doi.org/10.1175/JCLI-D-18-0778.1.

Deser, Clara and John M. Wallace (1990). "Large-Scale Atmospheric Circulation Features of Warm and Cold Episodes in the Tropical Pacific". In: *Journal of Climate* 3.11, pp. 1254–1281. DOI: https://doi.org/10.1175/1520-0442(1990)003<1254:LSACFO>2.0.CO;2.

Dessler, A. E. et al. (2008). "An analysis of the dependence of clear-sky top-of-atmosphere outgoing longwave radiation on atmospheric temperature and water vapor". In: *Journal of Geophysical Research: Atmospheres* 113.D17. DOI: https://doi.org/10.1029/2008JD010137.

Dong, Yue et al. (2019). "Attributing Historical and Future Evolution of Radiative Feedbacks to Regional Warming Patterns using a Green's Function Approach: The preeminence of the Western Pacific". In: *Journal of Climate*. ISSN: 08948755. DOI: 10.1175/JCLI-D-18-0843.1.

Emanuel, Kerry (Aug. 2006). "Hurricanes: Tempests in a greenhouse". In: *Physics Today* 59.8, pp. 74–75. DOI: 10.1063/1.2349743.

— (2008). "Chapter 7 Quasi-Equilibrium Dynamics of the Tropical Atmosphere". In: *The Global Circulation of the Atmosphere*. Ed. by Tapio Schneider and Adam H. Sobel. Princeton: Princeton University Press, pp. 186–218. ISBN: 9780691236919. DOI: doi:10.1515/9780691236919-009.

Emanuel, Kerry et al. (2013). "Influence of Tropical Tropopause Layer Cooling on Atlantic Hurricane Activity". In: *Journal of Climate* 26.7, pp. 2288–2301. DOI: https://doi.org/10.1175/JCLI-D-12-00242.1.

Emanuel, Kerry A. (1988). "Observational Evidence of Slantwise Convective Adjustment". In: *Monthly Weather Review* 116.9, pp. 1805–1816. DOI: https://doi.org/10.1175/1520-0493(1988)116<1805:OEOSCA>2.0.CO;2.

Emanuel, Kerry A., Maurizio Fantini, and Alan J. Thorpe (1987). "Baroclinic Instability in an Environment of Small Stability to Slantwise Moist Convection. Part I: Two-Dimensional Models". In: *Journal of Atmospheric Sciences* 44.12, pp. 1559–1573. DOI: https://doi.org/10.1175/1520-0469(1987)044<1559:BIIAEO>2.0.CO;2.

Epstein, Lewis C. (2002). *Thinking Physics: Understandable Practical Reality*. San Francisco, CA: Insight Press, Inc. ISBN: 978-0935218084.

Feldl, N. and G. H. Roe (2013a). "Four perspectives on climate feedbacks". In: *Geophysical Research Letters* 40.15, pp. 4007–4011. DOI: https://doi.org/10.1002/grl.50711.

Feldl, Nicole and Gerard H. Roe (2013b). "The Nonlinear and Nonlocal Nature of Climate Feedbacks". In: *Journal of Climate* 26.21, pp. 8289–8304. DOI: 10.1175/JCLI-D-12-00631.1.

Feng, Jing, David Paynter, and Raymond Menzel (2023). "How a Stable Greenhouse Effect on Earth Is Maintained Under Global Warming". In: *Journal of Geophysical Research: Atmospheres* 128.9, e2022JD038124. DOI: https://doi.org/10.1029/2022JD038124.

Flanner, M G et al. (2011). "Radiative forcing and albedo feedback from the Northern Hemisphere cryosphere between 1979 and 2008". In: *Nature Geoscience* 4.3, pp. 151–155. ISSN: 1752-0908. DOI: 10.1038/ngeo1062.

Forster, Piers et al. (Oct. 2021). "Chapter 7: The Earth's energy budget, climate feedbacks, and climate sensitivity". In: *Intergovernmenal Panel on Climate Change*. DOI: 10.25455/wgtn.16869671.v1.

Frierson, Dargan M. W. (2007). "The Dynamics of Idealized Convection Schemes and Their Effect on the Zonally Averaged Tropical Circulation". In: *Journal of the Atmospheric Sciences* 64.6, pp. 1959–1976. DOI: https://doi.org/10.1175/JAS3935.1.

Frierson, Dargan M. W., Isaac M. Held, and Pablo Zurita-Gotor (2006). "A Gray-Radiation Aquaplanet Moist GCM. Part I: Static Stability and Eddy Scale". In: *Journal of the Atmospheric Sciences* 63.10, pp. 2548–2566. DOI: https://doi.org/10.1175/JAS3753.1.

Fu, Q., M. Baker, and D. L. Hartmann (2002). "Tropical cirrus and water vapor: an effective Earth infrared iris feedback?" In: *Atmospheric Chemistry and Physics* 2.1, pp. 31–37. DOI: 10.5194/acp-2-31-2002.

Fu, Qiang (2006). "4 - Radiative Transfer". In: *Atmospheric Science (Second Edition)*. Ed. by John M. Wallace and Peter V. Hobbs. Second Edition. San Diego: Academic Press, pp. 113–152. ISBN: 978-0-12-732951-2. DOI: https://doi.org/10.1016/B978-0-12-732951-2.50009-0.

Fu, Qiang and K. N. Liou (1993). "Parameterization of the Radiative Properties of Cirrus Clouds". In: *Journal of Atmospheric Sciences* 50.13, pp. 2008–2025. DOI: https://doi.org/10.1175/1520-0469(1993)050<2008:POTRPO>2.0.CO;2.

Fueglistaler, S. (2019). "Observational Evidence for Two Modes of Coupling Between Sea Surface Temperatures, Tropospheric Temperature Profile, and Shortwave Cloud Radiative Effect in the Tropics". In: *Geophysical Research Letters* 46.16, pp. 9890–9898. DOI: https://doi.org/10.1029/2019GL083990.

Fueglistaler, S. et al. (2009). "Tropical tropopause layer". In: *Reviews of Geophysics* 47.1. DOI: https://doi.org/10.1029/2008RG000267.

Gasparini, B. et al. (2023). "Opinion: Tropical cirrus — From micro-scale processes to climate-scale impacts". In: *EGUsphere* 2023, pp. 1–47. DOI: 10.5194/egusphere-2023-1214.

Gasparini, Blaž et al. (2019). "What Drives the Life Cycle of Tropical Anvil Clouds?" In: *Journal of Advances in Modeling Earth Systems* 11.8, pp. 2586–2605. DOI: https://doi.org/10.1029/2019MS001736.

Goldenfeld, Nigel, Olivier Martin, and Y. Oono (Dec. 1989). "Intermediate asymptotics and renormalization group theory". In: *Journal of Scientific Computing* 4.4, pp. 355–372. DOI: 10.1007/BF01060993.

Gordon, I.E. et al. (2017). "The HITRAN2016 molecular spectroscopic database". In: *Journal of Quantitative Spectroscopy and Radiative Transfer* 203. HITRAN2016 Special Issue, pp. 3–69. ISSN: 0022-4073. DOI: https://doi.org/10.1016/j.jqsrt.2017.06.038.

Hansen, J. et al. (1984). "Climate Sensitivity: Analysis of Feedback Mechanisms". In: *Climate Processes and Climate Sensitivity*. American Geophysical Union (AGU), pp. 130–163. ISBN: 9781118666036. DOI: https://doi.org/10.1029/GM029p0130.

Harrop, Bryce E. and Dennis L. Hartmann (2012). "Testing the Role of Radiation in Determining Tropical Cloud-Top Temperature". In: *Journal of Climate* 25.17, pp. 5731–5747. DOI: https://doi.org/10.1175/JCLI-D-11-00445.1.

Hartmann, Dennis (2015). *Global Physical Climatology*. International Geophysics. Elsevier Science. ISBN: 9780080918624. URL: https://books.google.co.uk/books?id=RsScBAAAQBAJ.

Hartmann, Dennis and Kristin Larson (2002a). "An important constraint on tropical cloud - climate feedback". In: *Geophysical Research Letters* 29.20, pp. 12-1-12–4. DOI: https://doi.org/10.1029/2002GL015835.

Hartmann, Dennis L. (2016). "Tropical anvil clouds and climate sensitivity". In: *Proceedings of the National Academy of Sciences* 113.32, pp. 8897–8899. DOI: 10.1073/pnas.1610455113.

Hartmann, Dennis L. and Sara E. Berry (2017). "The balanced radiative effect of tropical anvil clouds". In: *Journal of Geophysical Research: Atmospheres* 122.9, pp. 5003–5020. DOI: https://doi.org/10.1002/2017JD026460.

Hartmann, Dennis L. and Kristin Larson (2002b). "An important constraint on tropical cloud - climate feedback". In: *Geophysical Research Letters* 29.20, pp. 12-1-12–4. DOI: https://doi.org/10.1029/2002GL015835.

Hartmann, Dennis L. and Marc L. Michelsen (1993). "Large-Scale Effects on the Regulation of Tropical Sea Surface Temperature". In: *Journal of Climate* 6.11, pp. 2049–2062. DOI: 10.1175/1520-0442(1993)006<2049:LSEOTR>2.0.CO;2.

— (2002). "NO EVIDENCE FOR IRIS". In: *Bulletin of the American Meteorological Society* 83.2, pp. 249–254. DOI: 10.1175/1520-0477(2002)083<0249:NEFI>2.3.CO;2.

He, Haozhe et al. (2023). "State dependence of CO2 forcing and its implications for climate sensitivity". In: *Science* 382.6674, pp. 1051–1056. DOI: 10.1126/science.abq6872.

Held, Isaac M. and Arthur Y. Hou (1980). "Nonlinear Axially Symmetric Circulations in a Nearly Inviscid Atmosphere". In: *Journal of Atmospheric Sciences* 37.3, pp. 515–533. DOI: 10.1175/1520-0469(1980)037<0515:NASCIA>2.0.CO;2.

Held, Isaac M. and Karen M. Shell (2012). "Using Relative Humidity as a State Variable in Climate Feedback Analysis". In: *Journal of Climate* 25.8, pp. 2578–2582. DOI: 10.1175/JCLI-D-11-00721.1.

Held, Isaac M. and Brian J. Soden (2000). "Water Vapor Feedback and Global Warming". In: *Annual Review of Energy and the Environment* 25.1, pp. 441–475. DOI: 10.1146/annurev.energy.25.1.441.

— (2006). "Robust Responses of the Hydrological Cycle to Global Warming". In: *Journal of Climate* 19.21, pp. 5686–5699. DOI: 10.1175/JCLI3990.1.

Held, Issac M. (1982). "On the Height of the Tropopause and the Static Stability of the Troposphere". In: *Journal of Atmospheric Sciences* 39.2, pp. 412–417. DOI: https://doi.org/10.1175/1520-0469(1982)039<0412:OTHOTT>2.0.CO;2.

Henry, Matthew et al. (2023). "State-Dependence of the Equilibrium Climate Sensitivity in a Clear-Sky GCM". In: *Geophysical Research Letters* 50.23, e2023GL104413. DOI: https://doi.org/10.1029/2023GL104413.

Hersbach, Hans et al. (2020). "The ERA5 global reanalysis". In: *Quarterly Journal of the Royal Meteorological Society* 146.730, pp. 1999–2049. DOI: https://doi.org/10.1002/qj.3803.

Highwood, E. J. and B. J. Hoskins (1998). "The tropical tropopause". In: *Quarterly Journal of the Royal Meteorological Society* 124.549, pp. 1579–1604. DOI: https://doi.org/10.1002/qj.49712454911.

Hu, Shineng and Geoffrey K. Vallis (2019). "Meridional structure and future changes of tropopause height and temperature". In: *Quarterly Journal of the Royal Meteorological Society* 145.723, pp. 2698–2717. DOI: https://doi.org/10.1002/qj.3587.

Igel, Matthew R., Aryeh J. Drager, and Susan C. van den Heever (2014). "A CloudSat cloud object partitioning technique and assessment and integration of deep convective anvil sensitivities to sea surface temperature". In: *Journal of Geophysical Research: Atmospheres* 119.17, pp. 10515–10535. DOI: https://doi.org/10.1002/2014JD021717.

Ingersoll, Andrew P. (2013). *Planetary Climates*. STU - Student edition. Princeton University Press. ISBN: 0691145059. (Visited on 01/18/2024).

Ingram, W. J. (2012). "Water vapor feedback in a small ensemble of GCMs: Two approaches". In: *Journal of Geophysical Research: Atmospheres* 117.D12. DOI: https://doi.org/10.1029/2011JD017221.

Ingram, William (2010). "A very simple model for the water vapour feedback on climate change". In: *Quarterly Journal of the Royal Meteorological Society* 136.646, pp. 30–40.

IPCC (2021). "Summary for Policymakers". In: *Climate Change 2021: The Physical Science Basis. Contribution of Working Group I to the Sixth Assessment Report of the Intergovernmental Panel on Climate Change*. Ed. by V. Masson-Delmotte et al. Cambridge, United Kingdom and New York, NY, USA: Cambridge University Press, 3-32. DOI: 10.1017/9781009157896.001.

Ito, Masato and Hirohiko Masunaga (2022). "Process-Level Assessment of the Iris Effect Over Tropical Oceans". In: *Geophysical Research Letters* 49.7, e2022GL097997. DOI: https://doi.org/10.1029/2022GL097997.

Jeevanjee, N. et al. (2021a). "An Analytical Model for Spatially Varying Clear-Sky CO2 Forcing". In: *Journal of Climate* 34.23, pp. 9463–9480. DOI: https://doi.org/10.1175/JCLI-D-19-0756.1.

Jeevanjee, Nadir (2018). *The physics of climate change: simple models in climate science*. arXiv: 1802.02695 [physics.ao-ph]. URL: http://arxiv.org/abs/1802.02695.

— (2022). "Three Rules for the Decrease of Tropical Convection With Global Warming". In: *Journal of Advances in Modeling Earth Systems* 14.11, e2022MS003285. DOI: https://doi.org/10.1029/2022MS003285.

— (Sept. 2023). "Climate sensitivity from radiative-convective equilibrium: A chalkboard approacha)". In: *American Journal of Physics* 91.9, pp. 731–745. ISSN: 0002-9505. DOI: 10.1119/5.0135727.

Jeevanjee, Nadir and Stephan Fueglistaler (2020a). "On the Cooling-to-Space Approximation". In: *Journal of the Atmospheric Sciences* 77.2, pp. 465–478. DOI: 10.1175/JAS-D-18-0352.1.

— (2020b). "Simple Spectral Models for Atmospheric Radiative Cooling". In: *Journal of the Atmospheric Sciences* 77.2, pp. 479–497. DOI: https://doi.org/10.1175/JAS-D-18-0347.1.

Jeevanjee, Nadir, Isaac Held, and V. Ramaswamy (2022). "Manabe's Radiative–Convective Equilibrium". In: *Bulletin of the American Meteorological Society* 103.11, E2559–E2569. DOI: 10.1175/BAMS-D-21-0351.1. URL: https://journals.ametsoc.org/view/journals/bams/103/11/BAMS-D-21-0351.1.xml.

Jeevanjee, Nadir, Daniel D. B. Koll, and Nicholas Lutsko (2021b). ""Simpson's Law" and the Spectral Cancellation of Climate Feedbacks". In: *Geophysical Research Letters* 48.14, e2021GL093699. DOI: https://doi.org/10.1029/2021GL093699.

Jeevanjee, Nadir and David M. Romps (2018). "Mean precipitation change from a deepening troposphere". In: *Proceedings of the National Academy of Sciences* 115.45, pp. 11465–11470. DOI: 10.1073/pnas.1720683115.

Jenney, A. M., D. A. Randall, and M. D. Branson (2020). "Understanding the Response of Tropical Ascent to Warming Using an Energy Balance Framework". In: *Journal of Advances in Modeling Earth Systems* 12.6, e2020MS002056. DOI: https://doi.org/10.1029/2020MS002056.

Johnson, Richard H. et al. (1999). "Trimodal Characteristics of Tropical Convection". In: *Journal of Climate* 12.8, pp. 2397–2418. DOI: 10.1175/1520-0442(1999)012<2397:TCOTC>2.0.CO;2.

Juckes, M. N. (2000). "The Static Stability of the Midlatitude Troposphere: The Relevance of Moisture". In: *Journal of the Atmospheric Sciences* 57.18, pp. 3050–3057. DOI: https://doi.org/10.1175/1520-0469(2000)057<3050:TSSOTM>2.0.CO;2.

Kang, Sarah M., Dargan M. W. Frierson, and Isaac M. Held (2009). "The Tropical Response to Extratropical Thermal Forcing in an Idealized GCM: The Importance of Radiative Feedbacks and Convective Parameterization". In: *Journal of the Atmospheric Sciences* 66.9, pp. 2812–2827. DOI: 10.1175/2009JAS2924.1.

Kardar, Mehran (2007). *Statistical Physics of Fields*. Cambridge University Press.

Kiehl, J. T. (1994). "On the Observed Near Cancellation between Longwave and Shortwave Cloud Forcing in Tropical Regions". In: *Journal of Climate* 7.4, pp. 559–565. DOI: 10.1175/1520-0442(1994)007<0559:OTONCB>2.0.CO;2.

Klein, Stephen A. et al. (Nov. 2017). "Low-Cloud Feedbacks from Cloud-Controlling Factors: A Review". In: *Surveys in Geophysics* 38.6, pp. 1307–1329. URL: https://doi.org/10.1007/s10712-017-9433-3.

Kluft, Lukas et al. (2021). "Temperature-dependence of the clear-sky feedback in radiative-convective equilibrium". In: *Geophysical Research Letters* Submitted. DOI: https://doi.org/10.1002/essoar.10506363.1.

Knutson, Thomas R. and Syukuro Manabe (1995). "Time-Mean Response over the Tropical Pacific to Increased CO 2 in a Coupled Ocean–Atmosphere Model". In: *Journal of Climate* 8.9, pp. 2181–2199. ISSN: 08948755, 15200442. (Visited on 02/20/2024).

Koll, D. D. B., N. Jeevanjee, and N. J. Lutsko (2023). "An Analytic Model for the Clear-Sky Longwave Feedback". In: *Journal of the Atmospheric Sciences*. DOI: https://doi.org/10.1175/JAS-D-22-0178.1.

Koll, Daniel D. B. and Timothy W. Cronin (2018). "Earth's outgoing longwave radiation linear due to H2O greenhouse effect". In: *Proceedings of the National Academy of Sciences* 115.41, pp. 10293–10298. DOI: 10.1073/pnas.1809868115.

— (Aug. 2019). *PyRADS: Python RADiation model for planetary atmosphereS*. ascl: 1908.009.

Kotarba, Andrzej Z. and Mateusz Solecki (2021). "Uncertainty Assessment of the Vertically-Resolved Cloud Amount for Joint CloudSat–CALIPSO Radar–Lidar Observations". In: *Remote Sensing* 13.4. ISSN: 2072-4292. DOI: 10.3390/rs13040807.

Kubar, Terence L. and Jonathan H. Jiang (2019). "Net Cloud Thinning, Low-Level Cloud Diminishment, and Hadley Circulation Weakening of Precipitating Clouds with Tropical West Pacific SST Using MISR and Other Satellite and Reanalysis Data". In: *Remote Sensing* 11.10. ISSN: 2072-4292. DOI: 10.3390/rs11101250.

L'Ecuyer, Tristan S. et al. (2019). "Reassessing the Effect of Cloud Type on Earth's Energy Balance in the Age of Active Spaceborne Observations. Part I: Top of Atmosphere and Surface". In: *Journal of Climate* 32.19, pp. 6197–6217. DOI: 10.1175/JCLI-D-18-0753.1.

Larson, Kristin, Dennis L. Hartmann, and Stephen A. Klein (1999). "The Role of Clouds, Water Vapor, Circulation, and Boundary Layer Structure in the Sensitivity of the Tropical Climate". In: *Journal of Climate* 12.8, pp. 2359–2374. DOI: 10.1175/1520-0442(1999)012<2359:TROCWV>2.0.CO;2.

Lau, K-M., H-T. Wu, and S. Bony (1997). "The Role of Large-Scale Atmospheric Circulation in the Relationship between Tropical Convection and Sea Surface Temperature". In: *Journal of Climate* 10.3, pp. 381–392. DOI: 10.1175/1520-0442(1997)010<0381:TROLSA>2.0.CO;2.

Li, R. L. et al. (2019). "A Positive Iris Feedback: Insights from Climate Simulations with Temperature-Sensitive Cloud–Rain Conversion". In: *Journal of Climate* 32.16, pp. 5305–5324. DOI: https://doi.org/10.1175/JCLI-D-18-0845.1.

Lin, Bing et al. (2002). "The Iris Hypothesis: A Negative or Positive Cloud Feedback?" In: *Journal of Climate* 15.1, pp. 3–7. DOI: 10.1175/1520-0442(2002)015<0003:TIHANO>2.0.CO;2.

Lin, Pu et al. (2017). "Changes of the Tropical Tropopause Layer under Global Warming". In: *Journal of Climate* 30.4, pp. 1245–1258. DOI: 10.1175/JCLI-D-16-0457.1. URL: https://journals.ametsoc.org/view/journals/clim/30/4/jcli-d-16-0457.1.xml.

Lindzen, Richard S., Ming-Dah Chou, and Arthur Y. Hou (2001). "Does the Earth Have an Adaptive Infrared Iris?" In: *Bulletin of the American Meteorological Society* 82.3, pp. 417–432. DOI: 10.1175/1520-0477(2001)082<0417:DTEHAA>2.3.CO;2.

Loeb, Norman G. et al. (2018). "Clouds and the Earth's Radiant Energy System (CERES) Energy Balanced and Filled (EBAF) Top-of-Atmosphere (TOA) Edition-4.0 Data Product". In: *Journal of Climate* 31.2, pp. 895–918. DOI: 10.1175/JCLI-D-17-0208.1.

Loeb, Norman G. et al. (2020). "Toward a Consistent Definition between Satellite and Model Clear-Sky Radiative Fluxes". In: *Journal of Climate* 33.1, pp. 61–75. DOI: 10.1175/JCLI-D-19-0381.1.

Lutsko, Nicholas J., Steven C. Sherwood, and Ming Zhao (2023). "Precipitation Efficiency and Climate Sensitivity". In: *Clouds and Their Climatic Impacts*. American Geophysical Union (AGU). Chap. 13, pp. 271–285. ISBN: 9781119700357. DOI: 10.1002/9781119700357.ch13.

Manabe, Syukuro and Robert F. Strickler (1964). "Thermal Equilibrium of the Atmosphere with a Convective Adjustment". In: *Journal of Atmospheric Sciences* 21.4, pp. 361–385. DOI: https://doi.org/10.1175/1520-0469(1964)021<0361:TEOTAW>2.0.CO;2.

Manabe, Syukuro and Richard T. Wetherald (1967). "Thermal Equilibrium of the Atmosphere with a Given Distribution of Relative Humidity". In: *Journal of Atmospheric Sciences* 24.3, pp. 241–259. DOI: 10.1175/1520-0469(1967)024<0241:TEOTAW>2.0.CO;2.

Marston, J.B. (2011). "Looking for new problems to solve? Consider the climate". In: *Physics* 4, p. 20.

Match, Aaron and Edwin P. Gerber (2022). "Tropospheric Expansion Under Global Warming Reduces Tropical Lower Stratospheric Ozone". In: *Geophysical Research Letters* 49.19, e2022GL099463. DOI: https://doi.org/10.1029/2022GL099463.

Mauritsen, Thorsten (2016). "Clouds cooled the Earth". In: *Nature Geoscience* 9.12, pp. 865–867. ISSN: 1752-0908. DOI: 10.1038/ngeo2838.

Mauritsen, Thorsten and Bjorn Stevens (2015). "Missing iris effect as a possible cause of muted hydrological change and high climate sensitivity in models". In: *Nature Geoscience* 8.April, pp. 8–13. DOI: 10.1038/ngeo2414.

McKay, Christopher P., James B. Pollack, and Régis Courtin (1991). "The Greenhouse and Antigreenhouse Effects on Titan". In: *Science* 253.5024, pp. 1118–1121. DOI: 10.1126/science.11538492.

McKim, Brett, Sandrine Bony, and Jean-Louis Dufresne (June 2023). "Physical and observational constraints on the anvil cloud area feedback". In: DOI: 10.22541/au.167769953.39966398/v2.

McKim, Brett A., Nadir Jeevanjee, and Geoffrey K. Vallis (2021). "Joint Dependence of Longwave Feedback on Surface Temperature and Relative Humidity". In: *Geophysical Research Letters* 48.18, e2021GL094074. DOI: https://doi.org/10.1029/2021GL094074.

Meraner, Katharina, Thorsten Mauritsen, and Aiko Voigt (2013). "Robust increase in equilibrium climate sensitivity under global warming". In: *Geophysical Research Letters* 40.22, pp. 5944–5948. DOI: https://doi.org/10.1002/2013GL058118.

Mlawer, Eli J. et al. (1997). "Radiative transfer for inhomogeneous atmospheres: RRTM, a validated correlated-k model for the longwave". In: *Journal of Geophysical Research: Atmospheres* 102.D14, pp. 16663–16682. DOI: https://doi.org/10.1029/97JD00237.

Morice, C. P. et al. (2021). "An Updated Assessment of Near-Surface Temperature Change From 1850: The HadCRUT5 Data Set". In: *Journal of Geophysical Research: Atmospheres* 126.3, e2019JD032361. DOI: https://doi.org/10.1029/2019JD032361.

Morrison, Hugh et al. (2020). "Confronting the Challenge of Modeling Cloud and Precipitation Microphysics". In: *Journal of Advances in Modeling Earth Systems* 12.8, e2019MS001689. DOI: https://doi.org/10.1029/2019MS001689.

Mote, Philip W. et al. (1996). "An atmospheric tape recorder: The imprint of tropical tropopause temperatures on stratospheric water vapor". In: *Journal of Geophysical Research: Atmospheres* 101.D2, pp. 3989–4006. DOI: https://doi.org/10.1029/95JD03422.

Myers, Timothy A et al. (2021). "Observational constraints on low cloud feedback reduce uncertainty of climate sensitivity". In: *Nature Climate Change* 11.6, pp. 501–507. ISSN: 1758-6798. DOI: 10.1038/s41558-021-01039-0.

Nakajima, Shinichi, Yoshi-Yuki Hayashi, and Yutaka Abe (1992). "A Study on the "Runaway Greenhouse Effect" with a One-Dimensional Radiative–Convective Equilibrium Model". In: *Journal of Atmospheric Sciences* 49.23, pp. 2256–2266. DOI: https://doi.org/10.1175/1520-0469(1992)049<2256:ASOTGE>2.0.CO;2.

NASA/LARC/SD/ASDC (Dec. 5, 2018). *CALIPSO Lidar Level 3 Cloud Occurrence Data, Standard V1-00*. URL: https://doi.org/10.5067/CALIOP/CALIPSO/L3_CLOUD_OCCURRENCE-STANDARD-V1-00.

Neale, R. B. and B. J. Hoskins (2000). "A standard test for AGCMs including their physical parametrizations: I: the proposal". In: *Atmospheric Science Letters* 1.2, pp. 101–107. DOI: https://doi.org/10.1006/asle.2000.0022.

Neelin, J. David and Isaac M. Held (1987). "Modeling Tropical Convergence Based on the Moist Static Energy Budget". In: *Monthly Weather Review* 115.1, pp. 3–12. DOI: 10.1175/1520-0493(1987)115<0003:MTCBOT>2.0.CO;2.

O'Gorman, Paul A. and Tapio Schneider (2008). "The Hydrological Cycle over a Wide Range of Climates Simulated with an Idealized GCM". In: *Journal of Climate* 21.15, p. 3815. DOI: 10.1175/2007JCLI2065.1.

O'Gorman, Paul A. (2011). "The Effective Static Stability Experienced by Eddies in a Moist Atmosphere". In: *Journal of the Atmospheric Sciences* 68.1, pp. 75–90. DOI: 10.1175/2010JAS3537.1.

Oreopoulos, Lazaros, Nayeong Cho, and Dongmin Lee (2022). "Revisiting cloud overlap with a merged dataset of liquid and ice cloud extinction from CloudSat and CALIPSO". In: *Frontiers in Remote Sensing* 3. ISSN: 2673-6187. DOI: 10.3389/frsen.2022.1076471.

Parodi, Antonio and Kerry Emanuel (2009). "A Theory for Buoyancy and Velocity Scales in Deep Moist Convection". In: *Journal of the Atmospheric Sciences* 66.11, pp. 3449–3463. DOI: 10.1175/2009JAS3103.1.

Phillips, Norman A. (1956). "The general circulation of the atmosphere: A numerical experiment". In: *Quarterly Journal of the Royal Meteorological Society* 82.352, pp. 123–164. DOI: https://doi.org/10.1002/qj.49708235202.

Pierrehumbert, R. T. (1995). "Thermostats, Radiator Fins, and the Local Runaway Greenhouse". In: *Journal of Atmospheric Sciences* 52.10, pp. 1784–1806. DOI: 10.1175/1520-0469(1995)052<1784:TRFATL>2.0.CO;2.

Pierrehumbert, Raymond T. (2010). *Principles of Planetary Climate*. Cambridge University Press. DOI: 10.1017/CBO9780511780783.

— (Jan. 2011). "Infrared radiation and planetary temperature". In: *Physics Today* 64.1, pp. 33–38. ISSN: 0031-9228. DOI: 10.1063/1.3541943. eprint: https://pubs.aip.org/physicstoday/article-pdf/64/1/33/9879821/33_1_online.pdf. URL: https://doi.org/10.1063/1.3541943.

Pierrehumbert, Raymond T. and Feng Ding (2016). "Dynamics of atmospheres with a non-dilute condensible component". In: *Proceedings of the Royal Society A: Mathematical, Physical and Engineering Sciences* 472.2190, p. 20160107. DOI: 10.1098/rspa.2016.0107.

Raghuraman, Shiv Priyam et al. (2023). "Greenhouse Gas Forcing and Climate Feedback Signatures Identified in Hyperspectral Infrared Satellite Observations". In: *Geophysical Research Letters* 50.24, e2023GL103947. DOI: https://doi.org/10.1029/2023GL103947.

Ramanathan, V and W Collins (1991). "Thermodynamic regulation of ocean warming by cirrus clouds deduced from observations of the 1987 El Niño". In: *Nature* 351.6321, pp. 27–32. ISSN: 1476-4687. DOI: 10.1038/351027a0.

Ramanathan, V. et al. (1989). "Cloud-Radiative Forcing and Climate: Results from the Earth Radiation Budget Experiment". In: *Science* 243.4887, pp. 57–63. DOI: 10.1126/science.243.4887.57.

Randel, William J. and Eric J. Jensen (Mar. 2013). "Physical processes in the tropical tropopause layer and their roles in a changing climate". In: *Nature Geoscience* 6.3, pp. 169–176. DOI: 10.1038/ngeo1733. URL: https://doi.org/10.1038/ngeo1733.

Raval, A., A. H. Oort, and V. Ramaswamy (1994). "Observed Dependence of Outgoing Longwave Radiation on Sea Surface Temperature and Moisture". In: *Journal of Climate* 7.5, pp. 807–821. DOI: 10.1175/1520-0442(1994)007<0807:ODOOLR>2.0.CO;2.

Raymond, David J. (1995). "Regulation of Moist Convection over the West Pacific Warm Pool". In: *Journal of Atmospheric Sciences* 52.22, pp. 3945–3959. DOI: 10.1175/1520-0469(1995)052<3945:ROMCOT>2.0.CO;2.

Riehl, H. and J.S. Malkus (1958). "On the Heat Balance in the Equatorial Trough Zone". In: *Geophysica* 3, pp. 503–538.

Robinson, T. D. and D. C. Catling (Jan. 2014). "Common 0.1 bar tropopause in thick atmospheres set by pressure-dependent infrared transparency". In: *Nature Geoscience* 7.1, pp. 12–15. DOI: 10.1038/ngeo2020.

Roe, Gerard (2009). "Feedbacks, Timescales, and Seeing Red". In: *Annual Review of Earth and Planetary Sciences* 37.1, pp. 93–115. DOI: 10.1146/annurev.earth.061008.134734.

Roemer, Florian E. et al. (May 2023). "Direct observation of Earth's spectral long-wave feedback parameter". In: *Nature Geoscience* 16.5, pp. 416–421. DOI: 10.1038/s41561-023-01175-6.

Romps, David M. (2014). "An Analytical Model for Tropical Relative Humidity". In: *Journal of Climate* 27.19, pp. 7432–7449. DOI: https://doi.org/10.1175/JCLI-D-14-00255.1.

— (2016). "Clausius–Clapeyron Scaling of CAPE from Analytical Solutions to RCE". In: *Journal of the Atmospheric Sciences* 73.9, pp. 3719–3737. DOI: https://doi.org/10.1175/JAS-D-15-0327.1.

— (Feb. 2020). "Fundamental Aspects of Turbulent Flows in Climate Dynamics". In: ed. by Freddy Bouchet et al. Vol. 109. Lecture Notes of the Les Houches Summer School August 2017. Oxford University Press. Chap. Theory of Tropical Moist Convection, pp. 1–45. DOI: 10.1093/oso/9780198855217.003.0001.

Saint-Lu, Marion, Sandrine Bony, and Jean-Louis Dufresne (2020). "Observational Evidence for a Stability Iris Effect in the Tropics". In: *Geophysical Research Letters* 47.14, e2020GL089059. DOI: https://doi.org/10.1029/2020GL089059.

— (2022). "Clear-sky control of anvils in response to increased CO2 or surface warming or volcanic eruptions". In: *npj Climate and Atmospheric Science* 5.1, p. 78. ISSN: 2397-3722. DOI: 10.1038/s41612-022-00304-z.

Schiermeier, Quirin (Apr. 2015). "Climatologists to physicists: your planet needs you". In: *Nature* 520.7546, pp. 140–141. DOI: 10.1038/520140a. URL: https://doi.org/10.1038/520140a.

Schneider, Tapio (2004). "The Tropopause and the Thermal Stratification in the Extratropics of a Dry Atmosphere". In: *Journal of the Atmospheric Sciences* 61.12, pp. 1317–1340. DOI: https://doi.org/10.1175/1520-0469(2004)061<1317:TTATTS>2.0.CO;2.

— (2008). "Chapter 3 The Thermal Stratification of the Extratropical Troposphere". In: *The Global Circulation of the Atmosphere*. Princeton: Princeton University Press, pp. 47–77. ISBN: 9780691236919. DOI: doi:10.1515/9780691236919-005.

Schneider, Tapio, Paul A. O'Gorman, and Xavier J. Levine (2010). "WATER VAPOR AND THE DYNAMICS OF CLIMATE CHANGES". In: *Reviews of Geophysics* 48.3. DOI: https://doi.org/10.1029/2009RG000302.

Schneider, Tapio and Paul A. O'Gorman (2008). "Moist Convection and the Thermal Stratification of the Extratropical Troposphere". In: *Journal of the Atmospheric Sciences* 65.11, pp. 3571–3583. DOI: 10.1175/2008JAS2652.1.

Seeley, Jacob T. and Nadir Jeevanjee (2020). "H2O Windows and CO2 Radiator Fins: A Clear-Sky Explanation for the Peak in Equilibrium Climate Sensitivity". In: *Geophysical Research Letters* 48.4, e2020GL089609. DOI: https://doi.org/10.1029/2020GL089609.

Seeley, Jacob T., Nadir Jeevanjee, and David M. Romps (2019). "FAT or FiTT: Are Anvil Clouds or the Tropopause Temperature Invariant?" In: *Geophysical Research Letters* 46.3, pp. 1842–1850. DOI: https://doi.org/10.1029/2018GL080096.

Seidel, Seth D. and Da Yang (2022). "Temperatures of Anvil Clouds and Radiative Tropopause in a Wide Array of Cloud-Resolving Simulations". In: *Journal of Climate* 35.24, pp. 8065–8078. DOI: https://doi.org/10.1175/JCLI-D-21-0962.1.

Sherwood, S. C. et al. (2020). "An Assessment of Earth's Climate Sensitivity Using Multiple Lines of Evidence". In: *Reviews of Geophysics* 58.4, e2019RG000678. DOI: https://doi.org/10.1029/2019RG000678.

Siebesma, A.P. et al. (2020). *Clouds and Climate: Climate Science's Greatest Challenge*. Cambridge University Press. ISBN: 9781107061071. URL: https://books.google.co.uk/books?id=rvXvDwAAQBAJ.

Simpson, G. C. (1928). "FURTHER STUDIES IN TERRESTRIAL RADIATION". In: *Monthly Weather Review* 56.8, pp. 322–323. DOI: https://doi.org/10.1175/1520-0493(1928)56<322:FSITR>2.0.CO;2.

Sobel, Adam H., Johan Nilsson, and Lorenzo M. Polvani (2001). "The Weak Temperature Gradient Approximation and Balanced Tropical Moisture Waves". In: *Journal of the Atmospheric Sciences* 58.23, pp. 3650–3665. DOI: 10.1175/1520-0469(2001)058<3650:TWTGAA>2.0.CO;2.

Soden, Brian J., Anthony J. Broccoli, and Richard S. Hemler (2004). "On the Use of Cloud Forcing to Estimate Cloud Feedback". In: *Journal of Climate* 17.19, pp. 3661–3665. DOI: 10.1175/1520-0442(2004)017<3661:OTUOCF>2.0.CO;2.

Soden, Brian J. and Isaac M. Held (2006). "An Assessment of Climate Feedbacks in Coupled Ocean–Atmosphere Models". In: *Journal of Climate* 19.14, pp. 3354–3360. DOI: 10.1175/JCLI3799.1.

Soden, Brian J. et al. (2008). "Quantifying Climate Feedbacks Using Radiative Kernels". In: *Journal of Climate* 21.14, pp. 3504–3520. DOI: 10.1175/2007JCLI2110.1.

Spaulding-Astudillo, Francisco E. and Jonathan L. Mitchell (2023). "Effects of Varying Saturation Vapor Pressure on Climate, Clouds, and Convection". In: *Journal of the Atmospheric Sciences* 80.5, pp. 1247–1266. DOI: https://doi.org/10.1175/JAS-D-22-0063.1.

Stauffer, C. L. and A. A. Wing (2023). "Explicitly Resolved Cloud Feedbacks in the Radiative-Convective Equilibrium Model Intercomparison Project". In: *Journal of Advances in Modeling Earth Systems* 15.11, e2023MS003738. DOI: https://doi.org/10.1029/2023MS003738.

Stauffer, Catherine L. and Allison A. Wing (2022). "Properties, Changes, and Controls of Deep-Convecting Clouds in Radiative-Convective Equilibrium". In: *Journal of Advances in Modeling Earth Systems* 14.6, e2021MS002917. DOI: https://doi.org/10.1029/2021MS002917.

Stevens, B. and L. Kluft (2023). "A Colorful look at Climate Sensitivity". In: *EGUsphere* 2023, pp. 1–24. DOI: 10.5194/egusphere-2022-1460.

Stevens, Bjorn and Sandrine Bony (June 2013). "Water in the atmosphere". In: *Physics Today* 66.6, pp. 29–34. ISSN: 0031-9228. DOI: 10.1063/PT.3.2009.

Stevens, Bjorn et al. (2016). "Prospects for narrowing bounds on Earth's equilibrium climate sensitivity". In: *Earth's Future* 4.11, pp. 512–522. DOI: https://doi.org/10.1002/2016EF000376.

Stevens, Bjorn et al. (Sept. 2019). "DYAMOND: the DYnamics of the Atmospheric general circulation Modeled On Non-hydrostatic Domains". In: *Progress in Earth and Planetary Science* 6.1, p. 61. DOI: 10.1186/s40645-019-0304-z.

Stommel, Henry (1948). "The westward intensification of wind-driven ocean currents". In: *Eos, Transactions American Geophysical Union* 29.2, pp. 202–206. DOI: https://doi.org/10.1029/TR029i002p00202.

Stone, Peter H. and John H. Carlson (1979). "Atmospheric Lapse Rate Regimes and Their Parameterization". In: *Journal of Atmospheric Sciences* 36.3, pp. 415–423. DOI: https://doi.org/10.1175/1520-0469(1979)036<0415:ALRRAT>2.0.CO;2.

Tan, Zhihong, Orli Lachmy, and Tiffany A. Shaw (2019). "The Sensitivity of the Jet Stream Response to Climate Change to Radiative Assumptions". In: *Journal of Advances in Modeling Earth Systems* 11.4, pp. 934–956. DOI: https://doi.org/10.1029/2018MS001492.

Thompson, David W. J., Sandrine Bony, and Ying Li (2017). "Thermodynamic constraint on the depth of the global tropospheric circulation". In: *Proceedings of the National Academy of Sciences* 114.31, pp. 8181–8186. DOI: 10.1073/pnas.1620493114.

Thompson, David W. J., Paulo Ceppi, and Ying Li (2019). "A Robust Constraint on the Temperature and Height of the Extratropical Tropopause". In: *Journal of Climate* 32.2, pp. 273–287. DOI: https://doi.org/10.1175/JCLI-D-18-0339.1.

Thuburn, John and George C. Craig (1997). "GCM Tests of Theories for the Height of the Tropopause". In: *Journal of the Atmospheric Sciences* 54.7, pp. 869–882. DOI: https://doi.org/10.1175/1520-0469(1997)054<0869:GTOTFT>2.0.CO;2.

— (2000). "Stratospheric Influence on Tropopause Height: The Radiative Constraint". In: *Journal of the Atmospheric Sciences* 57.1, pp. 17–28. DOI: https://doi.org/10.1175/1520-0469(2000)057<0017:SIOTHT>2.0.CO;2.

Thuburn, John and George C. Craig (2002). "On the temperature structure of the tropical substratosphere". In: *Journal of Geophysical Research: Atmospheres* 107.D2, ACL 10-1-ACL 10–10. DOI: https://doi.org/10.1029/2001JD000448.

Troen, I. B. and L. Mahrt (Oct. 1986). "A simple model of the atmospheric boundary layer; sensitivity to surface evaporation". In: *Boundary-Layer Meteorology* 37.1-2, pp. 129–148. DOI: 10.1007/BF00122760.

Vallis, G. K. et al. (2018). "Isca, v1.0: a framework for the global modelling of the atmospheres of Earth and other planets at varying levels of complexity". In: *Geoscientific Model Development* 11.3, pp. 843–859. DOI: 10.5194/gmd-11-843-2018.

Vallis, Geoffrey K. (2016). "Geophysical fluid dynamics: whence, whither and why?" In: *Proceedings of the Royal Society A: Mathematical, Physical and Engineering Sciences* 472.2192, p. 20160140. DOI: 10.1098/rspa.2016.0140.

— (2017). *Atmospheric and Oceanic Fluid Dynamics: Fundamentals and Large-Scale Circulation*. 2nd ed. Cambridge University Press. DOI: 10.1017/9781107588417.

— (June 2020). "The Trouble with Water: Condensation, Circulation and Climate". In: *The European Physical Journal Plus* 135.6, p. 478. DOI: 10.1140/epjp/s13360-020-00493-7.

Vallis, Geoffrey K. et al. (2015). "Response of the large-scale structure of the atmosphere to global warming". In: *Quarterly Journal of the Royal Meteorological Society* 141.690, pp. 1479–1501. DOI: https://doi.org/10.1002/qj.2456.

Vecchi, Gabriel A. and Brian J. Soden (2007). "Global Warming and the Weakening of the Tropical Circulation". In: *Journal of Climate* 20.17, pp. 4316–4340. DOI: 10.1175/JCLI4258.1.

Vogel, Raphaela et al. (2022). "Strong cloud–circulation coupling explains weak trade cumulus feedback". In: *Nature* 612.7941, pp. 696–700. ISSN: 1476-4687. DOI: 10.1038/s41586-022-05364-y.

Voigt, Aiko and Tiffany A. Shaw (Feb. 2015). "Circulation response to warming shaped by radiative changes of clouds and water vapour". In: *Nature Geoscience* 8.2, pp. 102–106. DOI: 10.1038/ngeo2345.

Wallace, John M. (May 1992). "Effect of deep convection on the regulation of tropical sea surface temperature". In: *Nature* 357.6375, pp. 230–231. DOI: 10.1038/357230a0.

Wettlaufer, J. S. (Apr. 2016). "Editorial: Climate Science: An Invitation for Physicists". In: *Phys. Rev. Lett.* 116 (15), p. 150002. DOI: 10.1103/PhysRevLett.116.150002.

Wettlaufer, John S. (May 2011). "The universe in a cup of coffee". In: *Physics Today* 64.5, pp. 66–67. ISSN: 0031-9228. DOI: 10.1063/1.3592018.

Williams, Ian N. and Raymond T. Pierrehumbert (2017). "Observational evidence against strongly stabilizing tropical cloud feedbacks". In: *Geophysical Research Letters* 44.3, pp. 1503–1510. DOI: https://doi.org/10.1002/2016GL072202.

Williams, Ian N., Raymond T. Pierrehumbert, and Matthew Huber (2009). "Global warming, convective threshold and false thermostats". In: *Geophysical Research Letters* 36.21. DOI: https://doi.org/10.1029/2009GL039849.

Wing, Allison A. et al. (2020). "Clouds and Convective Self-Aggregation in a Multimodel Ensemble of Radiative-Convective Equilibrium Simulations". In: *Journal of Advances in Modeling Earth Systems* 12.9, e2020MS002138. DOI: https://doi.org/10.1029/2020MS002138.

Winker, D. M. et al. (2010). "The CALIPSO Mission: A Global 3D View of Aerosols and Clouds". In: *Bulletin of the American Meteorological Society* 91.9, pp. 1211–1230. DOI: 10.1175/2010BAMS3009.1.

Xu, Chi et al. (2020). "Future of the human climate niche". In: *Proceedings of the National Academy of Sciences* 117.21, pp. 11350–11355. DOI: 10.1073/pnas.1910114117.

Yoshimori, Masakazu et al. (2020). "Fixed Anvil Temperature Feedback: Positive, Zero, or Negative?" In: *Journal of Climate* 33.7, pp. 2719–2739. DOI: 10.1175/JCLI-D-19-0108.1.

Zelinka, Mark D. and Dennis L. Hartmann (2010). "Why is longwave cloud feedback positive?" In: *Journal of Geophysical Research: Atmospheres* 115.D16. DOI: https://doi.org/10.1029/2010JD013817.

Zelinka, Mark D., Stephen A. Klein, and Dennis L. Hartmann (2012). "Computing and Partitioning Cloud Feedbacks Using Cloud Property Histograms. Part II: Attribution to Changes in Cloud Amount, Altitude, and Optical Depth". In: *Journal of Climate* 25.11, pp. 3736–3754. DOI: https://doi.org/10.1175/JCLI-D-11-00249.1.

Zelinka, Mark D. et al. (2020). "Causes of Higher Climate Sensitivity in CMIP6 Models". In: *Geophysical Research Letters* 47.1, e2019GL085782. DOI: https://doi.org/10.1029/2019GL085782.

Zelinka, Mark D. et al. (2022). "Evaluating Climate Models' Cloud Feedbacks Against Expert Judgment". In: *Journal of Geophysical Research: Atmospheres* 127.2, e2021JD035198. DOI: https://doi.org/10.1029/2021JD035198.

Zhang, Yi and Stephan Fueglistaler (2020). "How Tropical Convection Couples High Moist Static Energy Over Land and Ocean". In: *Geophysical Research Letters* 47.2, e2019GL086387. DOI: https://doi.org/10.1029/2019GL086387.

Zhang, Yi, Nadir Jeevanjee, and Stephan Fueglistaler (2020). "Linearity of Outgoing Longwave Radiation: From an Atmospheric Column to Global Climate Models". In: *Geophysical Research Letters* 47.17, e2020GL089235. DOI: https://doi.org/10.1029/2020GL089235.

Zurita-Gotor, Pablo and Richard S. Lindzen (2008). "Chapter 2 Theories of Baroclinic Adjustment and Eddy Equilibration". In: *The Global Circulation of the Atmosphere*. Princeton: Princeton University Press, pp. 22–46. ISBN: 9780691236919. DOI: doi:10.1515/9780691236919-004.

Zurita-Gotor, Pablo and Geoffrey K. Vallis (2011). "Dynamics of Midlatitude Tropopause Height in an Idealized Model". In: *Journal of the Atmospheric Sciences* 68.4, pp. 823–838. DOI: https://doi.org/10.1175/2010JAS3631.1.